The Impact of Grid-connected Photovoltaic Voltage Sourced Converter with Negative Sequence Decoupling Control on Protection Scheme Behavior

A Thesis

Presented in Partial Fulfillment of the Requirements for the

Degree of Master of Science

with a

Major in Electrical Engineering

in the

College of Graduate Studies

University of Idaho

by

Fahad Ata Allah Alhajeri

Major Professor: Brian K. Johnson, Ph.D.

Committee Members: Herbert Hess, Ph.D.; Ahmed Abdel-Rahim, Ph.D.

Department Administrator: Mohsen Guizani, Ph.D.

May 2018

Authorization to Submit Thesis

This thesis of Fahad Alhajeri, submitted for the degree of Master of Science with a major in Electrical Engineering and titled "The impact of grid-connected photovoltaic voltage sourced converter with negative sequence decoupling control on protection scheme behavior," has been reviewed in final form. Permission, as indicated by the signatures and dates given below, is now granted to submit final copies to the College of Graduate Studies for approval.

Major Professor: _____ Date: _____
Brian K. Johnson, Ph.D.

Committee Members: _____ Date: _____
Herbert Hess, Ph.D.

_____ Date: _____
Ahmed Abdel-Rahim, Ph.D.

Department Administrator: _____ Date: _____
Mohsen Guizani, Ph.D.

Abstract

This thesis focuses on grid-connected PV systems and their impact on protection scheme performance during system fault conditions. The main objective of this work is to design a simulation model that can simulate the response of the system during different fault applications. The ATP program is used to model the grid-connected PV system along with the VSC control schemes based on the decoupled double synchronous reference frame method. The ATP model can be used as a teaching tool in courses and for research purposes. Different types of faults are applied to the power distribution system, with a distance protection element (21) proposed to protect the distribution system. An inverse-time overcurrent element (51) is used to protect the collector system on the ac-side of the VSC. Due to the characteristics of the VSC, it is controlled to limit the fault current contribution to less than 1.2 pu of the maximum current value. This causes the protection elements to either not trip or not trip correctly. In addition, due to the limited fault current and the weak source of the grid-connected PV system compared to the grid system source, the mho distance element mislocates the fault location. It calculates that the apparent fault location is much closer to the PCC than it actually is. This study indicates that the performance of the supervised distance element and the inverse-time overcurrent element are impacted by the grid-connected PV system. Therefore, in the fault analysis study and the protection schemes settings, this type of system should not be modeled as a conventional power generator.

Acknowledgements

First and foremost, praises and thanks to God, the Almighty, for the unlimited and continuous blessings in my life.

I would like to thank and express my sincere gratitude to my major professor, Dr. Brian Johnson for his continuous support and guidance throughout my Master's program. Thank you for your patience, kindness, availability, and enthusiasm you provided during my thesis.

I would also like to thank the committee members, Dr. Herbert Hess and Dr. Ahmed Abdel-Rahim, for their valuable time and insightful suggestions.

I am also thankful to my colleagues, faculty, and staff of the ECE department who have been part of my Master's Degree completion.

Last but not the least, I would like to thank my family and friends for their sincere prayers, support, and believing in me throughout my personal and academic life.

Dedication

“To my beloved parents, for their love, prayers and support.”

Table of Contents

List of Figures

List of Tables

Acronyms

AC – Alternating Current

DC – Direct Current

VSC – Voltage Source Converter

ATP – Alternative Transient Program

COMTRADE – Common format for Transient Data Exchange for power systems

DLG – Double Line to Ground

DSRF – Double Synchronous Reference Frame

DDSRF – Decoupled-Double Synchronous Reference Frame

PLL – Phase Locked Loop

DDSRF-PLL – Decoupled-Double Synchronous Reference Frame – Phase-Locked Loop

LCOE – Levelized Cost of Energy

DOE – Department of Energy

NREL – National Renewable Energy Laboratory

HVDC – High Voltage Transmission Line

HV-side – High Voltage-side

LV-side – Low Voltage-side

IEEE – The Institute of Electrical and Electronics Engineers

NEC – National Electrical Code

ANSI – American National Standards Institute

UL – Underwriters Laboratories

LPF – Low Pass Filter

PI Controller – Proportional-Integral Controller

CT – Current Transformer

PT – Voltage Transformer

RMS – Root Mean Square

IGBT – Insulated-Gate Bipolar Transistor

IGCT – Integrated Gate-Commutated Thyristor

NPC – Neutral-Point Clamped

MPPT – Maximum Power Point Tracking

VCO – Voltage-Controlled Oscillator

VSAV – Voltage System Averaged

ECE529 – Utility Applications of Power Electronics Course

SLG – Single Line to Ground

MVA – Megavolt Ampere

VAR – Volt-Ampere Reactive

MW – Megawatt

PCC – Point of Common Coupling

PU – Per Unit

PV – Photovoltaic

RLC –Resistor Inductor Capacitor

SLG – Single Line to Ground

LL – Line to Line

Chapter 1: Introduction and Objective

1.1. Introduction

The installation of renewable power generation has increased significantly in the last decade and the number of new installations is still increasing in order to meet the growing demand for the electricity. One type of renewable power generation is grid-connected PV generation. In this thesis, a grid-connected PV system is studied and an appropriate system is designed and modeled. The electromagnetic transient program – ATP is utilized to model the grid-connected PV system, and extract current and voltage data, which are converted to COMTRADE files that are replayed in relay models implemented in Mathcad.

Chapter 2 introduces PV systems in general with basic concepts of operation and main system components. Chapter 3 discusses grid-connected PV systems, including interactions with the electrical power grid and the related standards and codes. Chapter 4 discusses the system design, different power converter topologies, control schemes and related mathematical equations. Chapter 5 discusses the electrical protection challenges due to the characteristics of the power converter that is coupled with the PV system. Chapter 6 presents detailed models of the grid-connected PV power system and its control schemes that are based on the decoupled double synchronous reference frame approach (DDSRF). The ATP model of the grid-connected PV system is discussed in chapter 6, and the Mathcad relay models are discussed in chapter 7. Chapter 7 discusses the results of the modeled simulation and protection scheme performance when electrical faults are applied on the distribution system of the power grid. Last but not least, Chapter 8 draws conclusions from this study and describes possible future work building on this study.

1.2. Objective

The objective of this thesis is to study and examine the performance of both distance and inverse-time overcurrent protection elements for a power system that is coupled with a PV system during short-circuit faults on the distribution line of the grid. The distance protection element is applied on the distribution system instead of the overcurrent element as an option to improve the protection performance. Due to the characteristics of the PV power converter, the control schemes limit the current contribution from the VSC, which causes misoperation of the protection elements. Also, part of the thesis objective is to build a model system in the ATP program that can simulate an appropriate response of the grid-connected PV system during normal and abnormal conditions. The ATP model can be used as a teaching tool in the ECE529 course and for research purposes.

Chapter 2: PV Systems

2.1. PV System Overview

A photovoltaic power system, often called a PV system, is a well-known power generation system that is used as a renewable energy source. The system is designed to supply electrical power by converting solar energy into direct current (DC) electricity through the photovoltaic effect [1], a phenomenon studied in physics. The system consists of several elements, including solar panels or arrays, power converters, controllers, distribution lines, and other electrical connections. The system features noiseless operation, is free of environmental emission, and contains no moving parts aside from potential cooling equipment for the power converters. The system can be used in a small scale such as electronic equipment, or to power houses or buildings. It could also be used in a very big scale in multi-megawatt electrical power generation facilities such as the solar generation farms [1].

As a renewable energy source, PV systems have big advantages over conventional energy sources. PV systems would reduce the emission of greenhouse gases and other pollutants during operation, creating employment opportunities, and improve the environmental security of the power system. Once fabricated, it does not require fuel and water, it requires a minimal maintenance, and has a lifetime up to 30 years, and it generates electricity whenever there is a light. Expanding the use of renewable energy sources would make the environment better, contribute to job creation in the technology manufacturing industries, and when coupled with hypothetical inexpensive energy storage systems enhance power system reliability and security by providing local energy generation [1]. Worldwide energy demand continues to increase. Fossil fuel based energy sources are limited and will

eventually run out. PV solar energy is a capable energy source that has a high potential to help fulfill the growing need for energy around the world [1].

PV energy generation has some drawbacks, some of which are; it cannot generate power during the absence of light, it requires a large area for the large-scale applications, and it has a high initial cost, as well as the environmental impact of PV cells fabrication. However, theses drawbacks are potentially minimal in comparison with the disadvantages of the traditional energy sources in the long run. Government policies have encouraged the adoption of PV systems, and driven down production costs through increased manufacturing scale. In the recent decades, there have been various projects and growing interests in the PV solar energy from both industry and from academic and national labs researchers. They are studying and investigating the PV solar energy and its behavior, and advancing the technology to its limits in all PV aspects: efficiency, costs, size, reliability, and performance. One of the notable ongoing projects is SunShot Initiative.

2.1.1. SunShot Initiative

The SunShot Initiative is a better-future promising project the U.S. Department of Energy (DOE) launched in 2011, in collaboration with the National Renewable Energy Laboratory (NREL), and other DOE national labs. The project has an aggressive target of making solar electricity cost-competitive with the traditional electricity generations by 2020. The goal of the project is to reduce the PV solar power prices by approximately 75% relative to its cost in 2010, across three sectors, residential, commercial, and utility-scale. The study expects this price reduction goal can increase the solar energy utilization in the U.S. electricity need by approximately 14% in 2030 and 27% in 2050. Along with a decline in the fossil fuel use, the development could decrease greenhouse gase emissions and other pollutants, and

create more employment opportunities in solar-related technology [2]. Due to significant change in the solar technology, its markets, and industry over the past five years, solar deployment in the U.S. has increased more than ten times. At the same time, the levelized cost of solar energy has gone down by 65%, and became much more affordable [2].

Due to the PV system cost reduction, the PV solar energy has grown from 0.1% of the total U.S. electricity generation in 2010 to 0.9% at the end of 2015. This growth has increased the PV deployment in the U.S. at a compound annual growth rate of 54% since 2010, varying from 25% to 54% to 74% in the commercial sector, the residential sector, and the utility-scale sector, respectively, as shown in Figure 2.1 [2]. Figures 2.1 and 2.2 are part of a study done by the U.S. Department of Energy from the "On the Path to SunShot" report released on May 2016. Figure 2.2 illustrates the PV system Levelized Cost of Energy, LCOE, in 2010, 2015, and the 2020 target, which is lowering the LCOE in utility, commercial (20 kW to 1 MW), and residential (less than 20 kW) sectors to 6, 7, and 9 cents per kWh, respectively, without subsidies and based on an average solar resource [2]. The cost, efficiency, reliability, and lifetime of PV modules, and the tradeoffs among them are the significant factors of LCOE.

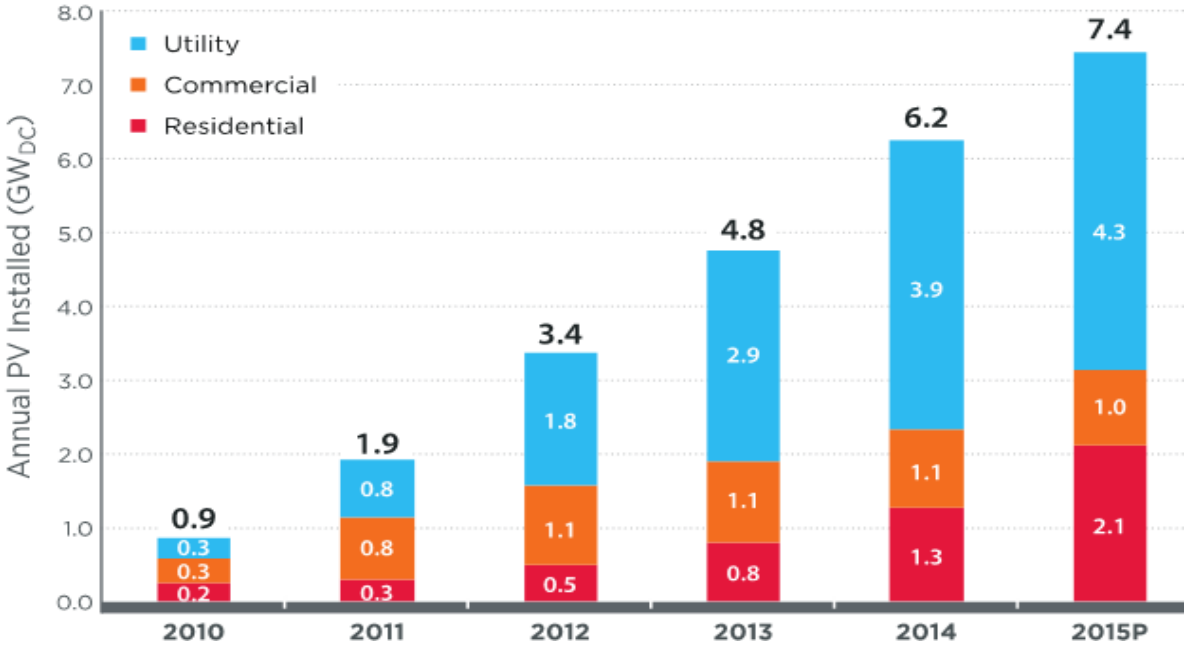

Figure 2.1: U.S.A. annual PV installations [2].

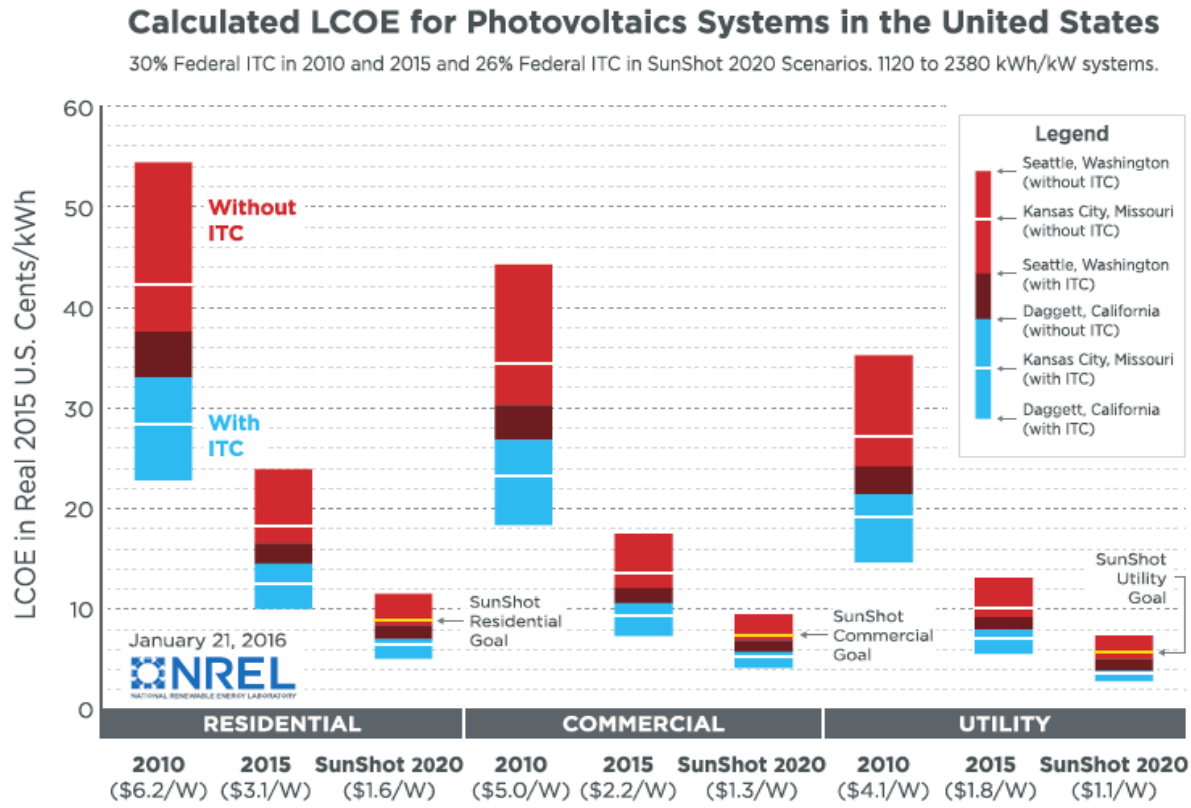

Figure 2.2: A statistical calculation of LCOE for photovoltaic systems in the U.S.A [2].

2.2. PV System Concept

Solar radiation can be directly converted into electricity in a semiconductor device that is called solar cell. This direct conversion is defined as a photovoltaic energy conversion since it is based on the photovoltaic effect, which generally means creating a potential difference at the junction of two different materials when exposed to light [1]. As shown in Figure 2.3, a group of solar cells is connected together in series-parallel configurations to create a solar panel or PV module to produce a particular voltage and current for their operation. The peak output power of PV modules may range from a few watts to more than 300 Watts depending on the intended application. The PV modules can be connected together to form a PV array, which can be used in large-scale applications, with a typical output power varying from 100 Watts to kilowatts [3]. Megawatt arrays are also available. The PV arrays are the heart of a complete PV system, which usually consists of PV arrays, DC/AC inverters, power controllers, batteries for energy storage, and other miscellaneous electrical setups depending on the application.

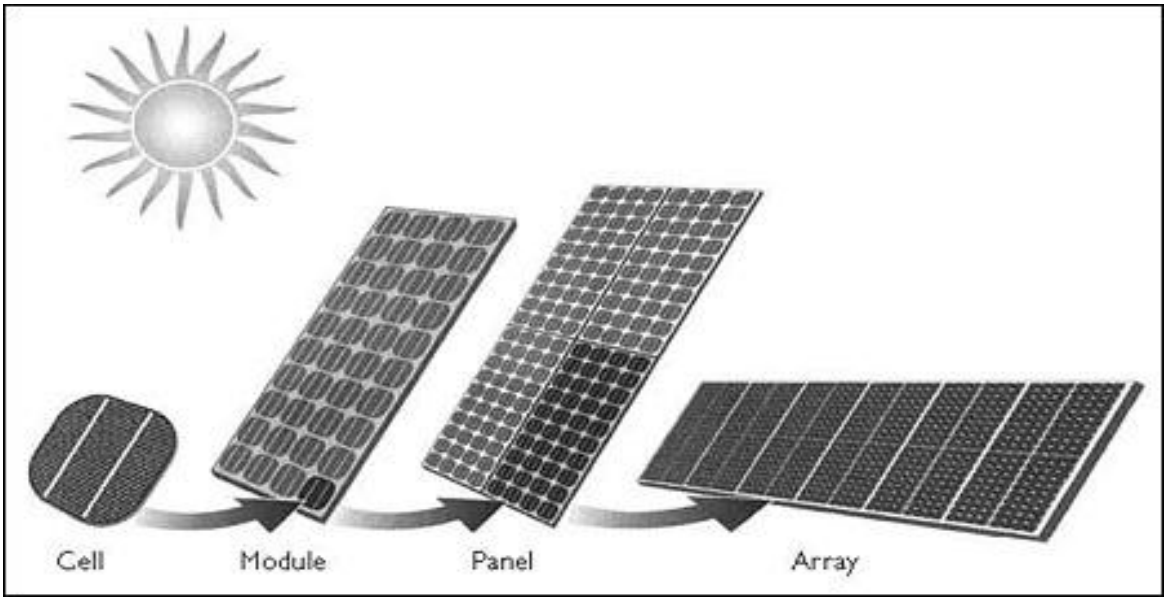

Figure 2.3: A PV array structure.

2.3. Types of PV System

The PV system can almost be utilized in any electrical system. It features both modularity and expandability, thus it can fit any system from a few watts to megawatts. This feature has led to many utilizations and varieties of PV systems. PV systems can be classified as stand-alone systems, hybrid systems, or grid-connected systems.

2.3.1. Stand-Alone

A stand-alone system has the ability to operate independently from the utility grid, and can be designed and sized to power certain DC and/or AC electrical loads. This type of system, illustrated in Figure 2.4, is generally utilized in remote areas where the nearest connection point utility grid is far away or not available. The system can be very simple, such as directly coupling a PV panel or array with a fan or a water pump, and it only works during sunlight hours. The system can be advanced when an energy storage is incorporated and used to power a whole village in a rural area or a space satellite along with other electrical components [3].

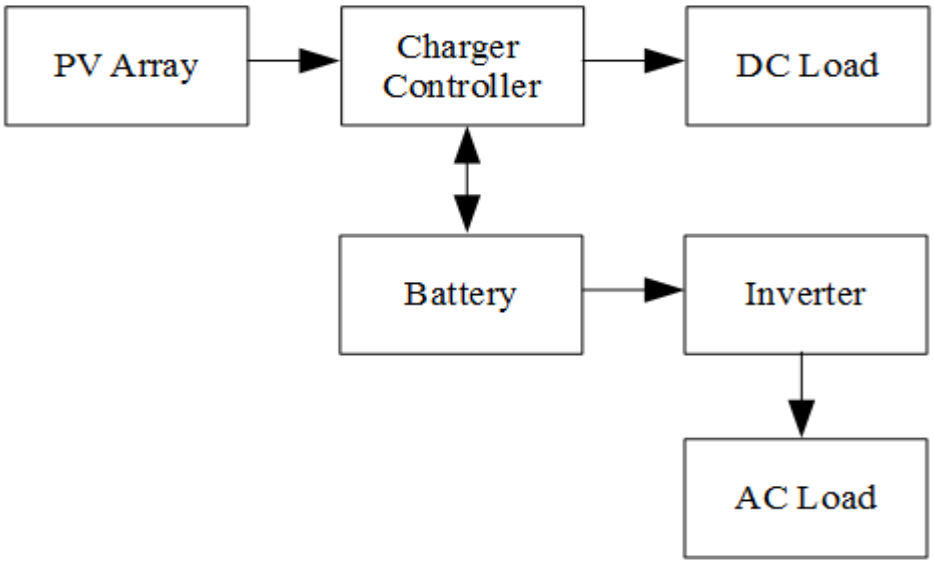

Figure 2.4: Stand-alone system

2.3.2. Hybrid

For stand-alone applications where using only PV arrays as a source of generation is not economical or practical, alternative types of generation can be used as a supplement to the PV output, such as wind turbines, or gasoline or diesel generators. Such a system is referred to as a hybrid system as shown in Figure 2.5. This type of system is sufficient when the winter peak sun is very low and instead of installing a large number of PV panels to meet the load demand, and wasting the energy produced from the extra panels during the summer, a different type of generation is utilized [3]. In such a system, the energy demand is met, at the same time the PV output is fully utilized.

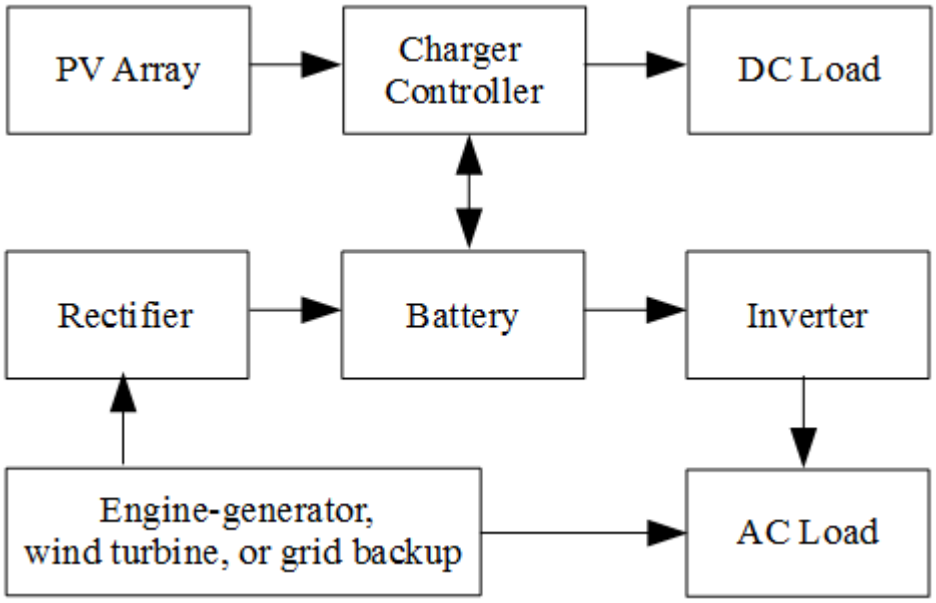

Figure 2.5: Hybrid system

2.3.3. Grid-Connected

The PV system can also be interconnected with the utility grid, with the incorporation of suitable electrical devices to interface with the major grid. This type of system is called a grid-connected PV system, where a basic block diagram is shown in Figure 2.6. The system must have a DC/AC inverter, electrical protective devices, and controllers to enhance the

interconnection and ensure the PV system will disconnect from the grid in case of grid failure and power outages. The grid-connected systems can be from a few kilowatts to the megawatt range. Residential systems are in the range of 1.5 to 5kW peak, commercial building units tend to be in the 15kW range, while large transmission grid-connected systems are in the megawatt range. This type of PV system is becoming more economically useful as the PV system costs continue to go down [3]. In addition, it holds the highest PV deployment amount in the U.S. with annual PV installation of 4.3GWdc in 2015 as indicated in Figure 2.1.

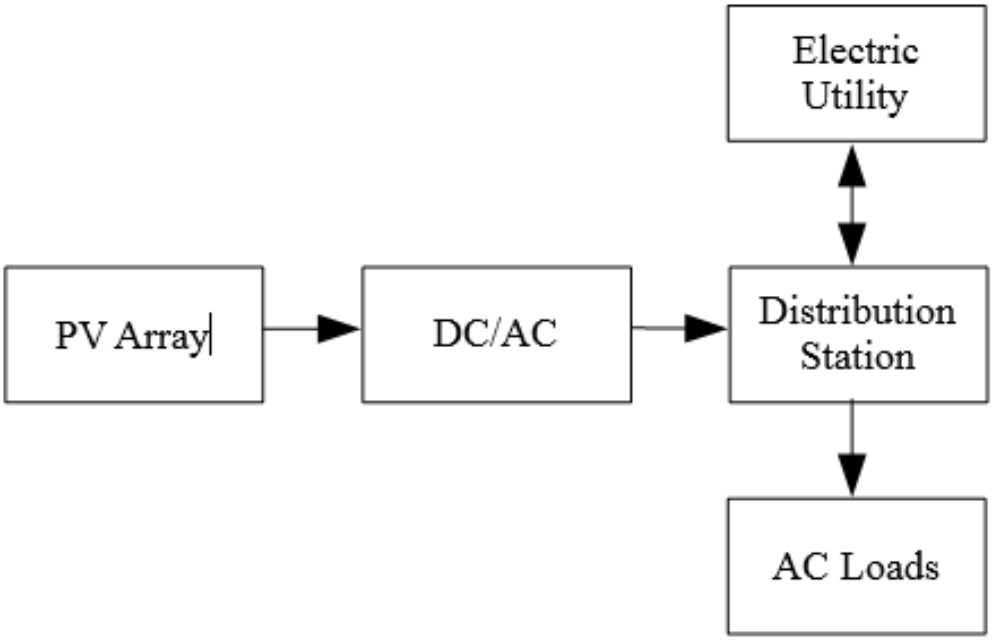

Figure 2.6: Grid-connected system

The remainder of this thesis will focus on this type of grid-connected PV system, and will discuss the system designs, necessary components needed for the interconnection, as well as the system contributions to the power grid, and the associated protective elements and their protection challenges. Later, a mathematical modeling is designed in the ATP program, to study the system behavior during both normal and abnormal conditions and analyze its response due to different system faults.

Chapter 3: Grid-Connected PV Systems

3.1. Overview

As discussed in Chapter 2, the cost of manufacturing PV modules and associated components is going down. More power producers and some utilities are building PV power plants in order to increase their power generation and meet state renewable energy portfolio standards. These PV power plants are of the grid-connected PV system type. This type of PV system can incorporate a battery bank for energy storage, however most of the large-scale applications do not include energy storage in their design because the generated power is directly supplied into the power grid to the customers.

Figure 3.1 illustrates the basic design of the grid-connected PV system. The generated power from the PV arrays is usually delivered to a DC-DC boost converter to increase the voltage level. The DC/AC inverter is then used to invert the boosted DC voltage to a three phase AC voltage before it is connected to the utility grid through a transformer. The system also consists of other electrical components such as power controllers, protective devices, voltage regulators, and more, in order to enhance the interconnection and guarantee the process of disconnection from the power utility during grid failure. Mechanical components might also be used, such as a sun-tracking system to increase the power generation.

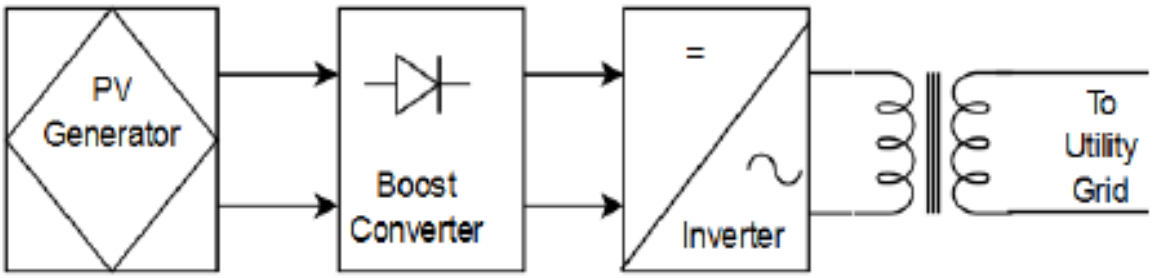

Figure 3.1: Block diagram of grid-connected PV system

3.1.1. Contributions and Advantages to the Electric Power Grid

Grid-connected PV systems could play a great role in supporting the future power grids while at the same time doing no harm to the environment. Beside the many advantages of the PV systems mentioned earlier, they would be an ideal distributed power generation source for remote and urban areas. Generators at the distribution level are near the load, which then helps in reducing some of the power losses that occur in transmitting power on a very long high-voltage transmission system like in the case of centralized power generation [4]. However, this is not necessarily an advantage for large grid-connected PV systems that are often being installed in rural areas.

In some cases, when connecting a PV system with a power grid, it reduces both energy and reactive power losses [5]. It also reduces transformers operating temperature both before and during the system peak, which then increases the transformers capacity and defers their maintenance and replacement [5]. Also in some cases, when a high capacity PV generation is implemented, it helps to relieve overloads on the transmission and distribution facilities, which may reduce the need for costly expansion of the transmission and distribution facilities [6]. Thus, power grid efficiency is improved and cost saving can be achieved in some cases.

In addition, grid-connected PV systems have an advantage that their energy peak production coincides with the utilities energy demand at its maximum. During the summer

season, utilities have a high peak energy demand primarily due to air conditioning load in mid-to late afternoon, which partially correlates with the peak energy production of the PV. Also, integrating PV system contributes to network reliability by alleviating summer peaking issues [4], [5], [6], and [7].

Another benefit of PV integration that some utilities have liked is the expandability feature. PV can be deployed on an incremental basis without having to consider standard footprint or capacity size requirements. It can be sized in a range of hundreds of kilowatts to hundreds of megawatts, and possibly be installed on roofs of buildings or parking structures. It also benefits in its construction schedule time that is significantly different than conventional natural gas and coal plants. A PV plant can be built and brought to operation within a six months, whereas natural gas facilities can range anywhere from three to five years to permit and construct [4].

3.2. Codes and Standards

The PV system is an energy source that can generate a high voltage, which can affect the power grid and cause hazard. Hence, sets of codes and standards have been made to standardize and uniform technical and practical requirements for the PV interconnection with the electric grid to ensure safety of people and property, grid reliability, efficiency, and performance. In general, the three main standards and codes that are related to the PV system interconnections are; the National Electric Code, NEC Article 690, and from the Institute of Electrical and Electronics Engineers, Standard IEEE 929-2000 and Standard IEEE 1547 [3]. These standards and codes are important not only to protect the end user, but also to ensure the safety of the maintenance technician.

1- NEC Article 690:

The NEC Article 690 is a set of codes for PV design engineers since it clearly states the acceptable practices for the PV system design, and talks about every topic where electrical safety and efficient utilization is a consideration. As it deals entirely with the PV systems it also refers to other articles that deal with system protective devices, grounding, and other components for the system installations [3].

2- IEEE 929-2000:

IEEE 929-2000 provides recommended practice for all concerns related to the interconnection of the PV system with the utility grid, and to standardize and set limits for related technical issues. It states all the concerns of power quality, voltage ratings, frequency, islanding protection, power factor, harmonic distortion, grounding, testing inverters, limitation of dc injection to the ac system, and disconnecting and reconnecting in the event of power grid failure and restoration. The IEEE 929-2000 also includes the general requirements of other standards such as UL 1741, IEEE 519-1992, and ANSI C84.1-1995 [3] and [8].

3- IEEE 1547:

IEEE 1547 is a standard that was developed to provide a guidance for interconnecting distributed generation and storage with electric power systems. It has been developed to establish criteria and requirements for distributed resources and provides a uniform standardization of the interconnection and its requirements for operation, performance, testing, safety, and maintenance [9]. The standard provides recommended best practices for implementation and uniform requirements for power quality, abnormal condition response, islanding protection, and testing procedures. Below are some additional related standards to the IEEE 1547:

- 1547.1: IEEE Standard Conformance Test Procedures for Equipment Interconnecting Distributed Resources with Electric Power Systems [10].
- 1547.2: IEEE Application Guide for IEEE Standard 1547, IEEE Standard for Interconnecting Distributed Resources with Electric Power Systems [11].
- 1547.3: IEEE Guide for Monitoring, Information Exchange, and Control of Distributed Resources Interconnected with Electric Power Systems [12].

Chapter 4: Grid-Connected PV System Design

4.1. Power Electronic Converter

For many years, power electronics have been widely utilized in many electrical applications in household, industrial, and information technology. In the past two decades, power semiconductor devices and microelectronics have become highly developed and gained more attention. As a result, power electronic devices are increasingly deployed in the electrical power system, for power compensation, correction, and filtering applications. One of the notable power electronic devices is the power-electronic converter [13].

The exchange of energy in the power system is not a straightforward job. Subsystems of different voltage or current waveforms, frequency, phase angle and number of phases cannot be directly interfaced with each other. The main function of the power converter is to assist the energy exchange between two or more subsystems in a precise manner at desired amounts. Based on the type of the subsystems that need to be interconnected and the requirements, each side of a power converter is categorized as AC or DC based on the subsystem it interfaces with. The power converters can be one of the following; a DC-to-DC converter to link two DC subsystems, a DC-to-AC converter to link a DC subsystem to an AC subsystem, or an AC-to-AC converter that links two AC subsystems [13] and [14].

For many years, the power-electronic converters had a limited use in the power system, largely in high-voltage DC (HVDC) transmission systems, and a lesser use in conventional static VAR compensators and synchronous machine exciters. However, for the past two decades, power-electronic converter utilizations have been continuously increasing in the electric power system; in distribution, transmission, generation, and energy exchange. One of

the many reasons behind the extensive power converter deployment is the fast and continuing advancement in technology of the power electronics and wide selections of the semiconductor switches for high-power applications. In addition, the environmental pollution problems and energy crisis associated with the traditional forms of energy resources (coal, natural gas, oil, and fossil fuel), have led toward further utilization of green energy. These renewable energy resources are regularly interconnected with the electric power system through the power-electronic converters. Due to the energy demand growth, more power electronic devices are used to improve the power stability in the electric power grid [13].

In addition, power electronic devices are expected to have a more impact on electric power systems, and will significantly grow, as there are more new strategies and ideas that are on the increase, such as the microgrids, active networks, and smart grids. The power electronics will have a great role in the efficiency and reliability improvement on the existing power system equipment and infrastructure. They facilitate large-scale renewable energy resources and storage system integration in the electric power grids. They also smooth the progress of integrating the small-scale distributed energy resources of both generations and storage units, especially at the sub-transmission and distribution voltage levels [13].

4.2. Voltage Sourced Converter (VSC)

Although there are many types of power electronic converters, the voltage-sourced converter (VSC) is the prominent type that is commonly utilized in electric power systems for all but the highest power rated applications. The VSC is a DC/AC type of converter that has the ability to convert a DC electric power to an AC electric power, and vice versa. Figure 4.1 shows a simplified power circuit diagram of a half-bridge converter that converts a DC current to a single phase AC current. The converter has two fully controllable and unidirectional

switches. The switches can be insulated-gate bipolar transistors (IGBT) or integrated gate-commutated thyristors (IGCT). This type of converter can be used as the building block for the construction of the three-phase VSC, which can have different configuration topologies. The two most commonly applied configurations of the three-phase VSC are a two-level VSC and a three-level neutral-point clamped (NPC).

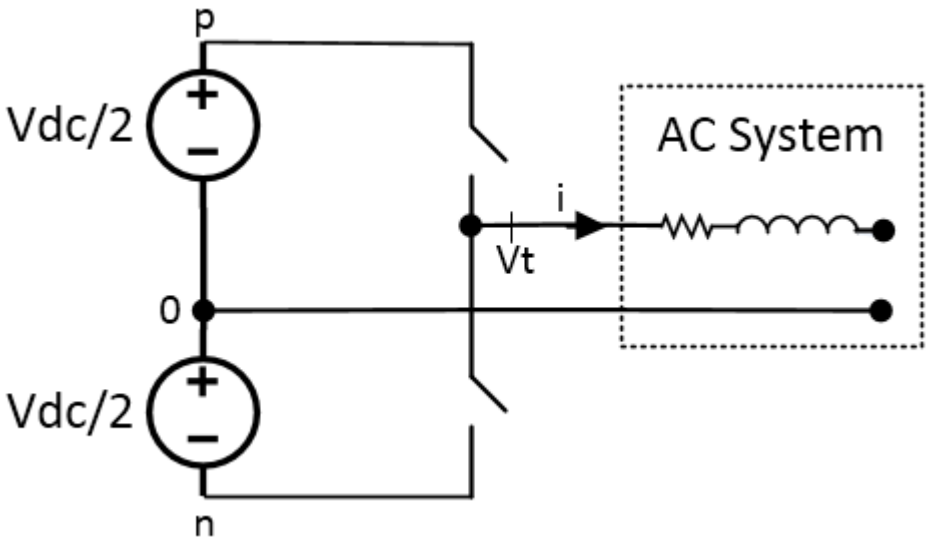

Figure 4.1: A simplified power circuit diagram of a half-bridge converter.

4.2.1. Two-Level Three Phase VSC

The two-level, three-phase VSC is the dominant converter utilized in a wide range of equipment in medium-to-high-power applications. The converter is a composition of three identical half-bridge converters as illustrated in Figure 4.2, which consists of six fully controllable and unidirectional switches. The AC-side terminal of each half-bridge converter is connected to one phase of the three-phase AC system, a, b, and c, whereas each DC-side of the three half-bridge converter shares a common ungrounded or center point grounded DC-side voltage source in a parallel connection. The converter has the ability to provide a bidirectional power-flow path between the three-phase AC system and the DC-side voltage

source [13]. Note that the two-level three-phase VSC shown in Figure 4.2 is a nonideal switching model of two-level VSC, which is not the scope of this thesis. The thesis will only focus on the ideal averaged model of the two-level VSC, which will be discussed later in this chapter, and whose three phase AC-side terminal voltages can be calculated by the following equations:

$$V_{ta}(t) = \frac{V_{DC}}{2} m_a(t), \tag{4.1}$$

$$V_{tb}(t) = \frac{V_{DC}}{2} m_b(t), \tag{4.2}$$

$$V_{tc}(t) = \frac{V_{DC}}{2} m_c(t), \tag{4.3}$$

V_{DC}: The ideal DC voltage source as a function of time

$V_{at}(t)$: Phase A dependent AC voltage source as a function of time

$V_{bt}(t)$: Phase B dependent AC voltage source as a function of time

$V_{ct}(t)$: Phase C dependent AC voltage source as a function of time

Where;

$$m_a(t) = m(t)\cos[\epsilon(t)], \tag{4.4}$$

$$m_b(t) = m(t)\cos[\epsilon(t) - \frac{2\pi}{3}], \tag{4.5}$$

$$m_c(t) = m(t)\cos[\epsilon(t) - \frac{4\pi}{3}], \tag{4.6}$$

$m_a(t)$: The modulating signal of phase A as a function of time

$m_b(t)$: The modulating signal of phase B as a function of time

$m_c(t)$: The modulating signal of phase C as a function of time

$\epsilon(t)$: The output of the phase-locked loop as a function of time

The modulating signals, $m_a(t)$, $m_b(t)$, and $m_c(t)$, are usually delivered by a closed-loop control scheme. Thus, the converter AC-side terminal voltages are found from the previous equations, and they can be controlled by the modulating signal, m (t), in $\frac{V_{DC}}{2}m(t)$.

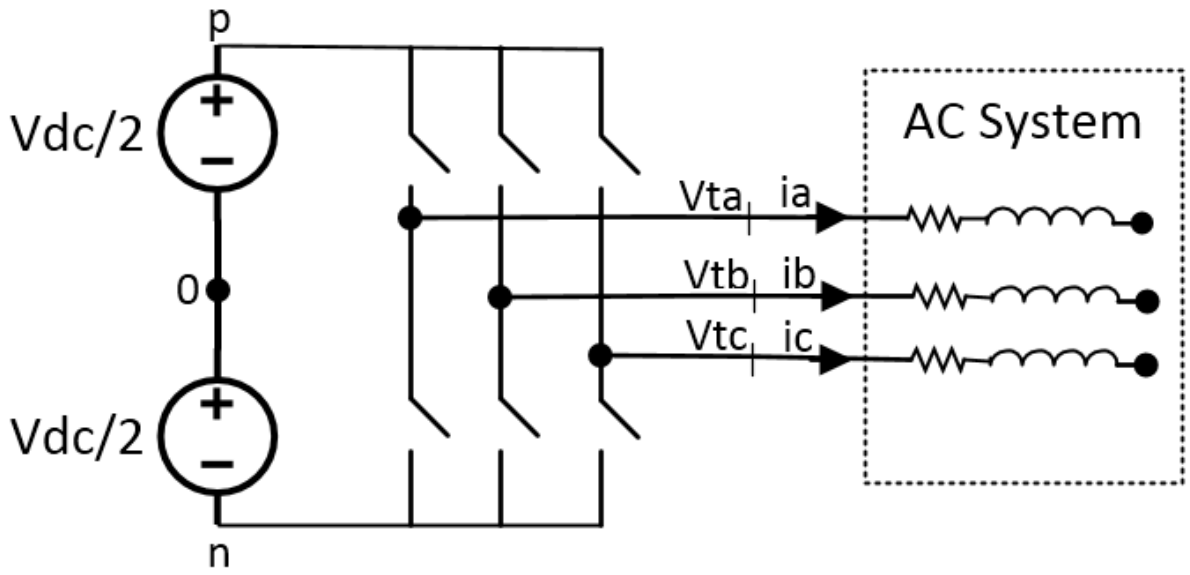

Figure 4.2: A schematic diagram of a nonideal two-level VSC.

4.2.2. Three-Level Three Phase (NPC) VSC

Another configuration of the three-phase VSC is the three-level, three-phase Neutral Point Clamped (NPC) VSC. As demonstrated in Figure 4.3, a combination of two two-level half-bridge converters is used to build a three-level half-bridge NPC, where one two-level half-bridge converter supplies a controlled positive AC voltage, and the other one supplies a controlled negative AC voltage. Then the three-level half-bridge NPC is used as the building block for the construction of the three-level three-phase NPC as shown in Figure 4.4, which is composed of three identical three-level half-bridge NPCs. The AC-side terminal of each

half-bridge NPC converter is connected to one phase of the three-phase AC system, a, b, and c, whereas the DC-sides of the half-bridge NPC converter are in a parallel connection and share the same split voltage source [13]. Thus this design makes it a multilevel converter whose switch cells can withstand the high-power/high-voltage applications.

Equations (4.1) - (4.6) are still applicable to the three-level NPC to calculate its three phase AC-side terminal voltages, $V_{at}(t)$, $V_{bt}(t)$, and $V_{ct}(t)$, and the modulating signal, $m_a(t)$, $m_b(t)$, and $m_c(t)$, with some minor modification.

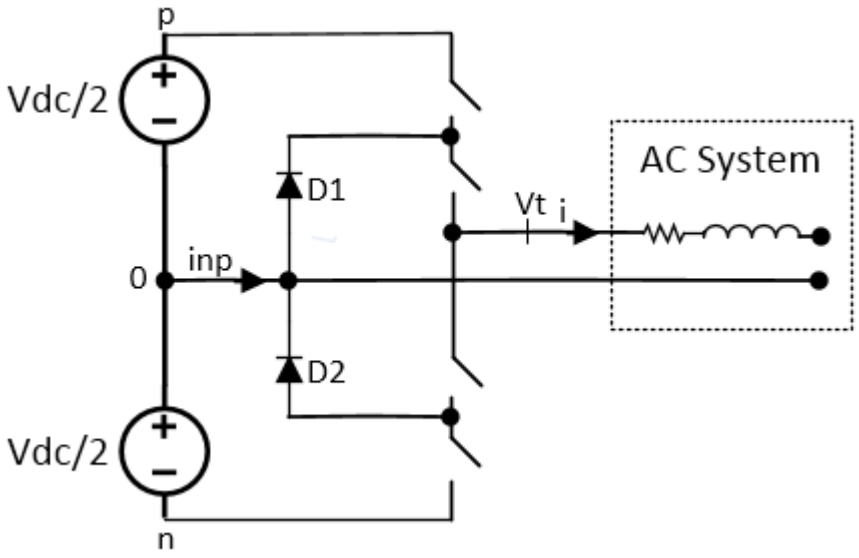

Figure 4.3: A circuit diagram of the three-level half-bridge NPC.

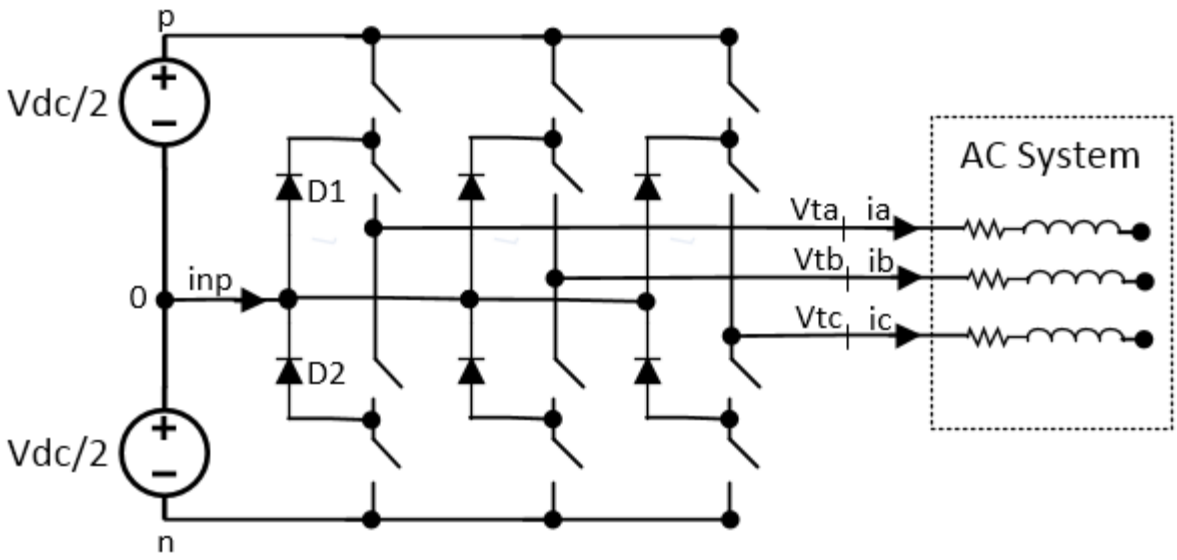

Figure 4.4: A schematic diagram of a three-level NPC VSC.

Compared to other high-power/high-voltage two-level converter topologies that have a number of lower voltage switches connected in series, the three-level NPC design offers an alternative approach that reduces the number of series-connected switches needed. It also avoids the need for the simultaneous gating and snubber circuits for the switches that guarantee equal voltage sharing among the switches and accurate timings, which are undesirable [13]. In the event of employing the two-level VSC in a high-power/high-voltage application, the switch cells must be rated for such applications and capable of withstanding the high DC voltage level. If the particular highly rated switches were selected, they would typically be expensive and may not fulfill the voltage requirements of most utility applications. In a comparison to a two-level VSC of the same rating, the three-level NPC provides three-phase AC voltage with a lower harmonic distortion, lower switching losses, and reduced switch stress levels [13].

4.2.3. Averaged Model of Two-level VSC

The switching model of the two-level VSC can describe the steady-state and dynamic behavior of the converter in an accurate way. Designing such an accurate converter with a

switching model would require more complicated models for the switching functions, which then provides high frequency components as well as the slow the transient and dynamic response due to the switching process. In the switching model, the relationships between the current-voltage variables and the modulating signals are not easily understood. Furthermore, when it comes the dynamic analysis and control design needs, the knowledge about the high frequency is not necessary. The reason is that the compensators and filters in the closed-loop control system usually include low-pass characteristics that do not respond to the components of the high frequency. Therefore for these reasons, using an averaged mode is more beneficial and practical, as we only care about the dynamics of the average values of variables, not the dynamics of the instantaneous values. The averaged model can also describe the converter dynamics as a function of the modulating signals [13]. Also, it takes less processing time compared to the switching model. Figure 4.5 shows the averaged equivalent circuit of the ideal two-level VSC, which will be modeled and studied in the ATP software in the thesis.

It is worth mentioning that equation (4.7) indicates both the expression for the DC-side current of the two-level VSC and the expression for the DC-side current of the three-level NPC. The reason is that in both configurations the power exchange is only supplied by the DC component of the DC-side current, and i_{np} in Figure 4.4 is equal to zero when the capacitor voltages are equal and stable. As mentioned earlier in the previous section that both two-level VSC and three-level NPC have the same equations, (4.1) - (4.6), to find their three phase AC-side terminal voltages and the modulating signals. Therefore, the averaged models of both the three-level NPC and the two-level VSC are the same, and this is another advantage of using the averaged model rather than the switching model. From now on, the thesis will

discuss the mathematical modeling, system behavior, and control design methodology for only the averaged model of a three-phase VSC.

$$V_{DC}(t)i_{DC}(t) = V_{ta}(t)i_a(t) + V_{tb}(t)i_b(t) + V_{tc}(t)i_c(t), \tag{4.7}$$

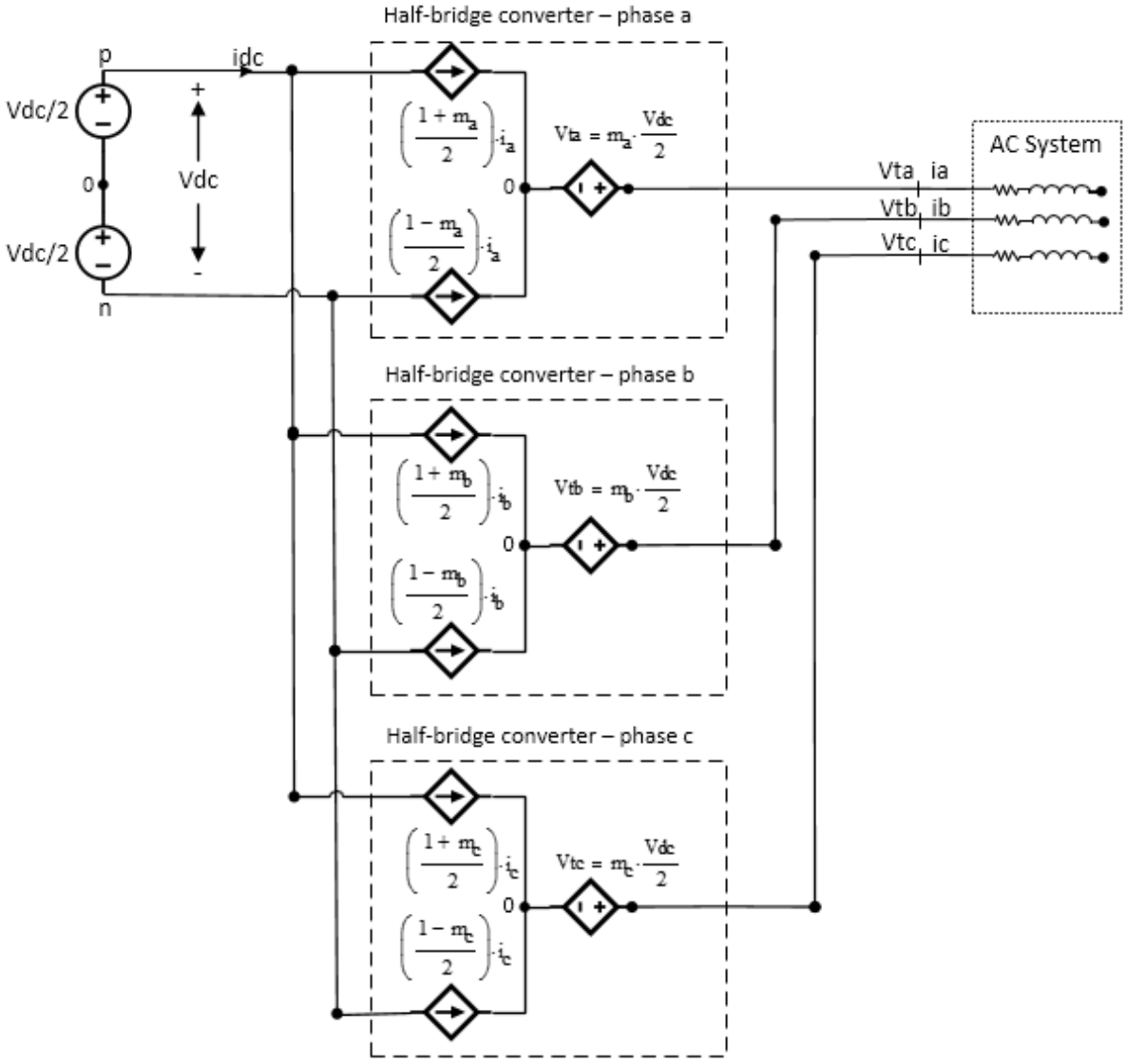

Figure 4.5: Averaged equivalent circuit of the ideal two-level VSC.

4.3. Clarke and Park's Transformations

Controlling a three-phase VSC system is not a straightforward task, as one is invariably interested in tracking sinusoidal voltage and current commands. The Clarke and Park's transformations are two-dimensional reference frames that are used to make the control

design adequately rapid and less complex. Both frames reduce the number of required control loops from three to two. The Clarke transformation transforms the abc quantities, such as voltages and currents, to a two axis stationary reference frame ($\alpha\beta$-frame). The inverse transformation will be used for the modulating signals, as shown in equations (4.8)-(4.13). Equation (4.10) calculates the zero sequence voltage. The same equations are applicable for calculating the currents by substituting the line currents instead of line to ground voltages.

$$V_\alpha(t) = \frac{2}{3}(V_a(t) - \frac{1}{2}V_b(t) - \frac{1}{2}V_c(t)), \tag{4.8}$$

$$V_\beta(t) = \frac{1}{\sqrt{3}}(V_b(t) - V_c(t)), \tag{4.9}$$

$$V_0(t) = \frac{1}{3}(V_a(t) + V_b(t) + V_c(t)), \tag{4.10}$$

V_a (t): Phase A line to ground voltage as a function of time

V_b (t): Phase B line to ground voltage as a function of time

V_c (t): Phase C line to ground voltage as a function of time

V_α (t): The real axis projection of the phase voltages as a function of time

V_β (t): The imaginary axis projection of the phase voltages as a function of time

V_0 (t): The zero sequence voltage as a function of time

Also, the modulating functions can be implemented as;

$$m_a(t) = m_\alpha(t), \tag{4.11}$$

$$m_b(t) = \frac{1}{2}(\sqrt{3}\, m_\beta(t) - m_\alpha(t)), \tag{4.12}$$

$$m_c(t) = \frac{1}{2}(\sqrt{3}\, m_\beta(t) + m_\alpha(t)), \tag{4.13}$$

$m_a(t)$: The modulating signal of phase A as a function of time

$m_b(t)$: The modulating signal of phase B as a function of time

$m_c(t)$: The modulating signal of phase C as a function of time

$m_\alpha(t)$: The real axis projection of the modulating signal as a function of time

$m_\beta(t)$: The imaginary axis projection of the modulating signal as a function of time

Similarly, the Park's transformation is used to convert the abc quantities and the modulating signals to a two axis rotating reference frame (dq-frame), direct- and quadrature-axis, respectively. The conversion from abc quantities to dq0 quantities can be done directly using equation (4.18). However for the sake of clarity, equations (4.14)-(4.17) convert the $\alpha\beta$ quantities to dq quantities. Equation (4.10) can be used to find $V_0(t)$. The same equations are applicable to calculate the currents by replacing the voltage quantities by current quantities. Figure 4.6 shows a typical dq-frame control scheme of a three-phase system, where abc quantities are converted to dq quantities.

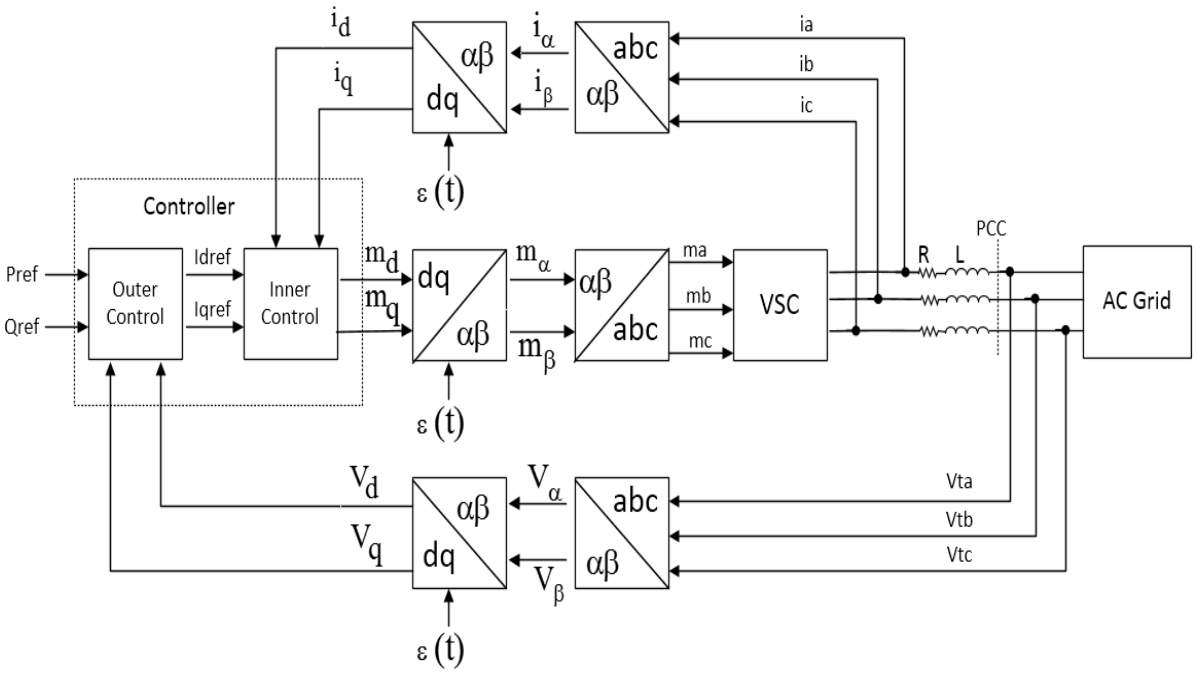

Figure 4.6: A typical three-phase control system diagram in the dq-frame.

$$V_d(t) = V_\beta(t)\sin\big(\theta(t)\big) + V_\alpha(t)\cos\big(\theta(t)\big), \tag{4.14}$$

$$V_q(t) = V_\beta(t)\cos\big(\theta(t)\big) - V_\alpha(t)\sin\big(\theta(t)\big), \tag{4.15}$$

$V_d(t)$: The voltage of the direct axis as a function of time

$V_q(t)$: The voltage of the quadrature axis as a function of time

$\theta(t)$: The phase locked loop (PLL) output angle as a function of time

Also;

$$m_\alpha(t) = m_d(t)\sin(\theta) + m_q(t)\cos(\theta), \tag{4.16}$$

$$m_\beta(t) = m_d(t)\cos(\theta) - m_q(t)\sin(\theta), \tag{4.17}$$

$m_d(t)$: The modulating signal of the direct axis as a function of time

$m_q(t)$: The modulating signal of quadrature axis as a function of time

Also, the direct conversion from abc quantities to dq reference frame is;

$$\begin{bmatrix} V_d \\ V_q \\ V_0 \end{bmatrix} = \frac{2}{3} * \begin{bmatrix} \cos(\theta) & \cos(\theta - \frac{2\pi}{3}) & \cos(\theta + \frac{2\pi}{3}) \\ -\sin(\theta) & -\sin(\theta - \frac{2\pi}{3}) & -\sin(\theta + \frac{2\pi}{3}) \\ \frac{1}{2} & \frac{1}{2} & \frac{1}{2} \end{bmatrix} * \begin{bmatrix} V_a \\ V_b \\ V_c \end{bmatrix} \quad (4.18)$$

The dq transformed voltages and currents can be used to calculate the real and reactive power using equations (4.19) and (4.20) respectively. If the converter is synchronized such that V_q equals zero then using equations (4.19) and (4.20), the real- and reactive-power components are proportional to the I_d and I_q respectively. This property is useful in the control of grid-connected three-phase VSC systems.

$$P(t) = \frac{3}{2}[V_d(t)I_d(t) + V_q(t)I_q(t)], \quad (4.19)$$

$$Q(t) = \frac{3}{2}[-V_d(t)I_q(t) + V_q(t)I_d(t)], \quad (4.20)$$

$P(t)$: The real power of the direct axis as a function of time

$Q(t)$: The reactive power of the quadrature axis as a function of time

$I_d(t)$: The current projected to the direct axis as a function of time

$I_q(t)$: The current projected to the quadrature axis as a function of time

As stated earlier, control in the $\alpha\beta$-frame reduces the number of required control loops from three to two, however, the converted signals and the feed-forward are still in sinusoidal functions of time. This poses a difficulty to have a satisfactory performance with small steady-state errors. A control design to track a 60Hz signal requires the compensators to be of higher

order to deal with the operating frequency. The bandwidths of the closed-loop control system should be large enough compared to the frequency of the reference commands.

By contrast, designing the control system in the synchronous dq-frame offers a solution to this problem, and it is often utilized in grid applications. In the synchronous dq-frame, the signals and variables are transformed to equivalent DC quantities in the steady-state. Thus, the control parameters are not at the operating frequency, and a conventional proportional-integral controller can be used in the system control scheme. This offers simpler structures with lower dynamic order for the compensators and it is more suitable representation for three-phase system for analysis and control design tasks [13] and [14].

In a grid-connected VSC system, the aim is usually to control the exchange of the real and reactive power with the power grid, and this is achieved by controlling the d- and q-axis parameters of the VSC AC-side current. In addition, large converters applied to power systems are often controlled and analyzed in the synchronous dq-frame; therefore representing VSC system in the dq-frame enables a unified framework for analysis and design of power system applications. Thus, the current-controlled VSC system modeled and controlled in dq-frame is the design that has been chosen in this thesis.

4.4. Synchronization using a Phase-Locked Loop

Designing the VSC control system in the dq-frame requires a synchronization mechanism, which can be achieved by using a phase-locked loop (PLL). The PLL synchronizes the output frequency and phase of the VSC to the frequency of the AC-side grid. This is mandatory in order to ensure the quality of the power delivered from the grid-connected VSC system to the utility grid, and guarantee its synchronization [14]. Also, the transformation to the synchronous dq reference frame requires frequency. Figure 4.7 shows a

schematic diagram of a possible PLL control system. The diagram shows the three-phase voltages are transformed to the dq-frame, and the rotational speed of the dq-frame, ω, is regulated to ensure that V_{sq} is equal to zero in the steady-state ensuring frequency and phase synchronization. Equations (4.21) and (4.22) respectively represent the direct- and quadrature-axis voltages in the PLL. Equation (4.23) represents the output of the PLL, and when the system is synchronized in the steady-state, V_d is equal to $\hat{V}_s$, and V_q is equal to zero.

$$V_d = \hat{V}_s \cos(\omega_0 t + \theta_0 - \rho(t)), \tag{4.21}$$

$$V_q = \hat{V}_s \sin(\omega_0 t + \theta_0 - \rho(t)), \tag{4.22}$$

Where;

$$\rho(t) = \omega_0 t + \theta_0, \tag{4.23}$$

$\hat{V}_s$: The peak value of the line-to-neutral voltage.

ω_0: The AC system (source) frequency.

θ_0: The initial source phase angle.

$\rho(t)$: The output of the PLL as a function of time.

In order to have a mechanism to regulate V_q to zero, a feedback loop is needed as shown in equation (4.24), where $H(P)$ is a linear transfer function (compensator), assuming a small angle approximation for $\sin(\omega_0 t)$ term, and P is a differentiation operator.

$$\omega(t) = H(P)\, V_{sq}(t)\,, \tag{4.24}$$

By substituting equation (4.22) into (4.24);

$$\omega(t) = H(P)\,\hat{V}_s \sin(\omega_0 t + \theta_0 - \rho), \qquad (4.25)$$

Thus, equation (4.25) describes a nonlinear dynamic system that is referred to as a PLL. The control output is limited by lower and upper limits of ω_{min} and ω_{max} respectively, and they are selected to be close to ω_0. In Figure 4.7, the voltage-controlled oscillator (VCO) is a resettable integrator whose output, ρ, is reset to zero every 2π radians.

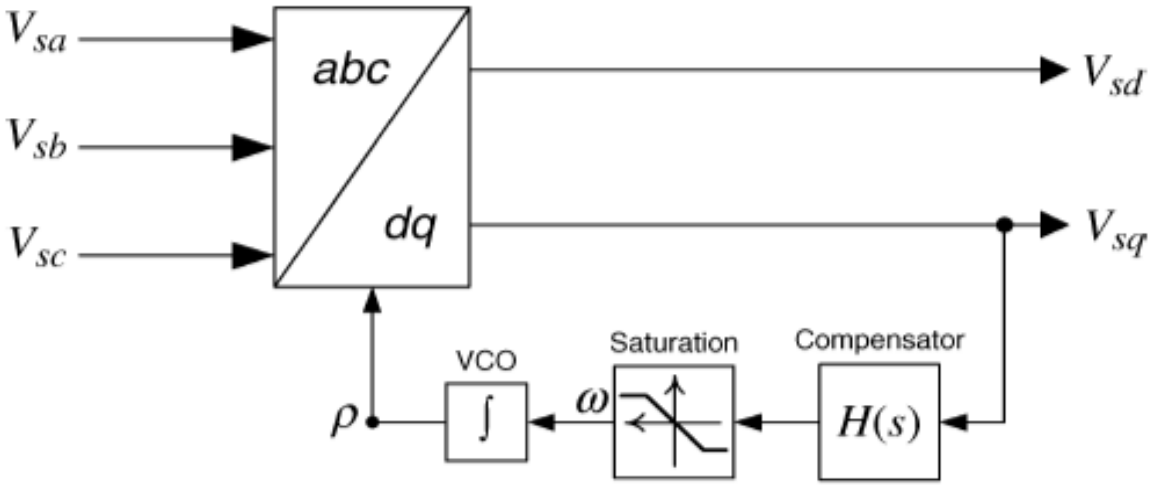

Figure 4.7: Schematic diagram of the PLL

4.5. Control Scheme

As mentioned earlier, in the grid-connected PV system the objective is often to control the power exchange from the PV generation and the utility grid. The target is to extract all generated power from the PV source. This can be achieved by using a maximum power point tracking (MPPT) strategy. The MPPT tracks the power point where the current and voltage from the PV array result in the possible maximum power, however this is out of the thesis scope. In this thesis the current-controlled real- and reactive-power controller is adopted [14], as Figure 4.8.a, and Figure 4.8.b demonstrate. Instead of using the MPPT scheme to provide the power reference, the controller is designed to have real- and reactive power reference sources as seen in both Figure 4.8.a and Figure 4.8.b. The controller is designed to have both

outer and inner controls. The outer controllers generate I_{dref} and I_{qref} which are then compared to their measured values before they enter the inner controller. The inner controller consists of a PI controller, voltage feed-forward compensator, and current decoupling compensator. Based on the reference currents, I_{dref} and I_{qref}, the inner controller is used to generate the modulating signals for both the direct- and quadrature-axis, which are m_d and m_q respectively. All the control, feed-forward, and feedback signals are DC quantities in steady-state. The PI controller can be a simple proportional-integral compensator to enable tracking of a DC reference command. The voltage feed-forward and current decoupling compensators are utilized to avoid any undesirable behavior due to transient and to decouple the VSC from the AC system dynamics. To protect the VSC, the reference currents are limited by corresponding saturation limits that are +1 and -1.

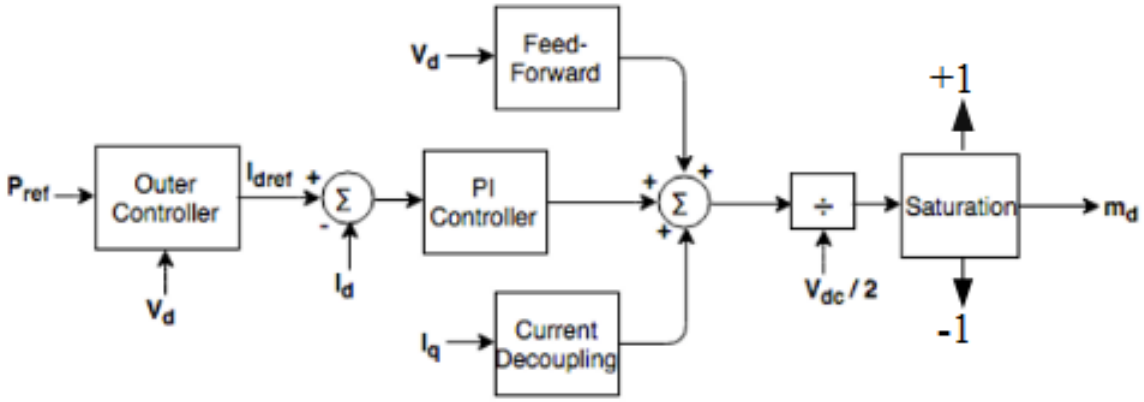

(a)

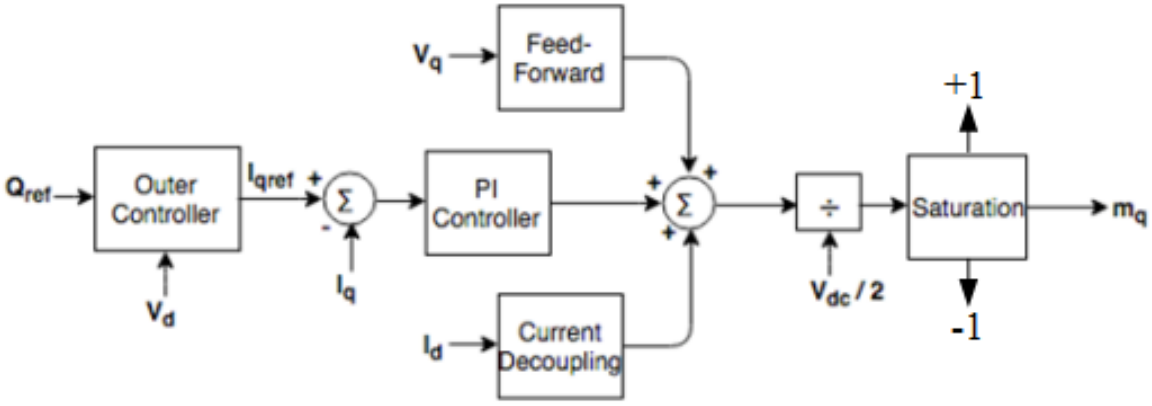

(b)

Figure 4.8: (a) block diagram of the current-controlled real-power controller and (b) block diagram of the current-controlled reactive-power controller.

Chapter 5: System Protection Challenges with Grid-Connected PV Systems

While synchronous generators are the dominant power generation in the power system by far compared to any other power source, the use of Voltage Sourced Converters (VSCs) in transmission and distribution systems is growing, as it is the core component of power conversion in the PV systems and type-3 and type 4 wind power generation, and many energy storage systems. When determining settings for protection equipment to respond to transmission system faults, utility protection engineers traditionally use impedance matrix algorithms to determine the magnitudes and angles of the fault currents in order to set the protective relays and perform coordination studies. Because VSCs limit their fault current contributions to slightly above their rated current, protection engineers used to neglect any power contributions from the PV and type 4 wind energy in their protection studies [15] and [16]. However, this has changed as more large-scale renewable power systems interface with the electric power system.

The VSC that is utilized in the interconnection of PV and type 4 wind turbine with the power system is designed as a regulated current source that has the ability to fully control its fault current injection to the grid as a self-protection from overcurrent. Therefore, it gives minimal fault current contribution above normal current, typically less than 1.2 per unit of its maximum current, and has small effect on overcurrent protection elements [16], [17], and [18]. This poses a major challenge in the power protection studies.

Another challenge is that when a fault is detected on the system and causes an under voltage condition, the VSC controller changes to a reactive current mode and supplies a

leading current to support the system voltage in order to meet grid interconnection codes as discussed in Chapter 3. In addition, the VSC controllers are manufactured to supply a balanced positive sequence current at all times with close to a unity power factor, even during a fault condition, thus it can fully transfer the real power generated to the grid [15] and [19]. These features of the VSC and its controlling nature present a hardship for protection engineers to create an accurate system model with the traditional fault programs.

5.1. Challenges

Protective devices such as relays and circuit breakers need to be connected on the transmission or distribution system in order to quickly remove and disconnect the electrical equipment or generation resources from the power system in case there is a fault condition or the power system is operating abnormally. During a system fault, the line protection relays must be reliable and perform with both dependability and security. However, due to the lack of fault current contribution and the absence of negative and zero sequence currents from the VSC and its controller, the operation of the protective relays could be impacted and they could misoperate.

5.1.1. Examples

Some examples of the misoperations that can occur in line protection schemes are:

- Due to the lack of fault current, distance protection scheme is impacted because the measured current flowing through the terminal does not exceed the current threshold to enable the element supervising the distance element. Incorporating a weak in-feed logic for a pilot protection scheme can help with this problem. Another option is to use a direct transfer trip to send a trip command from the strong terminal to the weak terminal [15], [16], and [20].

- A line current differential protection scheme can also be impacted. When it is used to protect the line between the power grid and the PV source, where there might not be enough fault current from the PV side to initiate the overcurrent relay that supervises the protection element in cases when a small number of PV modules are on-line early in the day or later in the day [15] and [21].
- Likewise when a directional protection element is used to supervise distance elements, they can misoperate because the most reliable directional elements for unbalanced faults are negative sequence directional elements. And the negative sequence directional elements are not active since, as mentioned earlier, the VSC controller does not provide much negative sequence current, thus the directional protection scheme will not be initiated and make any trip decision [15], [17], and [21]. Furthermore, in cases where the VSCs provide a leading current, to boost voltage during low voltage conditions, that can cause positive sequence directional elements to misoperate [17].

In case a circuit breaker fails to clear a fault, a breaker failure protection scheme is used to back it up and take action. This type of protection element combined with a minimal current scheme can be utilized to overcome the protection challenges associated with the lack of fault current contribution from the VSC. In addition, a direct transfer scheme can be incorporated to protect a line with a very weak in-feed by sending a trip message from the strong source to trip the circuit breaker at the weak source, yet it is not a secure method. Dual redundant communication paths should be used to increase the dependability and security of the scheme [15], [21], and [22].

5.1.2. Additional Challenges

Utilities operators might have a hard time dealing with the variable energy production from the PV system. The PV generation can rise and drop very rapidly due to a cloud cover, storms, or a sudden change in weather conditions [4]. This makes it hard to predict in advance and PV is typically not dispatchable since owners want to get maximum output power at all times, and regulatory standards support this. Thus utilities must take all of the generated power and modify other controllable generation to accommodate variations in output from renewables and fix their production curve. To do so, utilities maintain spinning reserves and quick-start natural gas generators. In some regions hydroelectric generation is used to offset variation in renewable generation output. Hence, when some utilities review project proposals for variable resources, they include additional cost for incorporating fast-response energy compensators or natural gas generators to overcome the sudden drops and rises of energy [4]. Another method that helps to mitigate the sudden production change is to scatter the PV farms over a wider geographic area. This helps to reduce the energy production variability of the entire portfolio. Furthermore, when a utility has high penetration levels of solar generation such as 10% or more [18], it might need to have a large number of flexible generators to compensate the PV energy as it decreases rapidly when the sun goes down [4].

Chapter 6: System Design and Controls Modeling

This chapter discusses the converter control and the main components of the grid-connected PV system in detail along with the ATP model. The scope of this thesis is to study the performance of different protection schemes during different grid fault conditions for the grid-connected PV system coupled through a VSC. Therefore, the main objective of this model is to design a system that can simulate an appropriate response of the system during fault conditions.

6.1. Power System Model Description

The overall model of the grid-connected PV system is illustrated in Figure 6.1, where the power system consists of five electrical subsystems. Figure 6.1 shows that a PV generation source is connected to a VSC, in order to convert the DC power to AC. A step-up transformer is used to couple the AC side of the VSC, on the collector circuit to the distribution side of the system. The generated PV power is then delivered to the grid system through the distribution line. The specifications of the different components are described in the following subsections

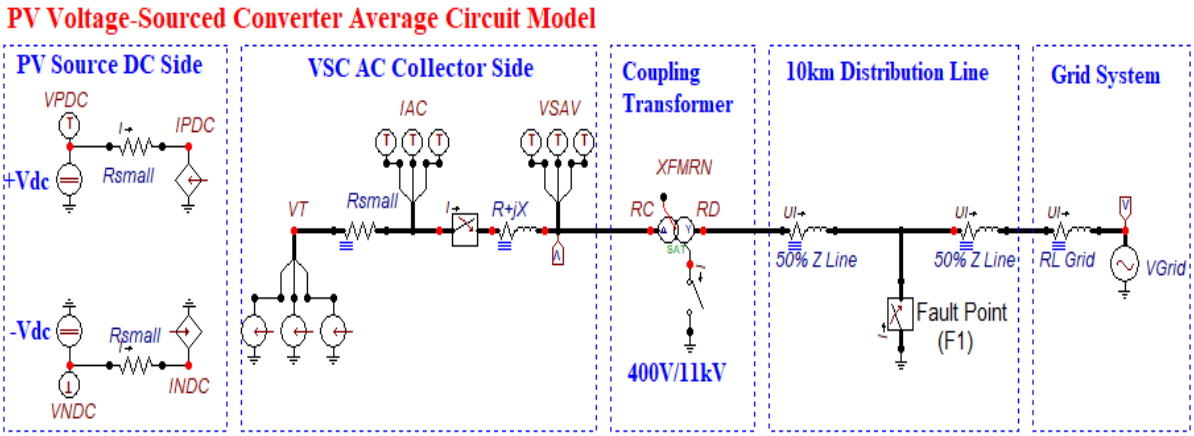

Figure 6.1: Grid-connected PV system model implemented in the ATP software.

6.1.1. PV Voltage-Sourced Converted Averaged Circuit Model

The PV source is represented by a constant 600V DC source with injected power controlled by a current-regulated power control scheme that is discussed later in this chapter. The PV source is connected to the averaged circuit model of the VSC whose AC-side terminal voltages depend on the dc PV voltage source related by the modulating signals $m_a(t)$, $m_b(t)$, and $m_c(t)$, as discussed in Chapter 4. The PV generation has a rated power of 1.5MW, and a rated current of 2,500A, whereas the VSC is sized to be 1.1 pu of the PV system ratings.

6.1.2. Coupling Transformer, Distribution Line, and Grid System Model

The transformer is a three phase and two windings step-up Delta-Y transformer modeled using the general saturable transformer type in ATP. It is used to raise the collector voltage level from 400V to 11kV, to match the distribution line voltage level. The HV-side of the transformer can be Y-grounded or Y-ungrounded for the different protection studies that are discussed in the Chapter 7. Similarly, the RC and RD in Figure 6.1 represent protection relay locations for the collector level and distribution level, respectively. The distribution line is chosen to be 10 km long, modeled with a simple RL line impedance of (0.2 + j3.762) Ω and (0.6 + j11.286) Ω for positive and zero sequence, respectively. A three phase time controlled switch is connected to the middle of the distribution line for different fault applications. The grid system is represented by a three phase Thevenin voltage of 11kV and a Thevenin impedance of (0.00588 + j0.260) Ω and (0.0176 + j0.78) Ω for positive and zero sequence, respectively.

6.2. Control System Model Description

As discussed earlier in Chapter 4, designing a grid-connected PV VSC requires a control system that assists the power exchange from the PV generation and the utility grid.

The control system is modeled in the ATP. The main parts are the decoupled double synchronous reference frame PLL (DDSRF-PLL) and the current-regulated real and reactive power control.

6.2.1. Decoupled Double Synchronous Reference Frame PLL (DDSRF-PLL) Control Model

As discussed previously, a proper synchronization mechanism is required when designing a control system for the grid-connected VSC. In the ATP model, an enhanced synchronization PLL model based on the decoupled double synchronous reference frame (DDSRF) is built. This type of PLL is suggested and described in reference [14]. The DDSRF-PLL is an enhanced version of the conventional synchronous reference frame PLL that was described in Chapter 4. The DDSRF-PLL allows the VSC controller to be accurately synchronized with the three phase grid system even under distorted and unbalanced grid operating conditions. Modelling this type of PLL is very useful and important especially when different types of unbalanced faults are applied to the distribution system and analyzed in the next chapter.

6.2.1.1. Decoupled Double Synchronous Reference Frame (DDSRF)

The DDSRF is a very helpful technique specially when dealing with three phase systems during abnormal/unbalanced operating conditions. The positive and the negative sequence components of voltage vector, V^{+1} and V^{-1}, respectively can be separated and independently controlled during system faults. This is done based on the double synchronous reference frame (DSRF) that is represented in equations (6.1) and (6.2) [14]. The same can be applied to the current by replacing the voltage quantities by current quantities.

$$v_{dq^{+1}} = \begin{bmatrix} v_{d^{+1}} \\ v_{q^{+1}} \end{bmatrix} = \left[T_{dq^{+1}}\right] * \ v_{\alpha\beta} = \ V^{+1} \begin{bmatrix} 1 \\ 0 \end{bmatrix} + \ V^{-1} \begin{bmatrix} \cos(-2\omega t) \\ \sin(-2\omega t) \end{bmatrix} \quad (6.1)$$

$$v_{dq^{-1}} = \begin{bmatrix} v_{d^{-1}} \\ v_{q^{-1}} \end{bmatrix} = \left[T_{dq^{-1}}\right] * \ v_{\alpha\beta} = \ V^{-1} \begin{bmatrix} 1 \\ 0 \end{bmatrix} + V^{+1} \begin{bmatrix} \cos(2\omega t) \\ \sin(2\omega t) \end{bmatrix} \quad (6.2)$$

Where,

$$\left[T_{dq^{+1}}\right] = \left[T_{dq^{-1}}\right]^T = \begin{bmatrix} \cos(\theta) & \sin(\theta) \\ -\sin(\theta) & \cos(\theta) \end{bmatrix} \quad (6.3)$$

The unbalanced voltage vector v expressed on the DSRF shown in the equations above consists of two of the rotating dq reference frames that were explained in Chapter 4. One is dq^{+1}, rotating with the positive speed ω and angular position θ, whereas the second one is dq^{-1}, rotating with the negative speed $-\omega$ and angular position $-\theta$. In the equations above, it was assumed that $\theta = \ \omega t$. What can be seen in equations (6.1) and (6.2) is that there is an oscillation at 2ω in the AC terms, the right side of the equations. These oscillation at 2ω is a consequence of the voltage vectors rotating in the opposite directions. In order to filter out such oscillations at 2ω, a decoupling network is used and modeled in the control system model.

6.2.1.2. Decoupling Network

A decoupling network is used to completely cancel out the effect of the double frequency oscillations generated from the DSRF on the synchronous reference frame voltage of the PLL. This allows an accurate grid synchronization even when the grid system is under unbalanced faults [23]. The decoupling network that is shown in Figure 6.2 is used to filter out the effects of the negative sequence voltage V^{-1} on the dq^{+1} frame signals. Figure 6.3 shows the same decoupling network implemented in ATP. To cancel out the oscillations in

the dq^{-1} frame signals, the same decoupling network can be used, but with swapping the -1 and +1 indexes in the figure. The $V_{d^{+1*}}$ and $V_{d^{-1*}}$ in Figure 6.2 are the voltage vector expressed on the dq^{+1} frame after filtering out the oscillations at 2ω. Similarly, the $V_{d^{-1**}}$ and $V_{q^{-1**}}$ terms are from another decoupling network for cancelling the effect of V^{+1}on the dq^{-1} frame signals. In addition, the signals go through a low pass filter, which will be discussed later in this chapter. As shown in the decoupling network in Figure 6.2, the angular position θ of the dq reference frame is the same as the PLL angle that is controlled by a feedback loop to regulate the q component to zero. The same decoupling network structure is used for the current quantities.

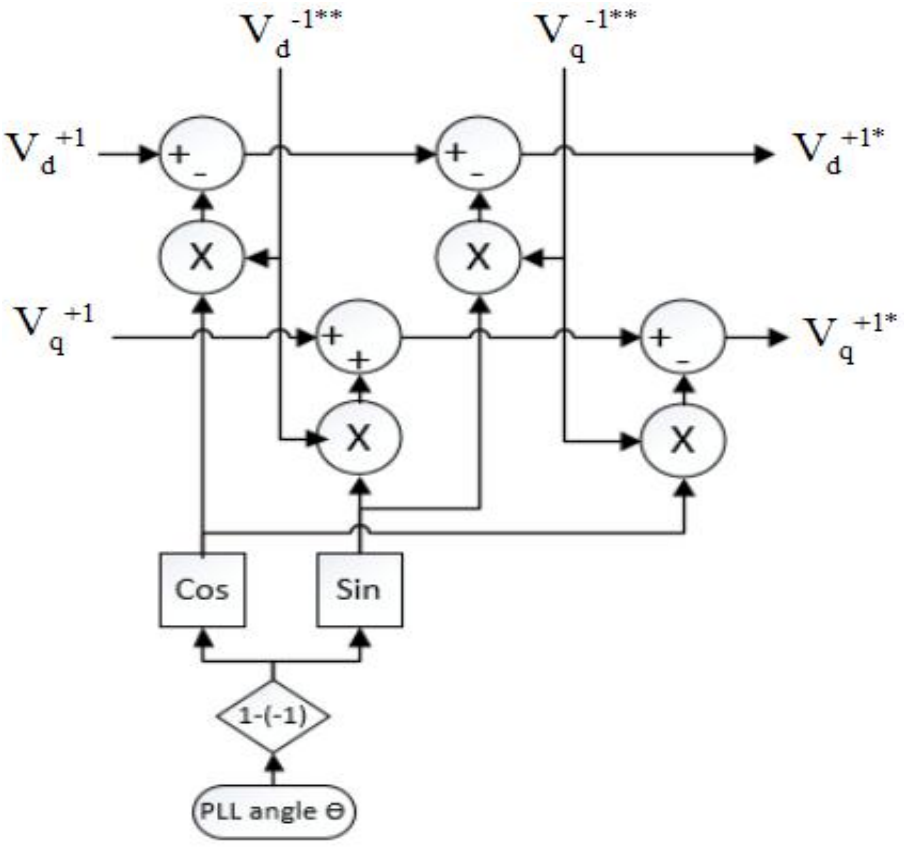

Figure 6.2: Decoupling network for eliminating the effect of V^{-1} on the dq^{+1} frame signals

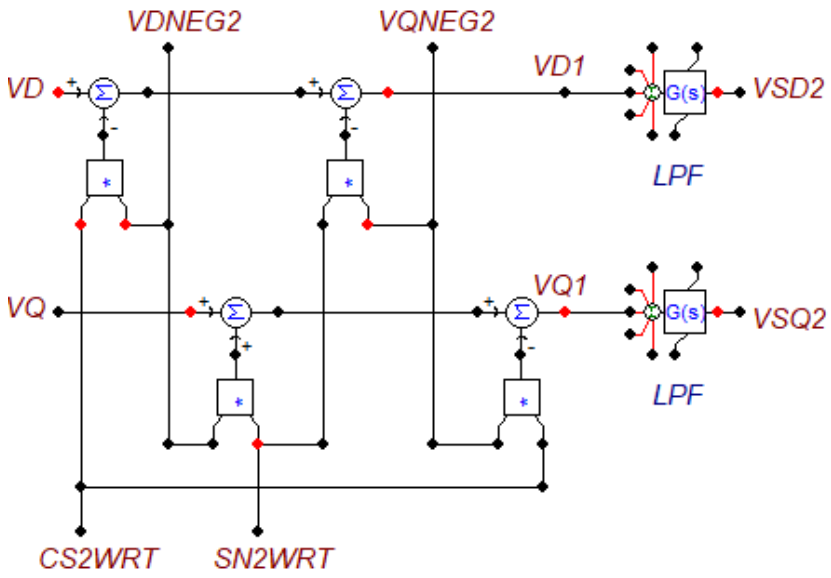

Figure 6.3: Decoupling network model implemented in ATP for cancelling the effect of V^{-1} on the dq^{+1} frame signals plus a low pass filter.

6.2.1.3. Structure of the DDSRF-PLL

The control scheme of the DDSRF-PLL that is shown in Figure 6.4 is an enhanced three-phase synchronous PLL based on using two synchronous reference frames. It completely cancels out the effects of the negative sequence components of the inputs on the positive sequence controller and the effects of the positive sequence components of the inputs on the negative sequence controller. Thus the real amplitude of the unbalanced input voltage sequence components is accurately detected. This makes it a useful tool for the current-regulated real and reactive power controller during unbalanced grid faults.

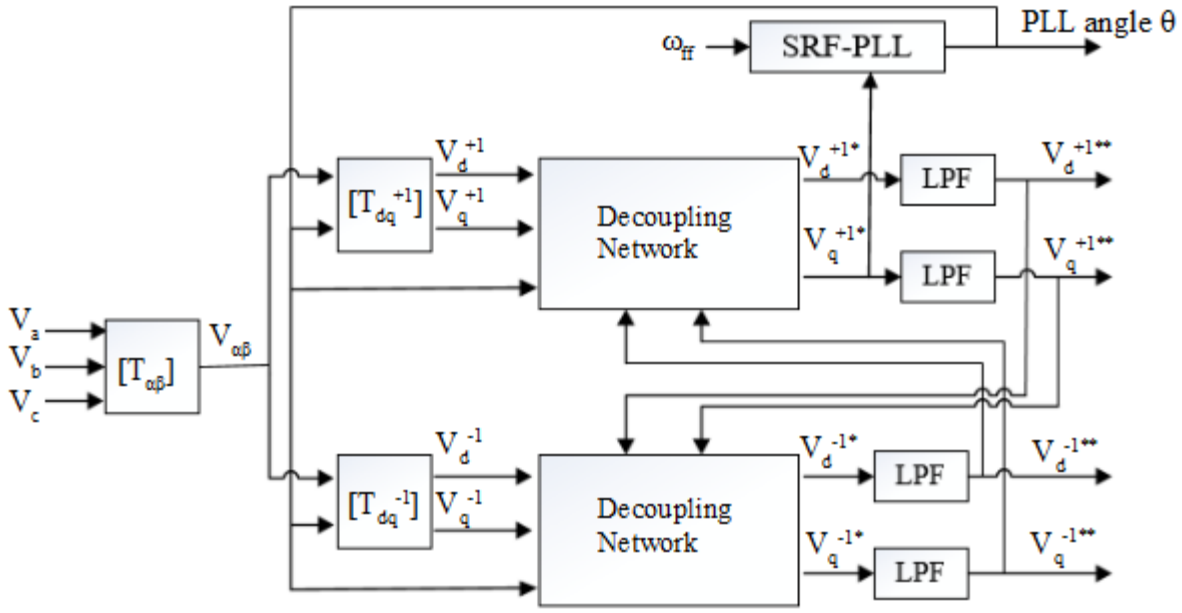

Figure 6.4: Structure of the decoupled double synchronous reference frame PLL (DDSRF-PLL) control scheme.

Figure 6.4 shows that the measured three-phase voltages at the collector side, V_a, V_b, and V_c (VSAV in Figure 6.1), are transformed to $V_{dq^{+1}}$ and $V_{dq^{-1}}$ by using equations (6.1) and (6.2). Then they enter the decoupling network together with the PLL angle θ to filter out the oscillations at 2ω. As a final filtering stage, the outputs of the decoupling network go through a low pass filter (LPF) to largely remove any remaining undesirable oscillations. Equation (6.4) shows the low pass filter, where its cut-off frequency is $\omega_f = \omega/\sqrt{2}\ rad/s$ [23]. The frequency ω in this case is the nominal fundamental frequency of the grid. The outputs of the low pass filters, $V_{d^{+1**}}$, $V_{q^{+1**}}$, $V_{d^{-1**}}$, and $V_{q^{-1**}}$, are the corrected voltage quantities from the DDSRF-PLL, and they are used as a feedback for the decoupling networks. The PLL that is shown in the figure is the same as the conventional synchronous reference frame PLL that was discussed in Chapter 4. The phase-angle error signal, $V_{q^{+1*}}$, is used as a feedback to the PLL in order to obtain a similar dynamic response for different voltage amplitudes in the grid.

In addition, the ω_{ff} in the PLL is the rated frequency of the grid and is used as a feed-forward parameter to expedite the process of the PLL.

$$LPF(s) = \frac{\omega_f}{s+\omega_f} \tag{6.4}$$

6.2.2. Current-regulated Real and Reactive Power Control Model

The current-regulated real and reactive power control that is used in this system is almost the same as was presented in Chapter 4. However, in this system the control scheme is based on the DDSRF method in order to make both the positive sequence and negative sequence current reference frames independent from each other. Thus, the same structure control of the DDSRF that is shown in Figure 6.4, excluding the PLL block diagram, has been applied to the measured currents, I_a, I_b, and I_c (IAC in Figure 6.1), in order to generate $I_{d^{+1**}}$, $I_{q^{+1**}}$, $I_{d^{-1**}}$, and $I_{q^{-1**}}$. Clearly, the oscillations at the 2ω on the synchronous reference frames should be filtered out in order to reach full control of the injected currents during unbalanced conditions [14].

Figure 6.5.a and Figure 6.5.b show the positive sequence current-regulated real and reactive power control schemes that are modeled in ATP. Likewise, Figure 6.6.a and Figure 6.6.b show the control schemes for the negative sequence current. In Figure 6.5.a, and Figure 6.5.b, the controller is built to have its real and reactive power reference values. The positive sequence real power reference is set to the PV rated power generation of 1.5MW, and both the positive and negative sequence reactive power references are set to zero. Then in the outer controller, the power references are divided by the $V_{d^{+1**}}$ to generate positive sequence I_{dref} and I_{qref} respectively. As mentioned previously, the rated current of the PV generation is 2,500A, and the VSC is rated at 110% of the PV system ratings. Therefore, in the current

regulator a 1.1 pu limiter is used to protect the VSC and limit the current delivered to the grid in order not to exceed the current limits of the power converter. However, in the negative sequence control schemes that are shown in Figure 6.6.a and Figure 6.6.b, the current references are set to zero such that the VSC produces only positive sequence current. Each of the reference currents, I_{dref}, I_{qref}, I_{dneg_ref}, and I_{qneg_ref} are then compared to their measured values before they enter the inner controller. Based on the reference currents, the inner controllers generate the modulating signals, m_d, m_q, m_{dneg}, and m_{qneg} for the dq reference frames for the positive and negative sequences. The dq modulating signals can be then transformed back to the three-phase modulating signals, m_a, m_b, and m_c, discussed in Chapter 4. The PI controller values, voltage feed-forward compensator and current decoupling compensator terms are calculated and shown in Appendix (C). The voltage feed-forward controller is used to stabilize the controller when there is a change in voltage. It also helps to smooth and speed the response of the controller when the VSC is starting up. The current decoupling controller is used to fully decouple the d-q axes controllers. In addition, the modulating signals are limited to +1 and -1 in order to prevent over-modulation and limit harmonics, as they regulate the current set points.

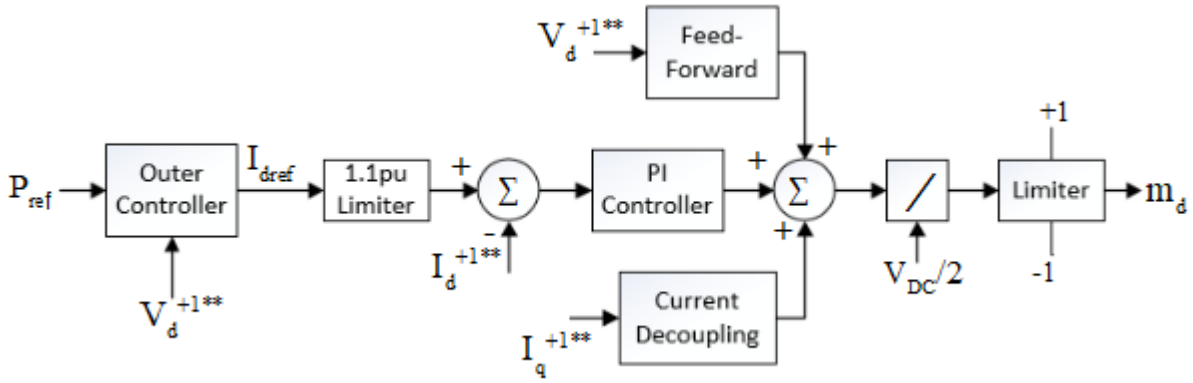

(a)

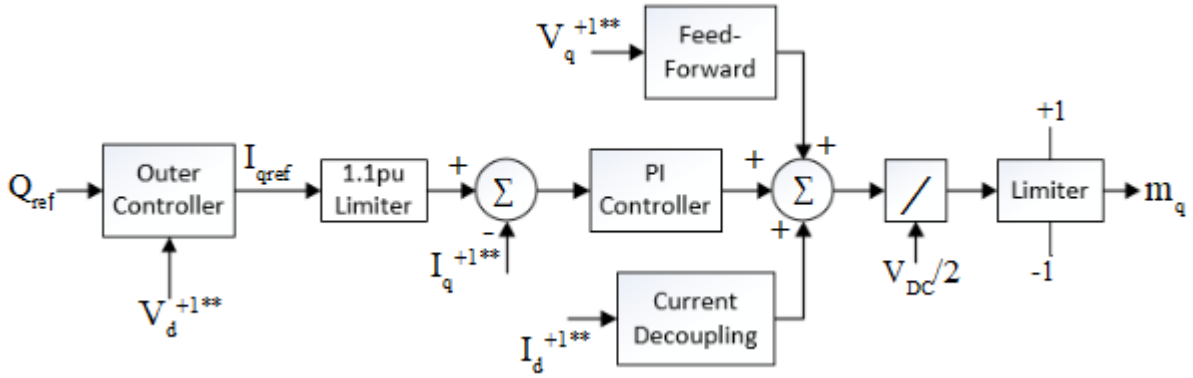

(b)

Figure 6.5: (a) positive sequence $I_{d^{+1**}}$, current-regulated real-power controller scheme and (b) positive sequence $I_{q^{+1**}}$, current-regulated reactive-power controller scheme.

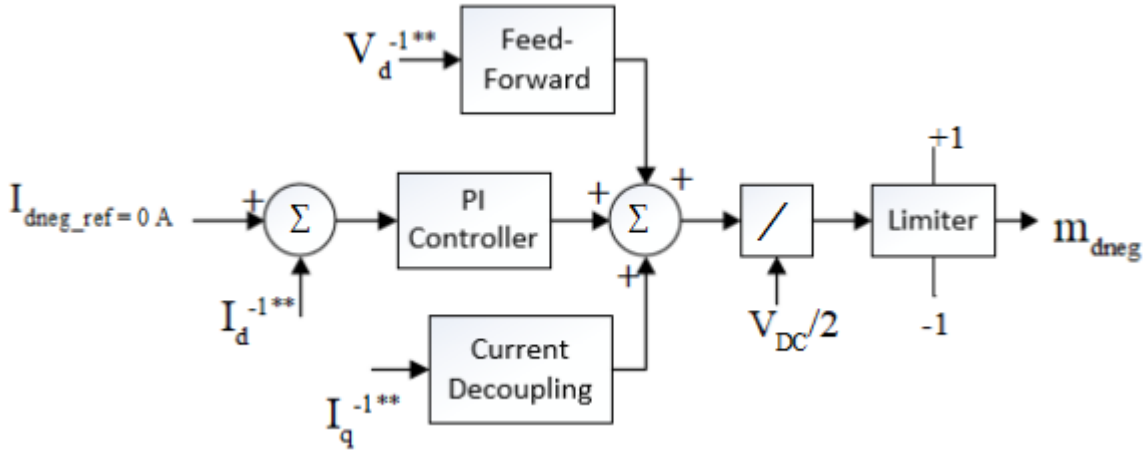

(a)

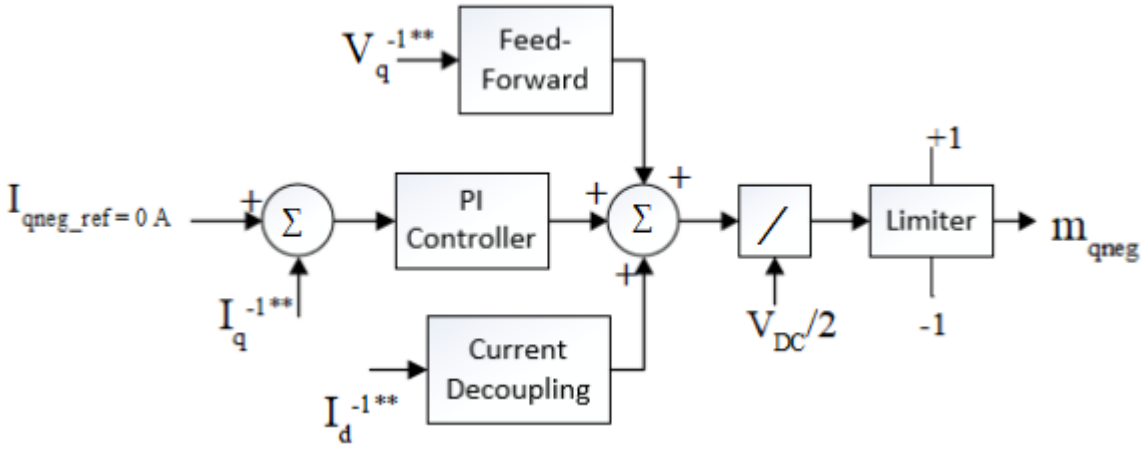

(b)

Figure 6.6: (a) negative sequence d reference $I_{d^{-1**}}$, current-regulated control scheme and (b) negative sequence q reference $I_{q^{-1**}}$, current-regulated controller scheme.

Chapter 7: System Simulation Results and Protection Performance

This chapter discusses the results from the simulation of the Grid-connected PV system modeled in the ATP software, and the impact of the PV on the performance of the associated protection elements. Distance and inverse-time overcurrent protection relay models are implemented using Mathcad software. COMTRADE files containing the measured voltages and currents for different case studies are recorded from the ATP simulation results are then replayed in the relay models.

7.1. Case Studies:

Case studies have been performed at both the collector system level and the distribution level. At the distribution level, distance protection performance is studied, whereas for the collector level, the performance of inverse time overcurrent protection elements is studied. In the study, it's assumed that the PV source is supplying rated power of 1.5MW at $600V_{DC}$, with a rated current of 2500A.

Figure 7.1 shows a one-line diagram of the grid-connected PV system under study. Two types of faults are applied to the middle of the distribution line at the fault point, F1. First, studies with SLG faults are performed, then with DLG faults applied.

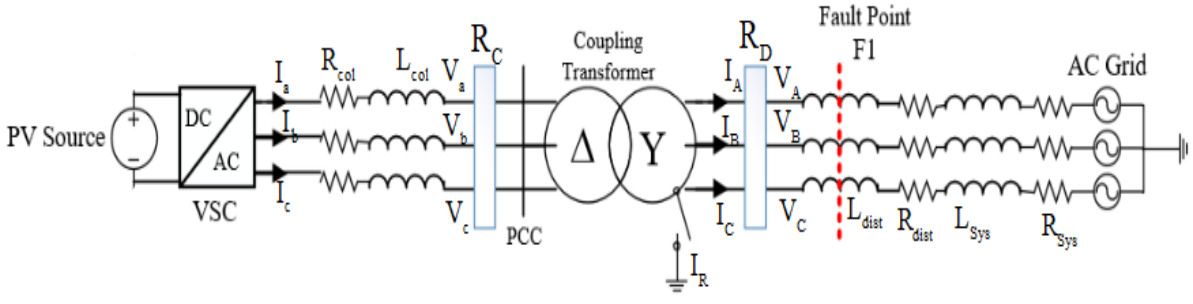

Figure 7.1: Simplified three-phase grid-connected PV system model.

7.2. Distribution Line Protection Study

The following protection relays are used for the distribution line protection study:

1- Instantaneous overcurrent protection scheme (ANSI/IEEE Type 50)

2- Distance protection scheme (ANSI/IEEE Type 21)

It is worth mentioning that the distance protection element is not normally used for the 11kV line. However, it is used here as an option to improve the protection performance since the overcurrent protection elements have limitations as it will be shown later in this chapter.

7.2.1. Instantaneous Overcurrent Element (50)

The instantaneous overcurrent element can be used to detect a fault when the measured current at the relay exceeds a set pickup value. The element has two levels of protection. Level 1 is the primary zone of protection, where the relay trips instantaneously when there is a fault. Level 2 is used as a backup zone for the relay. For the phase overcurrent element (50P), the minimum pickup value is set to be 1.5 pu of the maximum load current. The ground overcurrent element (50G) is set higher than the minimum unbalanced load current value, here 0.5 pu is chosen for the minimum pickup value. The minimum pickup values are based on the IEEE standard recommendation. In this study, the instantaneous overcurrent element is used as a supervisory protection element to supervise the distance protection element.

7.2.2. Distance Protection Element (21)

The distance element is used to protect the distribution line by performing a magnitude comparison between signals derived from the voltages and currents measured at the

distribution relay, R_D, in Figure 7.1, and the relay operating characteristics. Equation (7.1) shows the calculation of effective impendence measured by R_D.

$$\bar{Z}_{RD} = \frac{\bar{V}_{RD}}{\bar{I}_{RD}} \tag{7.1}$$

Where, $\bar{V}_{RD}$ is the voltage input signal measured at R_D,

$\bar{I}_{RD}$ is the current input signal measured at R_D.

During the normal operation, the effective impedance $\bar{Z}_{RD}$ is associated with the load flow in the distribution line. During a fault on the distribution line at the fault point F1 in Figure 7.1, $\bar{I}_{RD}$ increases and $\bar{V}_{RD}$ decreases, thus $\bar{Z}_{RD}$ in equation (7.1) goes below the predetermined set value, indicating a fault. The measured voltage at $\bar{V}_{RD}$ depends on the impedance between $\bar{V}_{RD}$ and the location of the fault, which can be mapped to distance. If the measured voltage at $\bar{V}_{RD}$ is smaller that means the fault is closer, and vice versa if it is further. Table 7.1 shows the voltage and current input signals used for $\bar{V}_{RD}$ and $\bar{I}_{RD}$ to the common phase and ground distance elements.

Table 7.1: Voltage and current input signals to the phase and ground distance elements [20].

Distance Elements		Voltage ($\bar{V}_{RD}$)	Current ($\bar{I}_{RD}$)
Phase Elements	AB	$\overline{V_A} - \overline{V_B}$	$\overline{I_A} - \overline{I_B}$
	BC	$\overline{V_B} - \overline{V_C}$	$\overline{I_B} - \overline{I_C}$
	CA	$\overline{V_C} - \overline{V_A}$	$\overline{I_C} - \overline{I_A}$
Ground Elements	AG	$\overline{V_A}$	$\overline{I_A} + \overline{k_0} * \overline{I_R}$
	BG	$\overline{V_B}$	$\overline{I_B} + \overline{k_0} * \overline{I_R}$
	CG	$\overline{V_C}$	$\overline{I_C} + \overline{k_0} * \overline{I_R}$

Where,

$\bar{V}_A, \bar{V}_B, \bar{V}_C$ are the measured phase to ground voltages at R_D,

$\bar{I}_A, \bar{I}_B, \bar{I}_C$ are the measured phase currents at R_D,

$\bar{I}_R = \bar{I}_A + \bar{I}_B + \bar{I}_C$ is the residual/neutral current,

$\bar{k}_0$ is a zero sequence correction factor for the ground distance element calculations [20].

The ground distance element requires the phase currents to be compensated for the zero sequence voltage drop by using the residual current $\bar{I}_R$ multiplied the factor $\bar{k}_0$, that is shown in equation (7.2)

$$\bar{k}_0 = \frac{\bar{Z}_{0L} - \bar{Z}_{1L}}{3 * \bar{Z}_{1L}} \tag{7.2}$$

where, $\bar{Z}_{1L}$ is the line positive sequence impedance,

$\bar{Z}_{0L}$ is the line zero sequence impedance.

In the distance element – mho type, a complex impedance plane, or R-X plane, is used to analyze the distance element operation. A representation of the impedance plane is shown in Figure 7.2, along with distance element protection zones, zone 1 and zone 2, and a representation of the line impedance. Zone-1 threshold is set to 80% of the line impedance, whereas Zone-2 threshold is set to 120%.

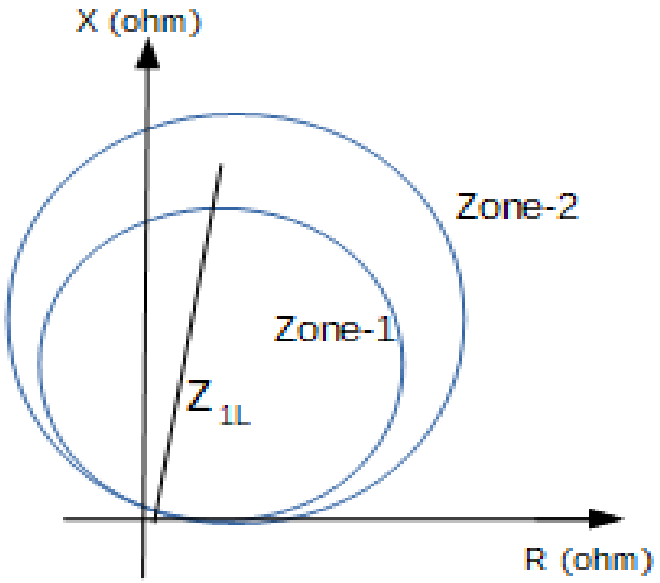

Figure 7.2: Static distance element Mho characteristics impedance plane.

Figure 7.3 shows both phase current and line to ground voltage waveforms on the distribution line during normal condition scaled by the CT and PT ratios. The ATP system model was simulated for a period of two seconds, however in the Mathcad relay model, the waveforms are scaled to cycles. The horizontal axis in Figure 7.3 is in the number of cycles. The vertical axis for both Figure 7.3.a and Figure 7.3.b are current (A) and voltage (V), respectively.

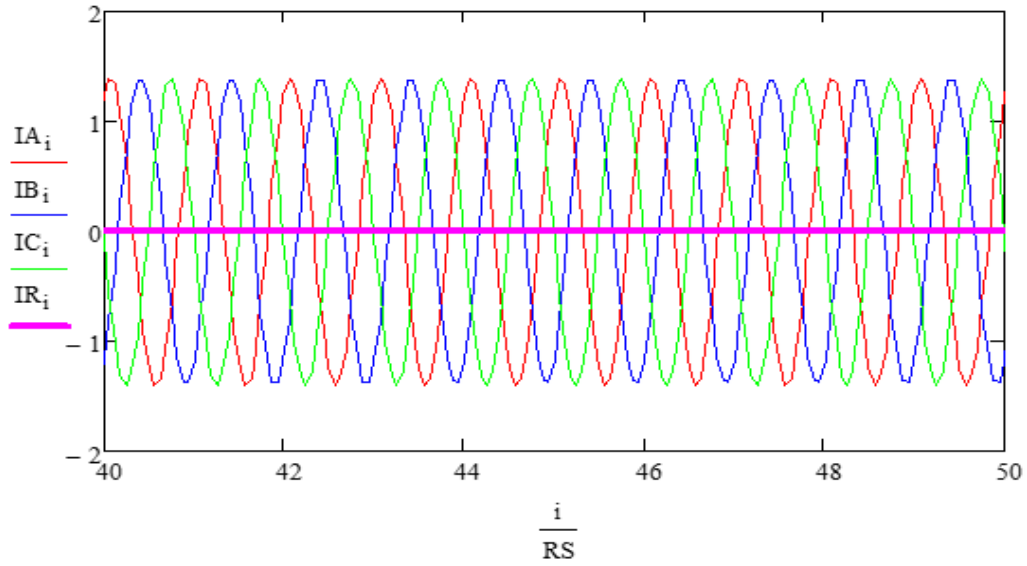

(a)

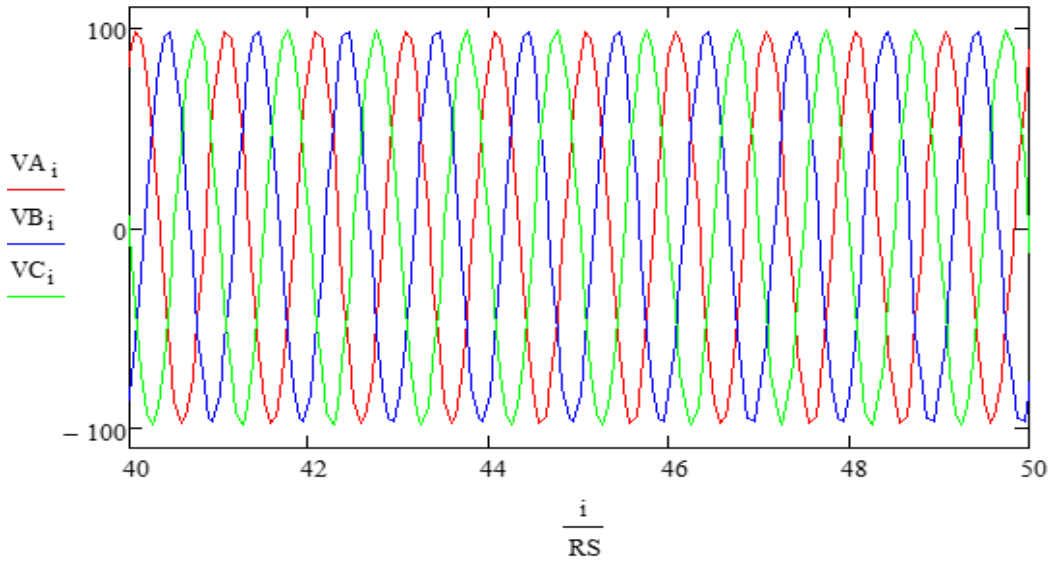

(b)

Figure 7.3: (a) phase current and (b) line to ground voltage waveforms on the distribution line during normal condition scaled by the CT and PT ratios.

The distribution level CT and PT ratios are set as shown in equations (7.3) and (7.4).

$$CTR = \frac{65A}{1A} \tag{7.3}$$

$$PTR = \frac{7.8kV}{69.5V} \tag{7.4}$$

In the system shown in Figure 7.1, the normal phase current and voltage values measured at the distribution relay R_D are 91A peak and 11kV peak respectively, whereas the residual current $\bar{I}_R$ is equal to zero since the system is balanced.

7.2.3. Case A: Delta-Y transformer

A SLG, AG, fault is applied at the 60th cycle, which evolves to an ABG at the 72nd cycle, as shown in Figure 7.4. The RMS current and voltage values are shown in Table 7.2 for the three operating states.

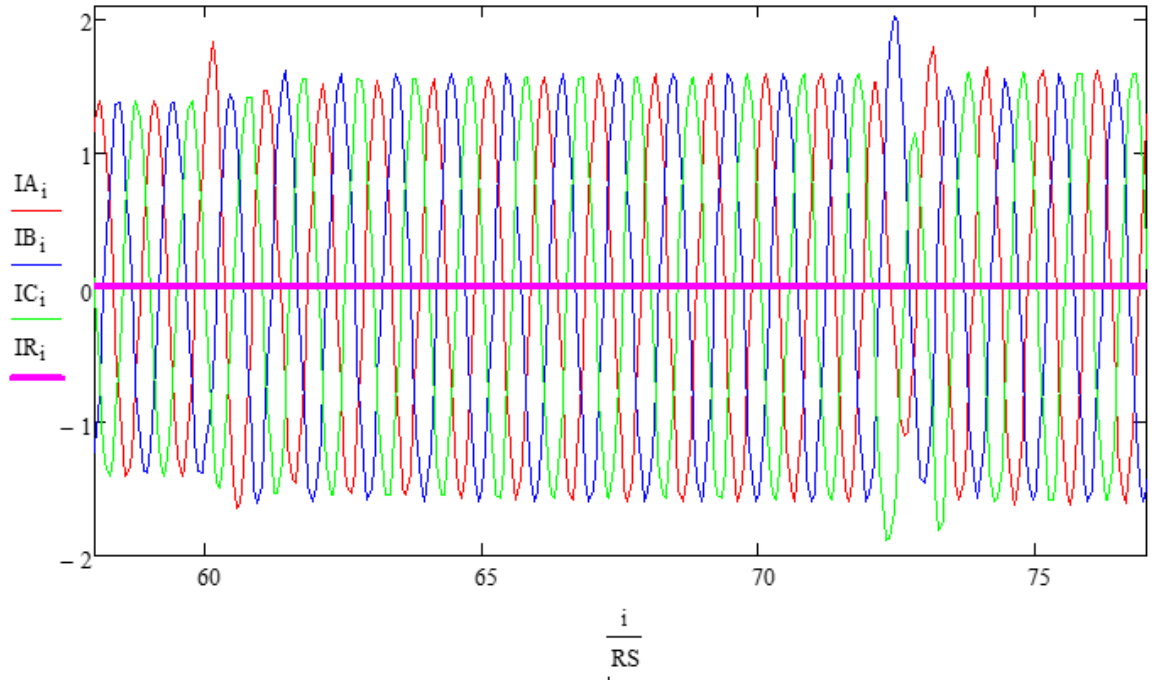

(a)

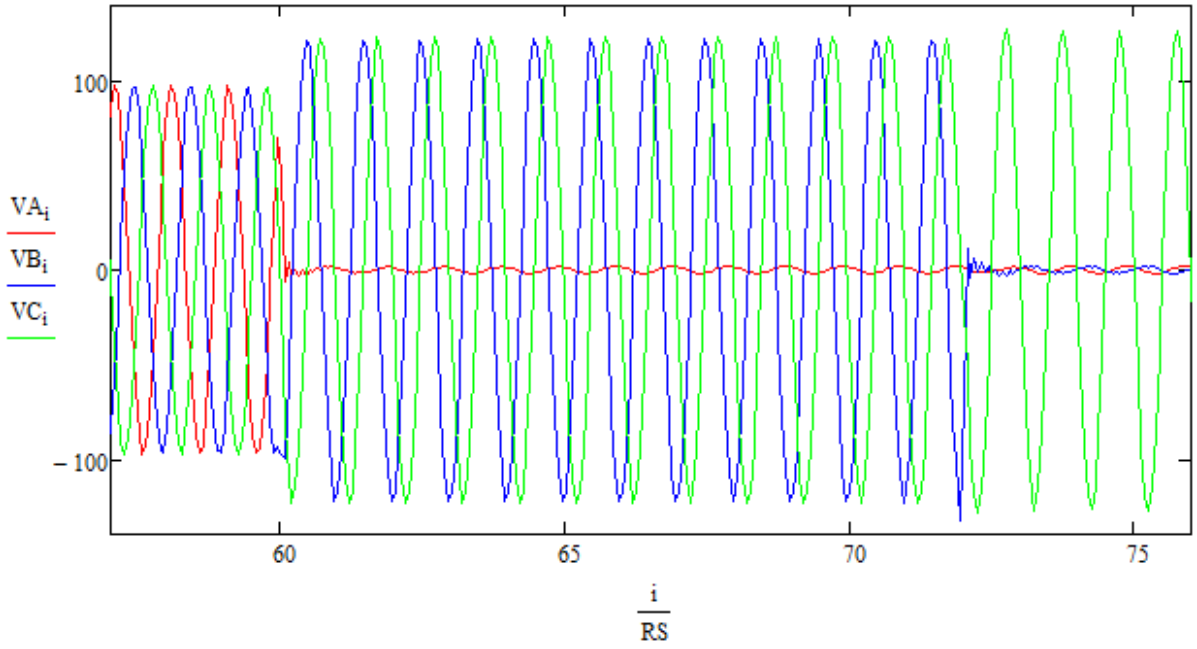

(b)

Figure 7.4: (a) phase current and (b) line to ground voltage waveforms on the distribution line during normal, SLG, and DLG conditions, respectively, for the Delta-Y transformer case study.

Table 7.2: Measured primary current and voltage values at R_D for normal, SLG, and DLG conditions, respectively, for Delta-Y transformer case study.

	Normal	SLG (AG)	DLG (AB)
IA	91.18A	102.83A	103.38A
IB	91A	103.53A	103.76A
IC	91.41A	102.51A	102.49A
VA	10.99kV	199V	203V
VB	10.86kV	13.71kV	222.2V
VC	11kv	13.87kV	14.246kV
IR	0A	0A	0A

By using the symmetrical component transformation in equation (7.5) to the digitally filtered currents, the sequence current magnitudes with a phase A reference can be plotted as shown in Figure 7.5.

$$\begin{bmatrix} IA0 \\ IA1 \\ IA2 \end{bmatrix} = \frac{1}{3} * \begin{bmatrix} 1 & 1 & 1 \\ 1 & a & a^2 \\ 1 & a^2 & a \end{bmatrix} * \begin{bmatrix} IA \\ IB \\ IC \end{bmatrix} \quad (7.5)$$

Where, a = 1∠120deg.

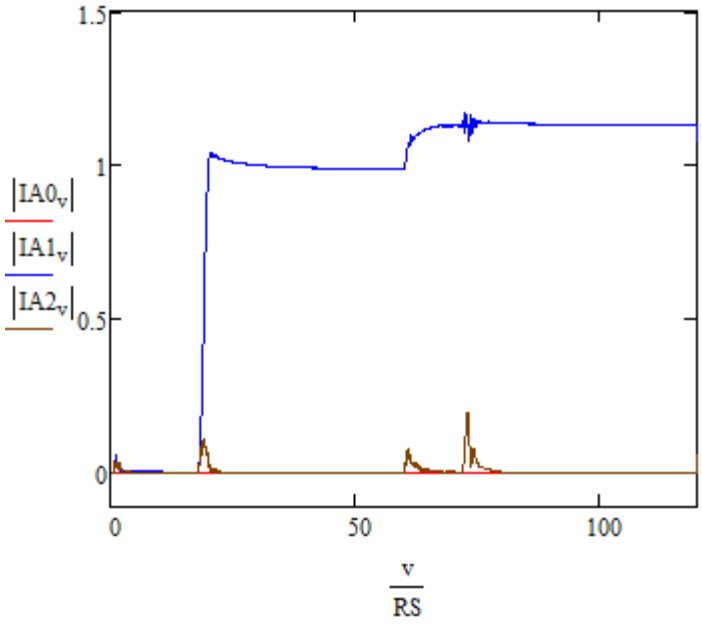

Figure 7.5: Sequence current magnitude waveforms of phase A during normal, SLG, and DLG fault conditions, for the Delta-Y transformer case study.

As shown in Figure 7.5, the positive sequence current magnitude of phase A during the three operating conditions is 1 pu, 1.128 pu, and 1.134 pu, respectively. As discussed in Chapter 4, the challenge with the grid-connected PV system is that the VSC controllers limit the fault current to 1.1 to 1.2 pu to protect the VSC devices from overcurrent. Figure 7.5 shows both the negative and zero sequence currents are largely absent even for the unbalanced fault conditions.

7.2.3.1. Instantaneous Overcurrent Element Response

Figure 7.6 shows the response of the instantaneous overcurrent relay in the Mathcad relay model, described in detail in Appendix (A). The phase overcurrent element (50P) did not trip because the phase currents, shown in Table 7.2 did not exceed the relay pickup value. Also, the ground overcurrent element (50G) did not trip since the zero sequence is equal to zero.

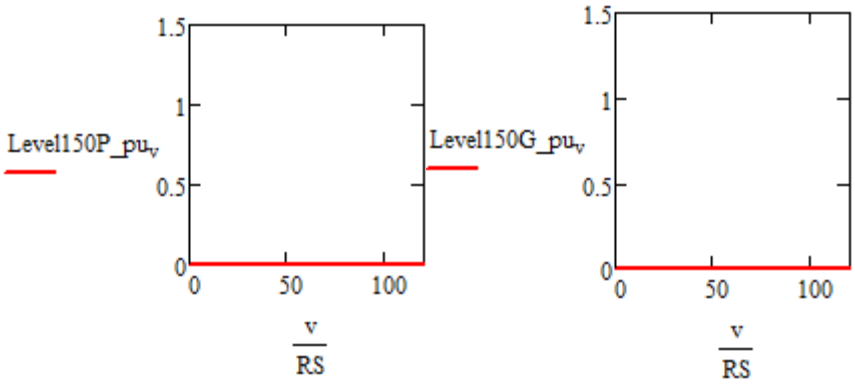

Figure 7.6: Phase and ground instantaneous overcurrent relay response of the system for the Delta-Y transformer case.

7.2.3.2. Distance Relay Response

As shown in Figure 7.7 (b), the ground distance element has picked up the SLG fault at the 60th cycle. Similarly, Figure 7.8 (b) shows that the phase distance element detected the DLG fault at the 72nd cycle, since $\bar{Z}_{RD}$, in equation (7.1) has become lower than the threshold value. What can be observed from the mho characteristics in both Figures 7.7 (a), and 7.8 (a), is that both types of faults were applied to the middle 50% of the distribution line. However, the mho plots show the effective location of the faults seen by the relay is about 30% of the distribution line, closer toward the PCC. The reason is that because the PV source is very weak compared to the grid system source, as well as the limited current contribution from the VSC. Thus, the measured voltage, $\bar{V}_{RD}$ at the distribution relay R_D in Figure 7.1, will experience too much drop, and is almost the same as the voltage at the fault point F1.

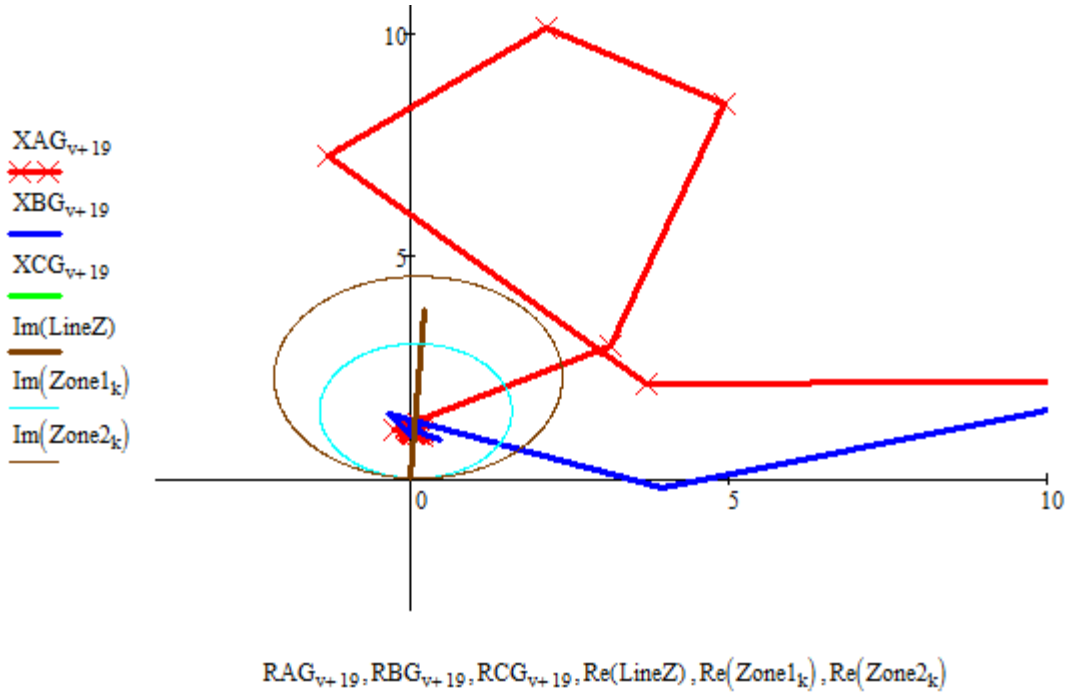

(a)

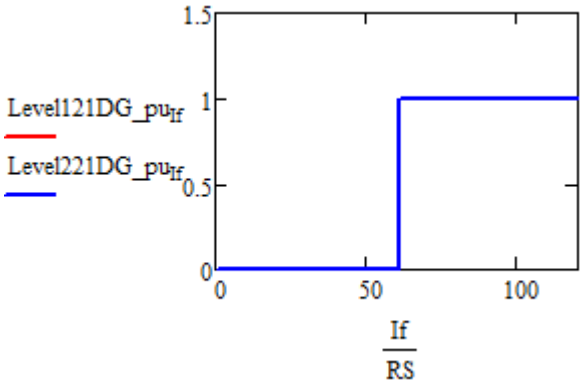

(b)

Figure 7.7: (a) Mho characteristic plot and (b) ground distance element response to SLG and DLG, for the Delta-Y transformer case.

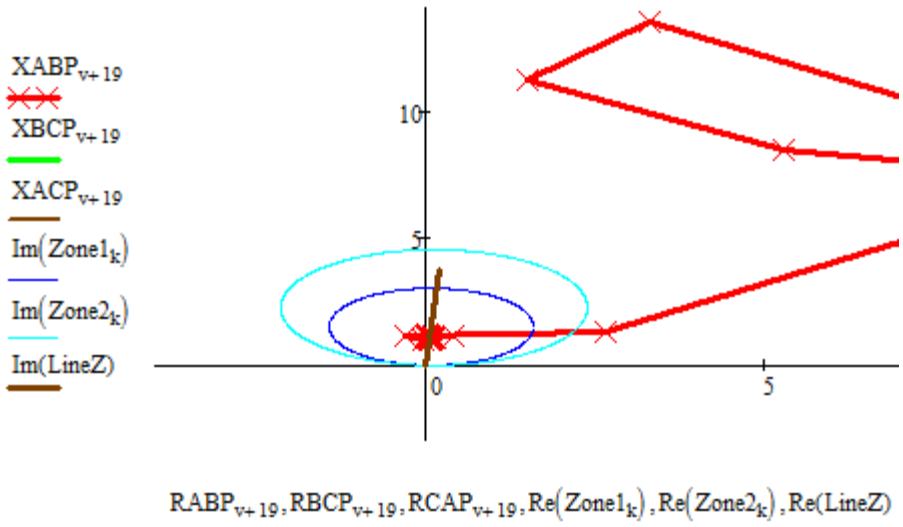

(a)

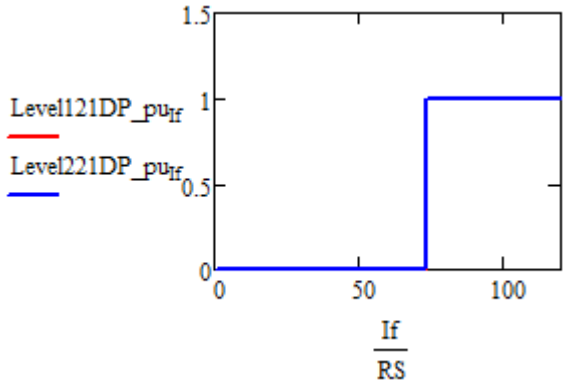

(b)

Figure 7.8: (a) Mho characteristic plot and (b) phase distance element response to SLG and DLG, for the Delta-Y transformer case.

Based on the trip logic diagram shown in Figure 7.9, the distance element that is supervised by an instantaneous overcurrent element did not trip for the faults, as shown in Figure 7.10. Even though both the phase and ground distance element picked up the fault, the supervisory instantaneous overcurrent element did not, as shown in Figure 7.6.

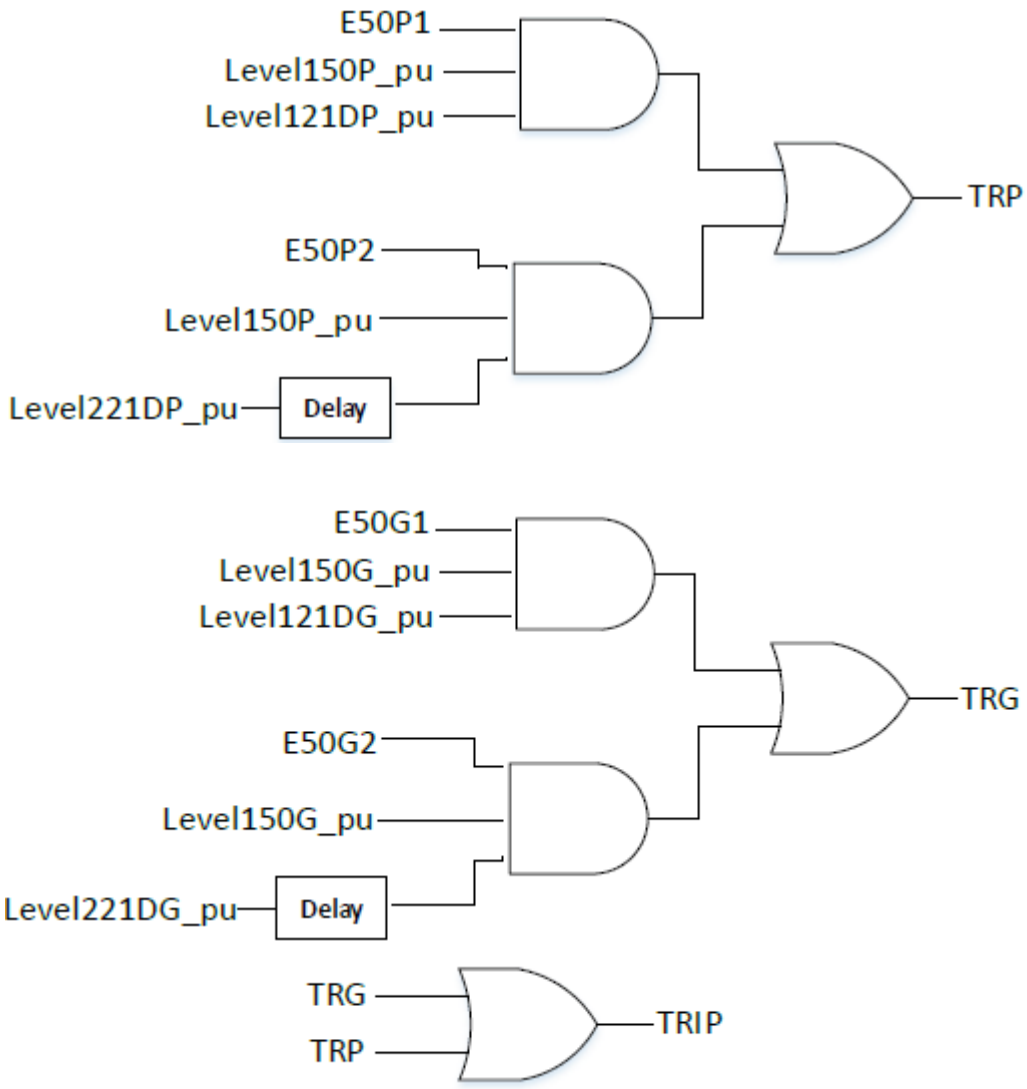

Figure 7.9: Trip logic diagram of the distance protection scheme supervised by an instantaneous overcurrent elements, phase and ground elements.

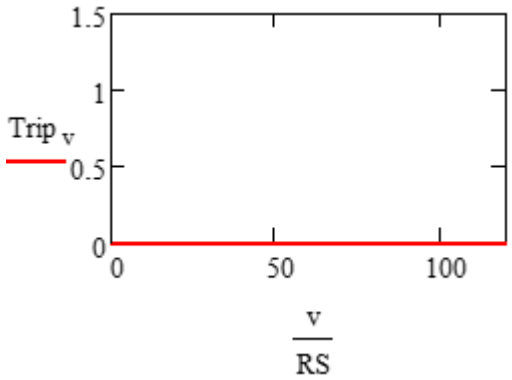

Figure 7.10: Supervised distance relay trip logic response for the Delta-Y transformer case.

7.2.4. Case B: Delta-Y-Grounded transformer

Figure 7.11 shows the same types of faults were applied to the system, this time the Y-side, HV-side, of the transformer is solidly grounded. Both current and voltage values are shown in Table 7.3 for the three operating conditions.

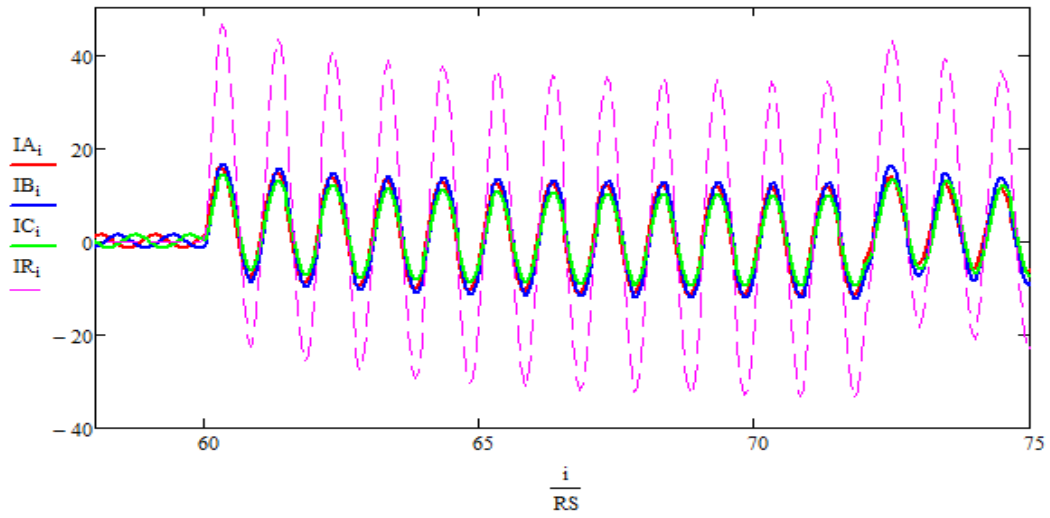

(a)

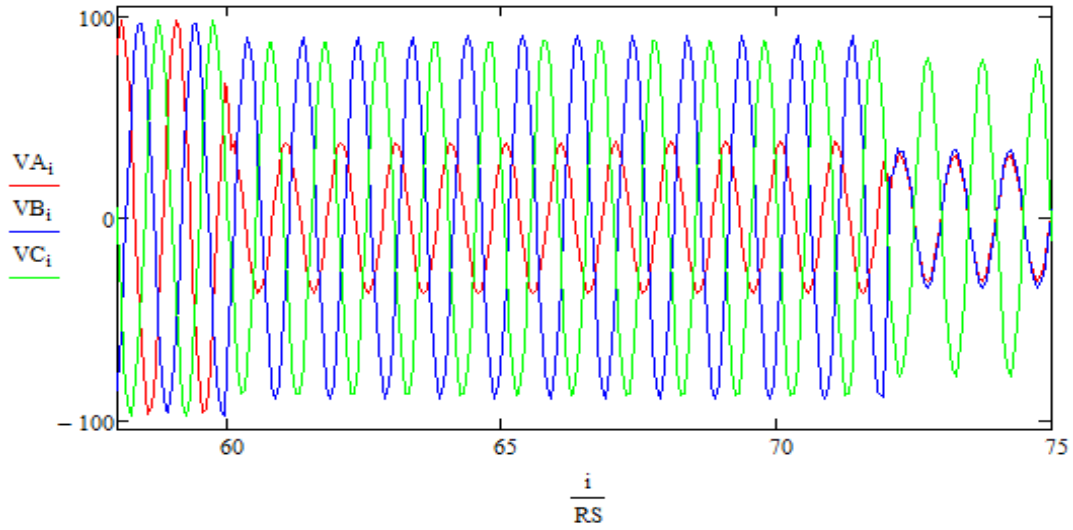

(b)

Figure 7.11: (a) Phase current and (b) line to ground voltage waveforms on the distribution line during normal, SLG, and DLG conditions, respectively, for the Delta-Y-grounded transformer case study.

Table 7.3: Measured primary current and voltage values for normal, SLG, and DLG conditions, respectively, for the Delta-Y-grounded transformer case study.

	Normal	SLG (AG)	DLG (AB)
IA	90.53A	830A	653A
IB	89.94A	864A	825A
IC	90.68A	695A	685A
VA	11kV	4.22kV	3.53kV
VB	10.84kV	10.12kV	3.84kV
VC	11kv	9.83kV	8.92kV
IR	0A	2.56kA	2.18kA

Similarly, by using the symmetrical component transformation in equation (7.5), the sequence current magnitudes with a phase A reference can be plotted as shown in Figure 7.12.

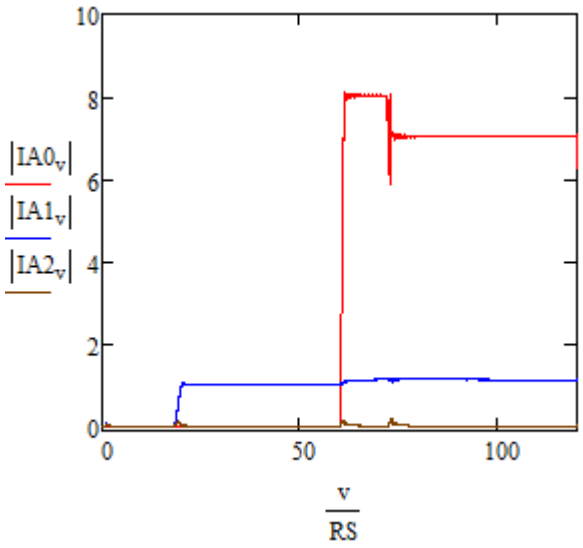

Figure 7.12: Sequence current magnitude waveforms of phase A during normal, SLG, and DLG fault conditions, for the Delta-Y-grounded transformer case study.

As shown in Figure 7.12, the positive sequence current magnitude of phase A during the three operating conditions is 1 pu, 1.127 pu, and 1.13 pu, respectively. Again, the VSC controllers limit the fault current to less than 1.2 pu to protect the VSC from overcurrent. The negative sequence is zero since the VSC injects only positive sequence current. The zero sequence current however is quite high, 8 pu and 7 pu, for SLG and DLG, respectively. This is because the HV-side of the transformer is grounded and is circulating zero sequence current from the remote source.

7.2.4.1. Instantaneous Overcurrent Element Response

The Mathcad instantaneous overcurrent relay response is shown in Figure 7.13. Both the phase overcurrent element (50P) and the ground overcurrent element (50G) have successfully detected the faults, since the measured currents, shown in Table 7.3, exceeded the relay minimum pickup values.

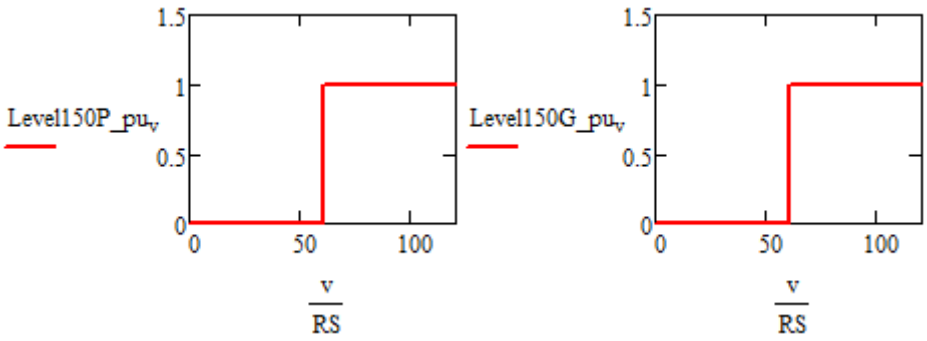

Figure 7.13: Phase and ground instantaneous overcurrent relay response of the system for the Delta-Y-grounded transformer case.

7.2.4.2. Distance Protection Relay Response

As shown in Figures 7.14 (b) and 7.15 (b), both the ground distance element and the phase distance element have picked up the faults since $\bar{Z}_{RD}$, in equation (7.1) became lower than the predetermined threshold values. The mho characteristic circle in Figure 7.14 (a) shows that the AG fault has happened first then followed by the ABG fault. Figure 7.14 (a)

and Figure 7.15 (a) show that the distance elements locate the faults about 30% of the distribution line much closer to the PCC, even though the faults were applied 50% of the distribution line. This is again due to the limited current and the weak effective source of the PV, which leads $\bar{Z}_{RD}$ to be much smaller than it actually is and which leads to incorrect the faults locations in the relay.

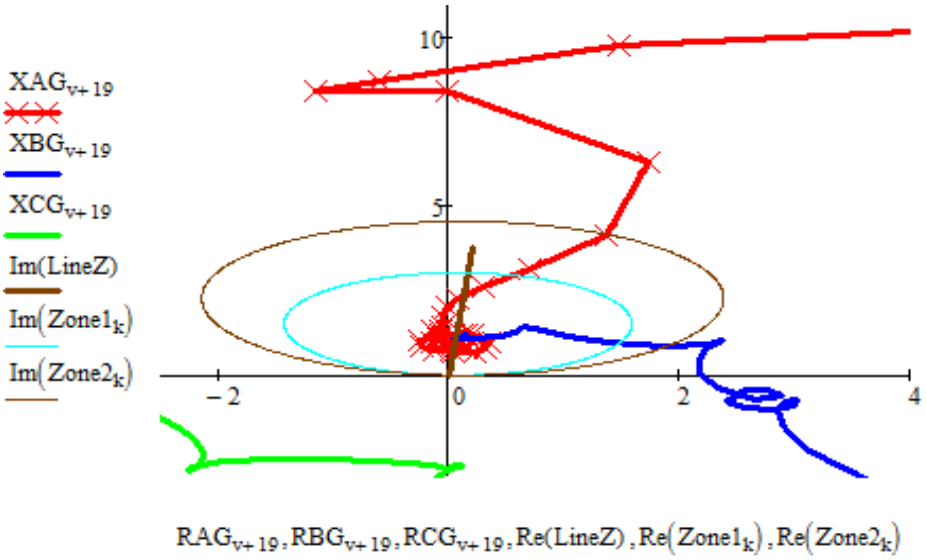

(a)

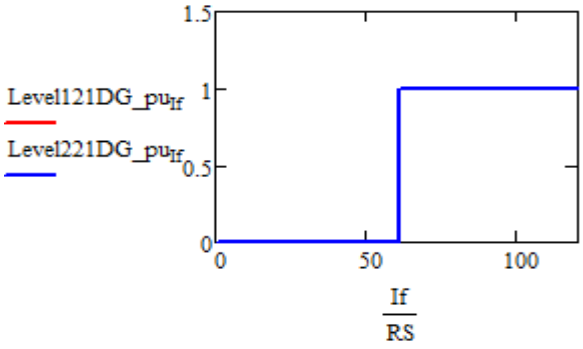

(b)

Figure 7.14: (a) Mho characteristic plot and (b) ground distance element response to SLG and DLG, for the Delta-Y-grounded transformer case.

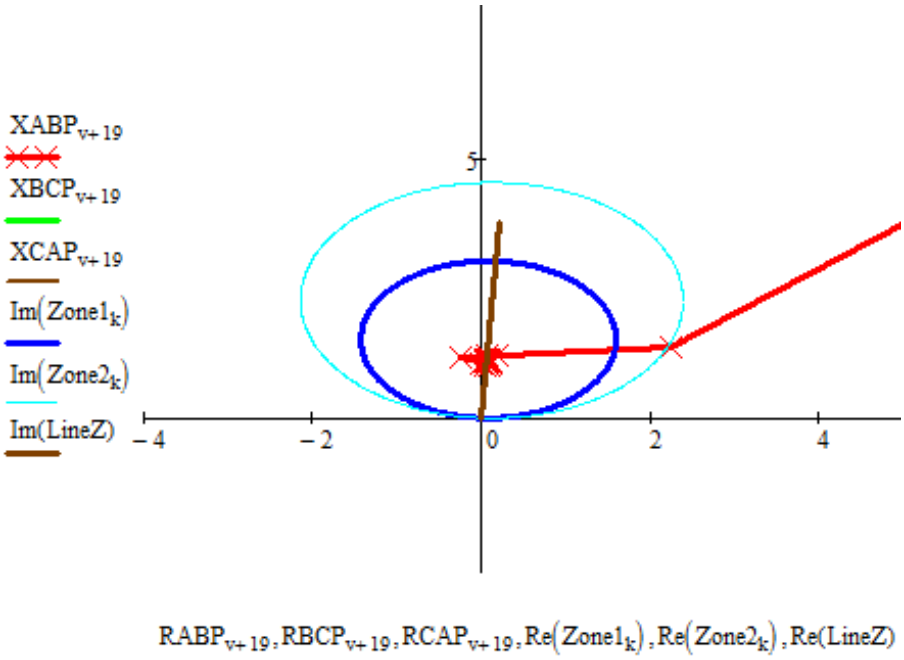

(a)

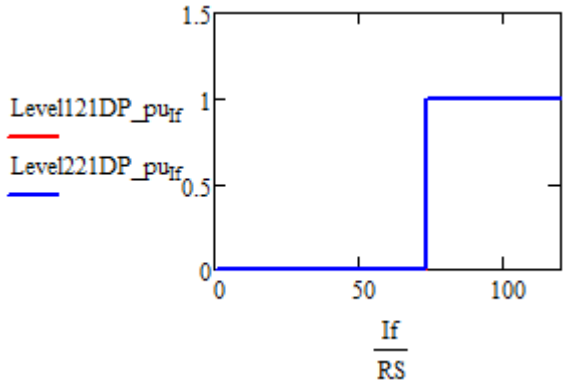

(b)

Figure 7.15: (a) Mho characteristic plot and (b) phase distance element response to SLG and DLG, for the Delta-Y-grounded transformer case.

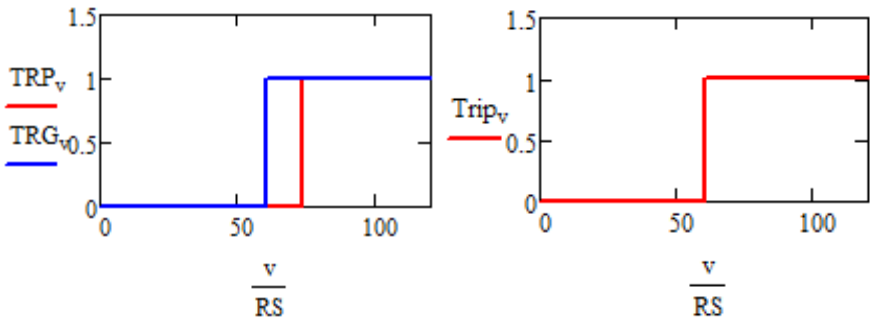

(a) (b)

Figure 7.16: (a) Phase and ground distance elements trip logic response, and (b) supervised distance element final trip logic response for the Delta-Y-grounded transformer case.

Based on the trip logic diagram shown in Figure 7.9, both phase and ground distance elements picked up the faults, as shown in Figure 7.16 (a). The supervisory instantaneous overcurrent element also responded to the fault, as shown in Figure 7.13. As a result, the final trip logic successfully tripped the fault, as shown in Figure 7.16 (b).

In a case when only a LL fault is applied to the middle of the distribution line, the supervised distance element will not trip for the fault. The reason is the fault current will be limited by the VSC and will not be enough to activate the supervisory phase overcurrent element. Also, the ground instantaneous overcurrent element will not detect the fault because there is no zero sequence current for that fault type.

7.3. Collector Line Protection Study

7.3.1. Inverse-time Overcurrent Element (51)

An inverse-time overcurrent protection scheme (ANSI/IEEE Type 51) is applied for the collector line protection. Unlike the instantaneous overcurrent element (50) with a fixed time delay, the inverse-time overcurrent element (51) operating time is inversely proportional to the fault current, meaning that as the current magnitude increases, the operating time taken to trip the fault decreases [21]. The relay has a standard inverse-time-overcurrent

characteristic curve for operation. In this study, the very inverse time-current characteristics equation (U3) is used, as shown in the Mathcad relay model in Appendix (B). In the inverse-time overcurrent element, the minimum pickup value for the phase element (51P) is set to be 1.5 pu of the maximum load current. The minimum pickup values for negative sequence element (51Q) and ground element (51G) are set to 0.1 pu. The minimum pickup values are based on the IEEE standard recommendation. In this part of the study, the performance of the collector inverse-time overcurrent relay is evaluated when the same types of the faults are applied to the middle of the distribution line at the fault point, F1, as shown in Figure 7.1. The inverse-time overcurrent relay is used as a backup element for the distribution line protection.

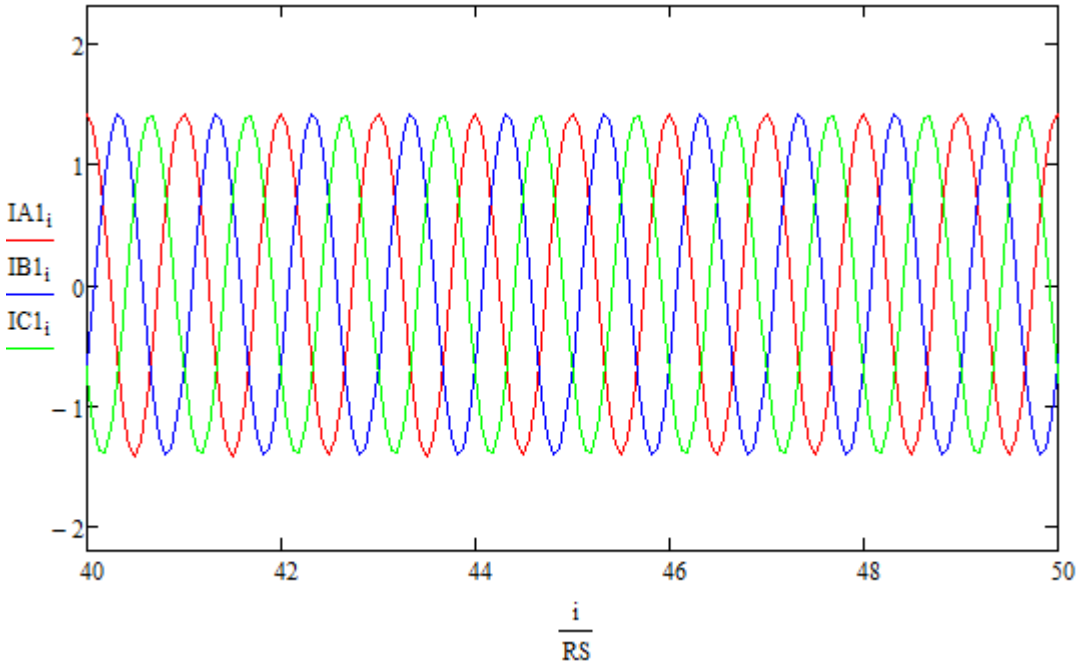

Figure 7.17: Phase current waveforms on the collector line during normal condition scaled by the CT ratio.

Figure 7.17 shows the phase current waveforms on the collector line during normal operation as scaled by the CT ratio, which is calculated as per equation (7.6). The ATP system model was simulated for a period of two seconds, however in the Mathcad relay model, the

waveform is scaled to cycles. The horizontal axis in Figure 7.17 is in the number of cycles, whereas the vertical axis is in current (A). In the system shown in Figure 7.1, the normal phase currents measured at the collector relay R_C is 2500A peak per phase.

$$CTR = \frac{\frac{2500}{\sqrt{2}}A}{1A} \tag{7.6}$$

7.3.2. Case A: Delta-Y transformer

A SLG, AG, fault is applied at the 60th cycle, which then evolves to an ABG at the 72nd cycle, as shown in Figure 7.18. The currents measured at the collector relay R_C are shown in Table 7.4 for the three operating conditions.

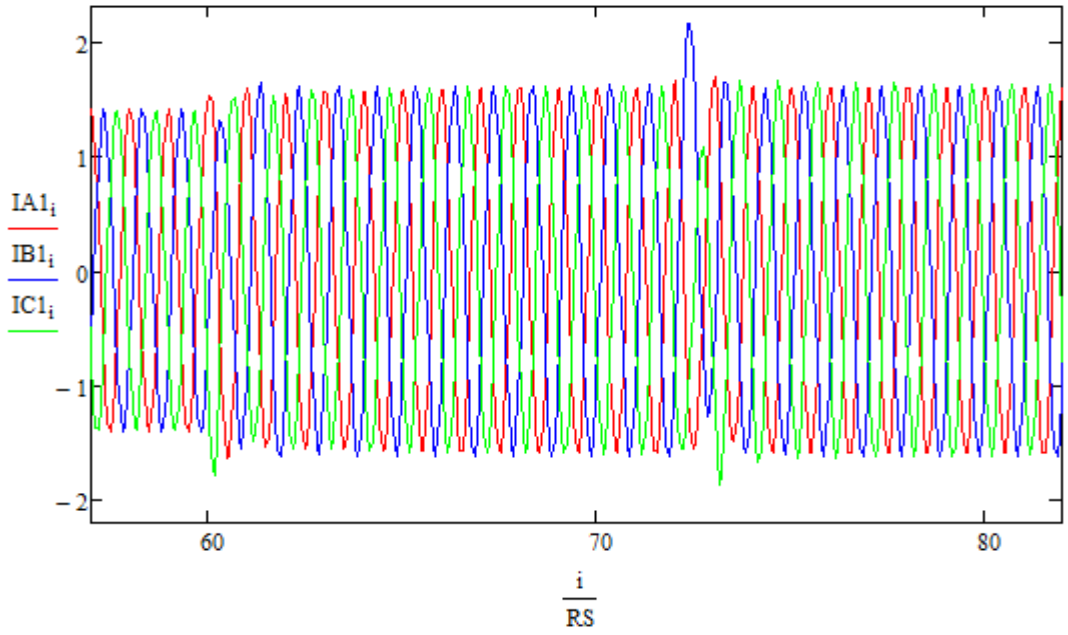

Figure 7.18: Phase current waveforms on the collector line during normal, SLG, and DLG conditions, respectively, for the Delta-Y transformer case.

Table 7.4: Measured current values for normal, SLG, and DLG operations, respectively, for the Delta-Y transformer case.

	Normal	SLG (AG)	DLG (AB)
IA	2,498A	2,820A	2,809A
IB	2,488A	2,850A	2,836A
IC	2,460A	2,840A	2,850A

By using equation (7.5), the sequence current magnitudes with a phase A reference can be plotted as shown in Figure 7.18.

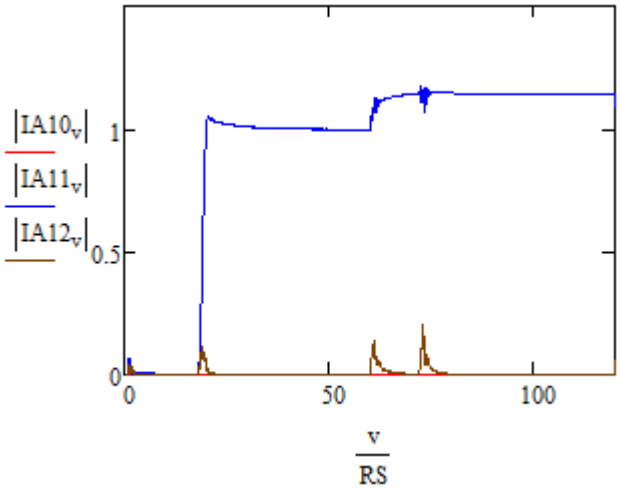

Figure 7.19: Sequence current magnitude waveforms with a phase A reference during normal, SLG, and DLG fault conditions, for the Delta-Y transformer case.

As shown in Figure 7.19, the positive sequence current magnitude of phase A during the three operating conditions is 1 pu, 1.135 pu, and 1.142 pu, respectively. The fault current was limited to below 1.2 pu by the VSC controllers. Both the negative and zero sequences are equal to zero.

7.3.2.1. Inverse-time Overcurrent Element Response

Figure 7.20 shows the trip logic diagram of the inverse-time overcurrent element in the Mathcad relay model. Based on this trip logic, the phase overcurrent element (51P) did not respond to the fault, as shown in Figure 7.21 (a). The reason is because the phase currents did not exceed the relay minimum pickup value for the specific time period the system was simulated. Figure 7.21 (a) also shows that the ground element (51G) and negative sequence element (51Q) did not trip, since currents for each are equal to zero, as shown in Figure 7.19. As a result, the final trip logic of the relay did not trip neither the SLG fault nor the DLG as shown in Figure 7.21 (b).

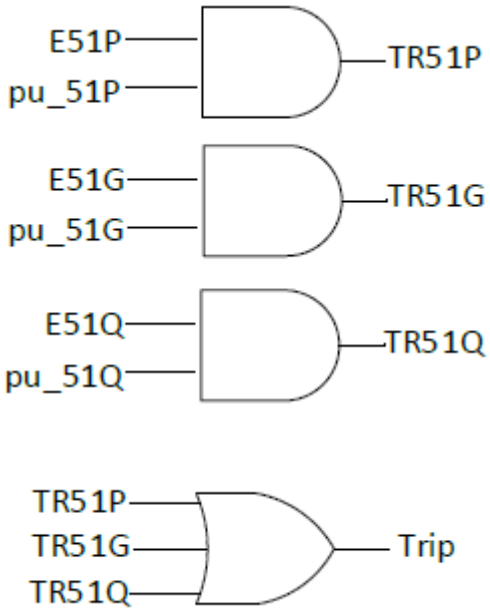

Figure 7.20: Trip logic diagram of the inverse-time overcurrent protection scheme.

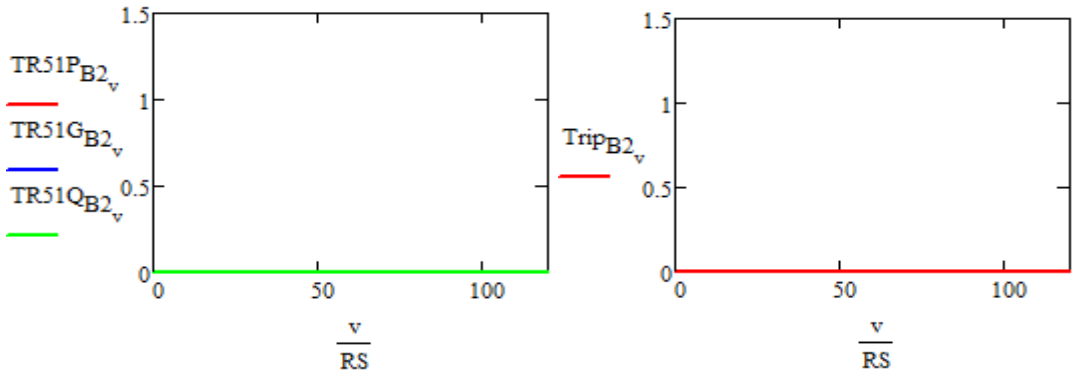

(a) (b)

Figure 7.21: (a) response of phase, ground, and negative sequence inverse-time overcurrent elements and (b) final trip logic response for the Delta-Y transformer case.

7.3.3. Case B: Delta-Y-Grounded transformer

Figure 7.22 shows response when the same types of faults were applied to the system, this time the Y-side, HV-side, of the transformer is solidly grounded. The current measurements at the collector relay R_C are shown in Table 7.5 for the three operating conditions.

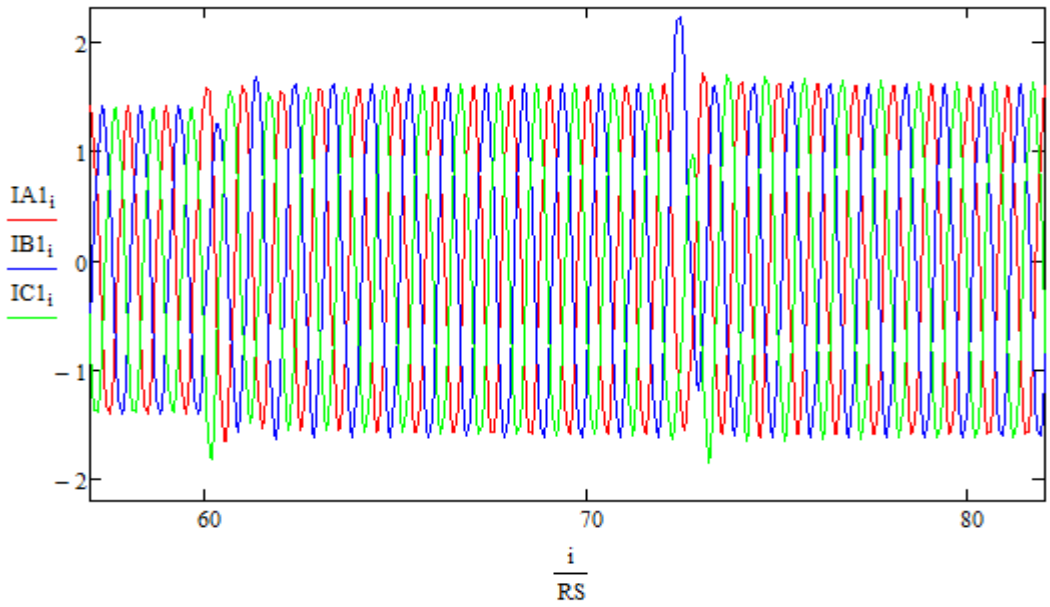

Figure 7.22: Phase current waveforms on the collector line during normal, SLG, and DLG conditions, respectively, for the Delta-Y-grounded transformer case.

Table 7.5: Measured current values for normal, SLG, and DLG operations, respectively, for the Delta-Y-grounded transformer case.

	Normal	SLG (AG)	DLG (AB)
IA	2,498A	2,800A	2,818A
IB	2,489A	2,848A	2,822A
IC	2,461A	2,840A	2,843A

By using equation (7.5), the sequence current magnitudes with a phase A reference can be plotted as shown in Figure 7.23.

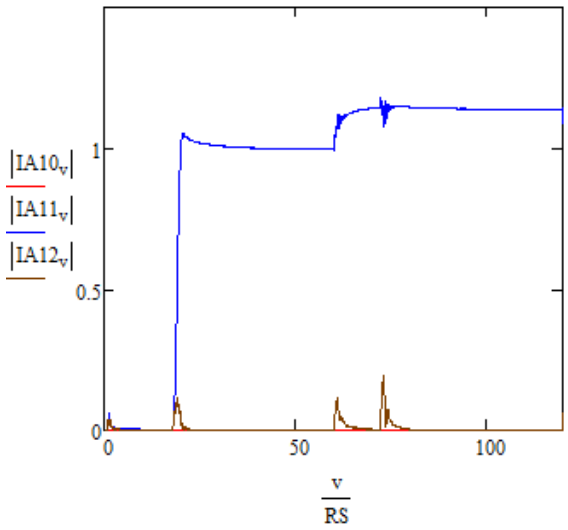

Figure 7.23: Sequence current magnitude waveforms with phase A reference during normal, SLG, and DLG fault conditions, for the Delta-Y-grounded transformer case.

As shown in Figure 7.23, the positive sequence current magnitude of phase A during the three operating conditions is 1 pu, 1.138 pu, and 1.14 pu, respectively. Both the negative and zero sequences are equal to zero. As expected, the sequence currents of phase A during the three operating conditions for the Delta-Y-grounded transformer are almost the same as the ones from the Delta-Y transformer case study. The reason is that these currents are only

supplied from the ungrounded VSC, and there is no path for zero sequence current due to the delta connection of the LV-side of the transformer.

7.3.3.1. Inverse-time Overcurrent Element Response

The protection settings for inverse-time overcurrent element are the same for both case studies, grounded and ungrounded HV-side of the transformer. The Mathcad relay model for Delta-Y-grounded transformer case study is shown in Appendix (B).

Since all the three phase currents, ground, and the negative sequence currents did not exceed their minimum pickup values, their protection elements did not operate, as Figure 7.24 (a) shows. Thus, the final trip logic of the relay did not trip for the faults as shown in Figure 7.24 (b).

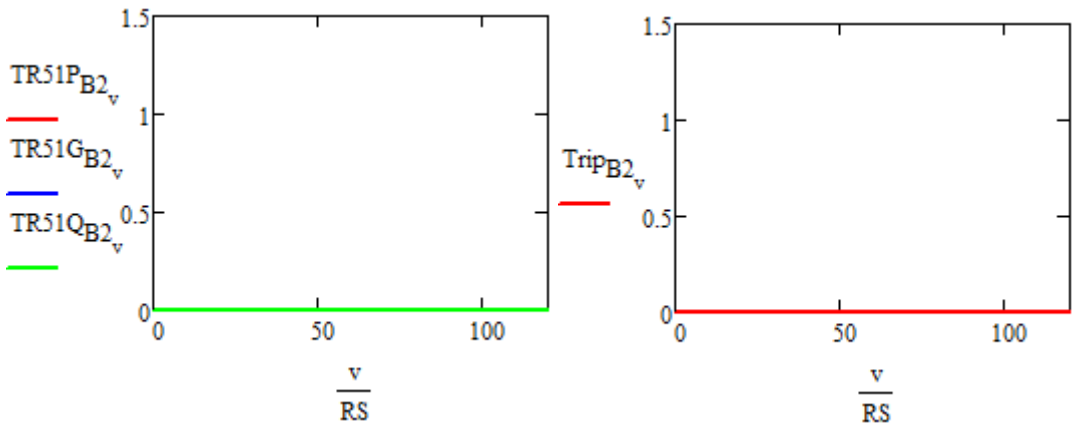

(a) (b)

Figure 7.24: (a) response of phase, ground, and negative sequence inverse-time overcurrent elements and (b) final trip logic for the Delta-Y-grounded transformer case.

7.4. System Results and Protection Performance without DDSRF Control

In this section, the same grid-connected PV system is studied however without the utilization of the decoupled double synchronous reference frame (DDSRF) control that was discussed in Chapter 6 and which was applied in the cases in Section 7.2 and 7.3. The same case studies performed in the previous sections are applied here in order to compare the grid-connected PV system protection performance with and without the utilization of the DDSRF control.

7.4.1. Distribution Line Protection Study

In the distribution line protection study, distance protection relay supervised by an instantaneous overcurrent protection element is used. Two case studies are performed for the system for the same types of fault applications to the middle of the distribution line. One case study is when the HV-side of the system has a delta-Y transformer configuration, whereas the second case study is when the HV-side of the system has a delta-Y-grounded transformer configuration.

7.4.1.1. Case A: Delta-Y transformer

By using the symmetrical component transformation equation from (7.5), the system sequence current magnitudes with a phase A reference can be plotted as shown in Figure 7.25.

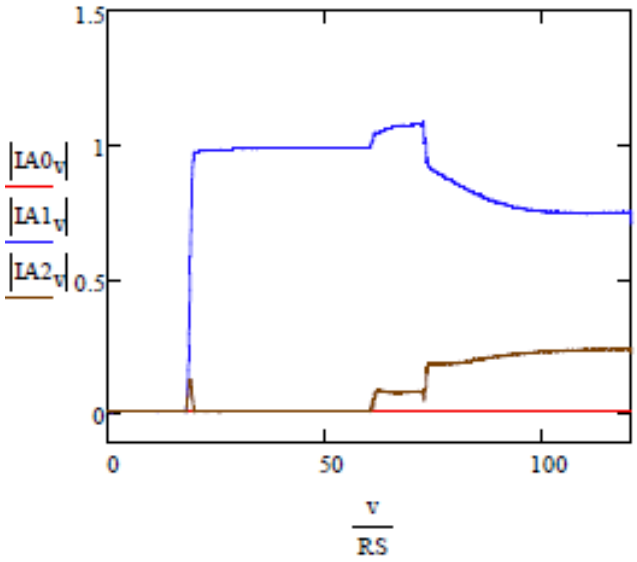

Figure 7.25: Sequence current magnitude waveforms of phase A during normal, SLG, and DLG fault conditions, when running the system without DDSRF control with a Delta-Y transformer configuration.

As shown in Figure 7.25, the positive sequence current magnitude of phase A during the three operating conditions is 1 pu, 1.065 pu, and 0.95 pu that continues to decrease to 0.75 pu for the simulation time period of 2 seconds. What can be observed in Figure 7.23 is that negative sequence current is present during the fault when the system is not using the DDSRF control. The negative sequence current during the three operating conditions is 0 pu, 0.073 pu, and 0.17 pu which keeps increasing to 0.235 pu. In comparison to the previous cases where the DDSRF control is used, the positive and negative sequence current components are not independently controlled and separated during unbalanced conditions. The zero sequence current is equal to zero since both the VSC and the HV-side of the transformer are ungrounded.

7.4.1.1.1 Instantaneous Overcurrent Element Response

The Mathcad instantaneous overcurrent relay response is shown in Figure 7.26. Neither the phase overcurrent element (50P) nor the ground overcurrent element (50G), in Figure 7.26 (a) and Figure 7.26 (b), detected the fault since the measured phase and ground

currents did not exceed their minimum pickup values. However, the negative sequence overcurrent element (50Q), Figure 7.26 (c), picked up for the fault because the negative sequence current exceeded the minimum pickup that is set to be 0.1667 in the Mathcad relay model.

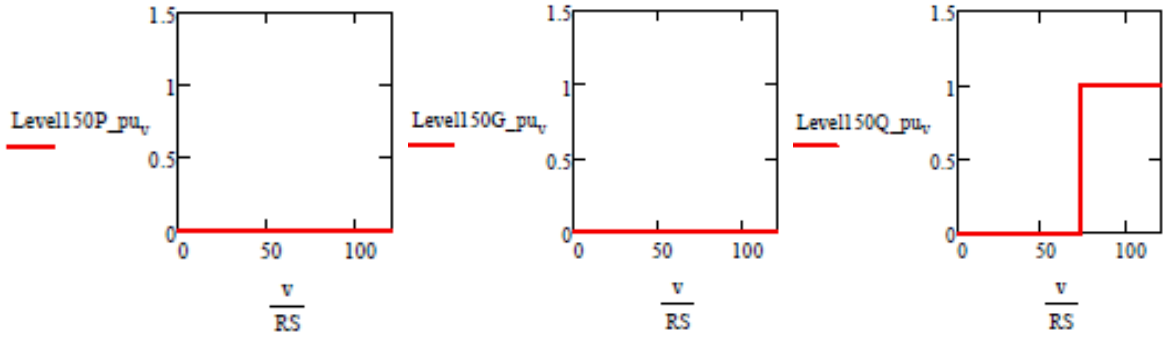

(a) (b) (c)

Figure 7.26: (a) phase, (b) ground, and (c) negative sequence instantaneous overcurrent relay response of the system when running without DDSRF control with a Delta-Y transformer configuration.

7.4.1.1.2 Distance Protection Relay Response

The response of the distance protection element for the case where the converter is not using the DDSRF control is the same as the response of the distance protection element in the previous system, where the DDSRF control was utilized.

Figure 7.27 illustrates two final trip responses of the supervised distance element, $Trip_V$ and $Tripalt_V$. $Trip_V$, in Figure 7.27, is the final trip logic response based on the trip logic diagram illustrated in Figure 7.9, when the distance element is supervised by only phase and ground instantaneous overcurrent elements. Whereas $Tripalt_V$, in Figure 7.27, is the final trip logic response, based on the trip logic diagram shown in Figure 7.28, when the distance element is supervised by the negative sequence instantaneous overcurrent element. Figure 7.27 shows that when supervising the distance element by the phase and ground instantaneous

overcurrent elements, the supervised distance element will fail to trip the faults. On the other hand, when the distance element is supervised by the negative sequence instantaneous overcurrent element, it will successfully trip for the fault, since the negative sequence supervisory element picked up for the fault, as shown in Figure 7.26 (c).

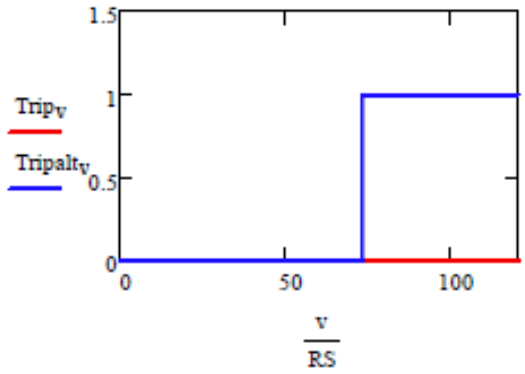

Figure 7.27: Supervised distance element final trip logic response for the system when running without DDSRF control, for the Delta-Y transformer case study.

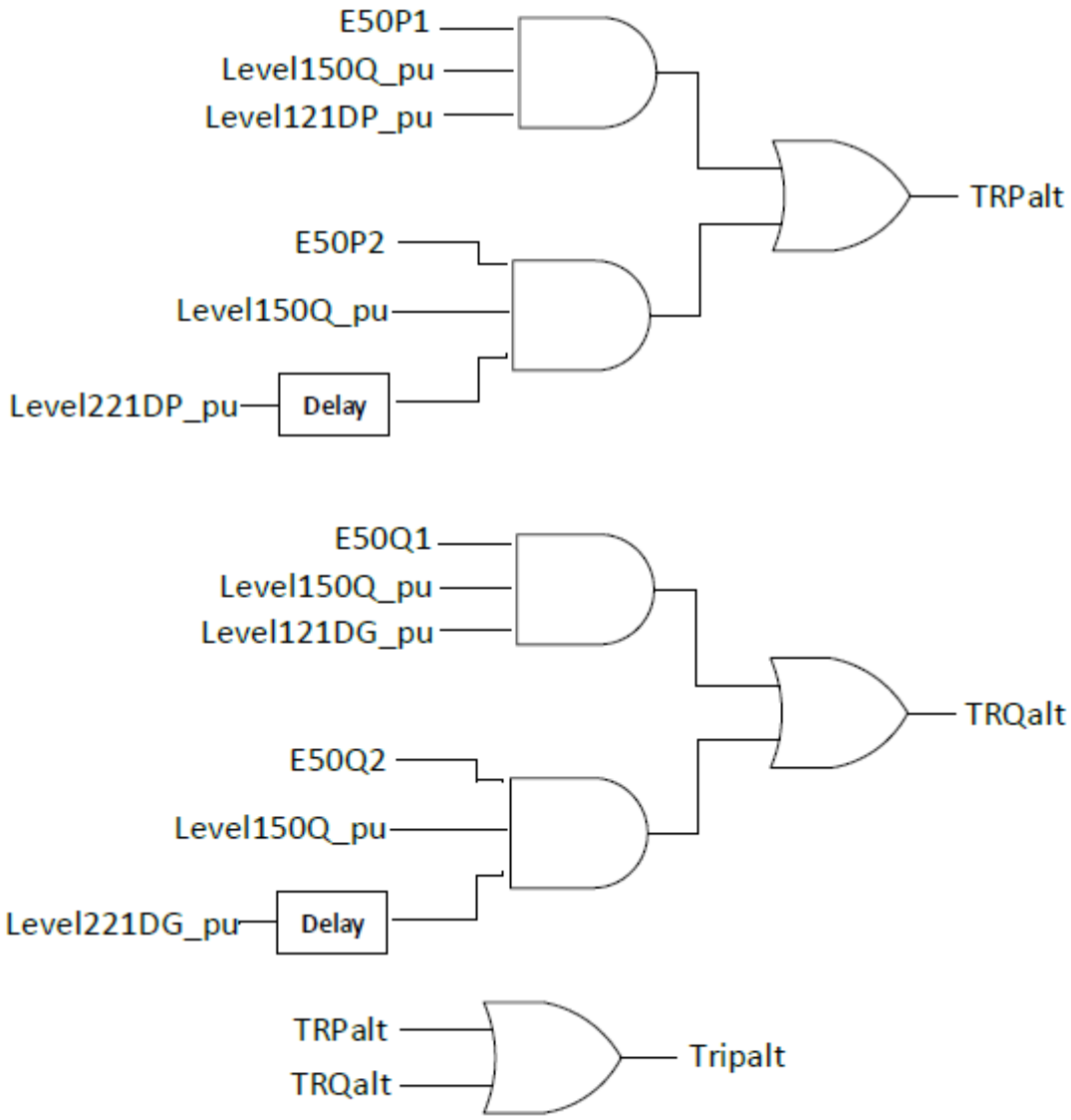

Figure 7.28: Trip logic diagram of the distance protection scheme supervised by the negative sequence instantaneous overcurrent element.

7.4.1.2. Case B: Delta-Y-Grounded transformer

The sequence current magnitudes with a phase A reference can be plotted as shown in Figure 7.26 for the case with a delta-Y-grounded transformer where the converter control does not use the DDSRF.

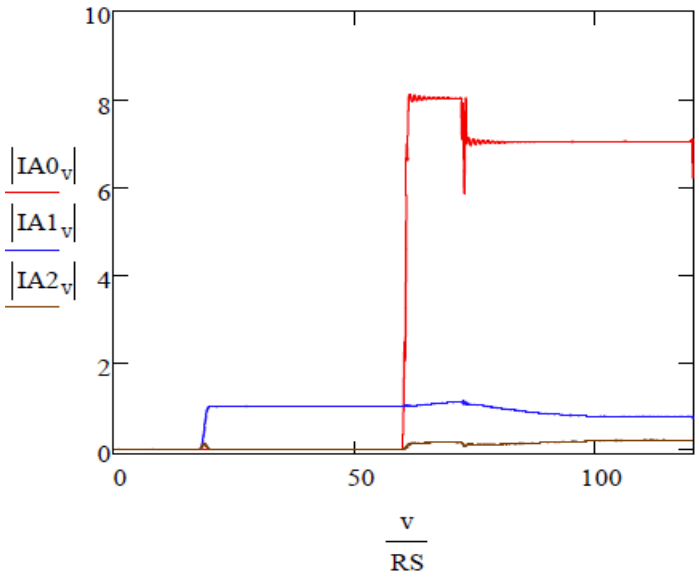

Figure 7.29: Sequence current magnitude waveforms of phase A during normal, SLG, and DLG fault conditions, when running the system without DDSRF control with a Delta-Y-grounded transformer configuration.

Figure 7.29 shows that the positive sequence current magnitude of phase A during the three operating conditions is 1 pu, 1.056 pu, and 1.075 pu that continues to decrease to 0.75 pu. Once again negative sequence current is present during the fault since the DDSRF control is not used in the system. As shown in Figure 7.29, the negative sequence current during the three operating conditions is 0 pu, 0.155 pu, and 0.11 pu which subsequently increase to 0.215 pu. The zero sequence current is quite high as expected, since the HV-side of the transformer is grounded and is circulating zero sequence current from the remote end of the line. The zero sequence current is 8 pu and 7 pu, for SLG and DLG faults, respectively.

7.4.1.2.1 Instantaneous Overcurrent Element Response

The Mathcad instantaneous overcurrent relay response is shown in Figure 7.30. Figure 7.30 (a), (b), and (c) show that the three supervisory overcurrent elements, phase (50P), ground (50G), the negative sequence element (50Q), all detected the fault since their measured current values exceeded their minimum pickup values. In this case study, the negative sequence

element (50Q), Figure 7.30 (c), detected the fault a little bit later than the phase and ground elements. This is because the measured negative sequence current did not exceed the relay minimum pickup value until the 91st cycle.

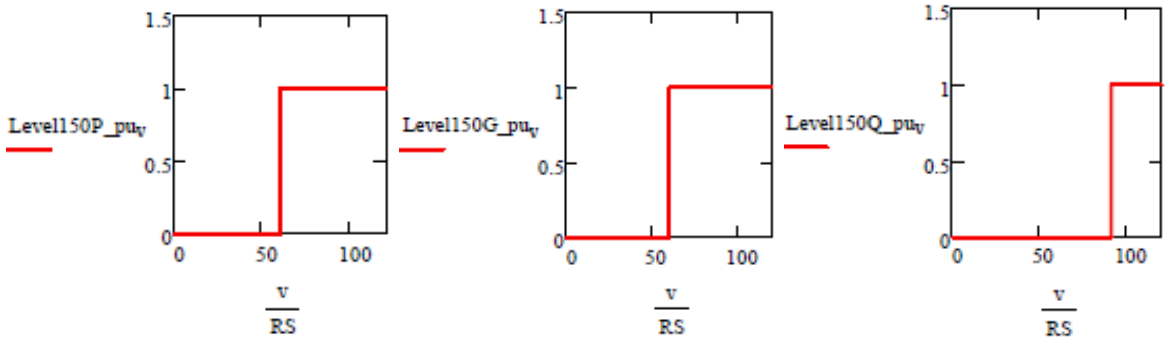

(a) (b) (c)

Figure 7.30: (a) phase, (b) ground, and (c) negative sequence instantaneous overcurrent relay response of the system when running without DDSRF control with a Delta-Y-grounded transformer configuration.

7.4.1.2.2 Distance Protection Relay Response

The distance protection element response is the same both when the system is running with and without utilization of the DDSRF control. Figure 7.31 shows the final trip logic response of the supervised distance element for both $Trip_V$ and $Tripalt_V$. In this case study, the distance element supervised by the phase and ground overcurrent element, $Trip_V$, trips the fault faster than the distance element that is supervised by the negative sequence element, $Tripalt_V$. This is because the phase and ground current based supervisory elements, detect the fault faster than the negative sequence current based element, as illustrated in Figure 7.30.

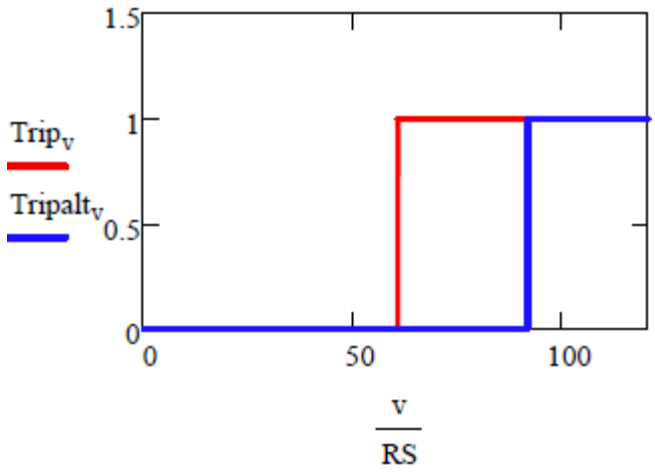

Figure 7.31: Supervised distance element final trip logic response for the system when running both with and without DDSRF control, for the Delta-Y-grounded transformer case study.

7.4.2. Collector Line Protection Study

The inverse-time overcurrent protection element is once again used to protect the collector side of the system when the same types of faults, SLG and DLG, are applied to the middle of the distribution line. Two case studies are performed for the system; the first case study is when the HV-side of the transformer is delta-Y connected, whereas the second case is when the HV-side of the transformer is a delta-Y-grounded connected.

7.4.2.1. Case A: Delta-Y transformer

The sequence current magnitudes with a phase A reference can be plotted as shown in Figure 7.32.

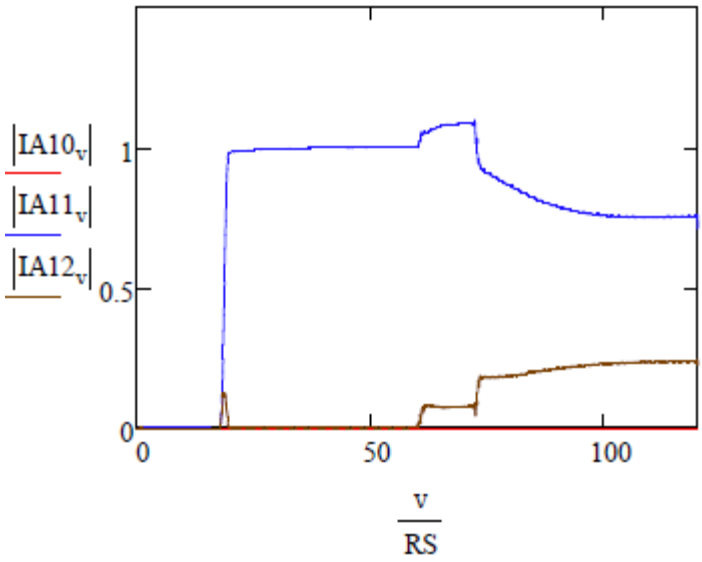

Figure 7.32: Sequence current magnitude waveforms of phase A during normal, SLG, and DLG fault conditions, when running the system without DDSRF control with a Delta-Y transformer configuration

Figure 7.32 shows the positive sequence current magnitude of phase A during the three operating conditions is 1 pu, 1.077 pu, and 0.92 pu that subsequently continues to decrease to 0.778 pu for the simulation time period of 2 seconds. Since the DDSRF control is not utilized in this system, the negative sequence current is present during the fault. As shown in Figure 7.32, the negative sequence current magnitude is 0 pu, 0.08 pu, and 0.188 pu which continues to increase to 0.245 pu, for the three operating conditions. The zero sequence is equal to zero since the VSC is ungrounded and there is no path for the zero sequence current to circulate to the fault on the distribution system.

7.4.2.1.1 Inverse-time Overcurrent Element Response

Figure 7.33 illustrates the response of the inverse-time overcurrent relay in the Mathcad relay model. Figure 7.33 (a) shows that the trip logic of the phase element (51P) and the ground element (51G) did not respond to the fault because their measured currents did not exceed the relay minimum pickup value for the specific time period the system was running

for. However, the trip logic for the negative sequence current element (51Q) successfully detected the fault since the negative sequence current exceeded the relay minimum pickup value and was large enough to trip within the simulation period, as shown in Figure 7.33 (a). As a result, based on the trip logic diagram illustrated in Figure 7.20, the relay final trip logic response has tripped during the DLG fault as shown in Figure 7.33 (b).

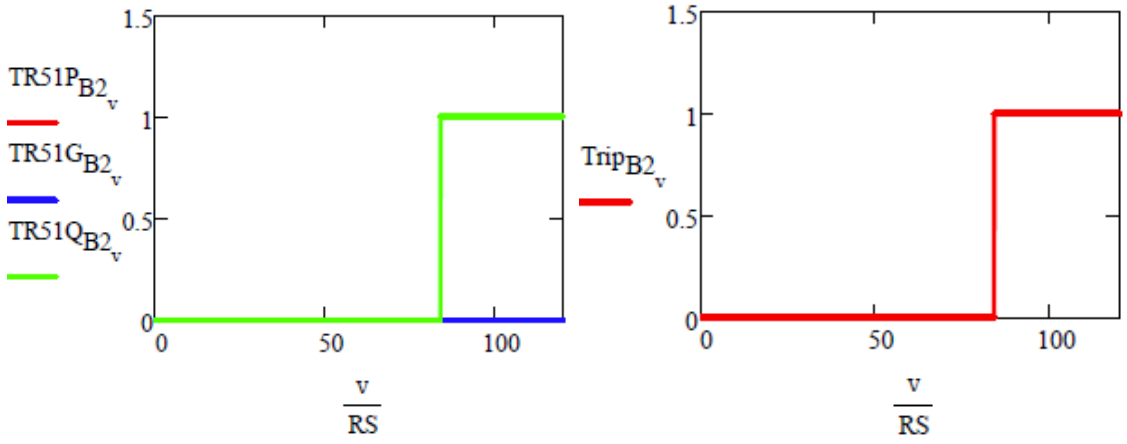

Figure 7.33: (a) response of phase, ground, and negative sequence inverse-time overcurrent elements and (b) final trip logic for the Delta-Y transformer case, when the system is running without DDSRF control.

7.4.2.2. Case B: Delta-Y-Grounded transformer

The sequence current magnitudes with a phase A reference can be plotted as shown in Figure 7.34.

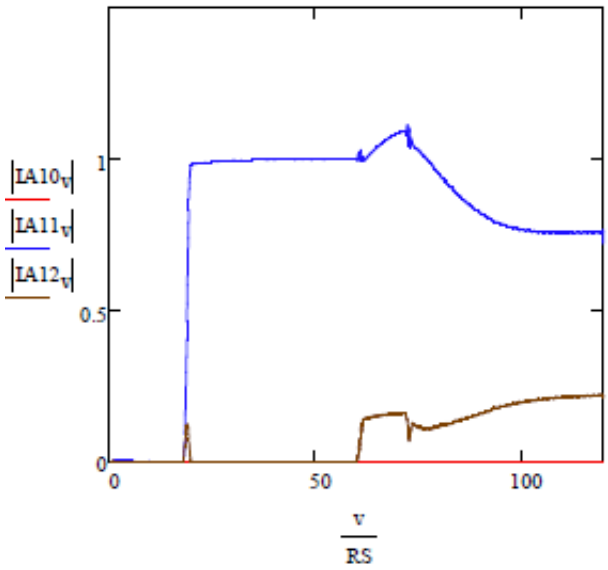

Figure 7.34: Sequence current magnitude waveforms of phase A during normal, SLG, and DLG fault conditions, when running the system without DDSRF control with a Delta-Y-grounded transformer configuration

Figure 7.34 shows the positive sequence current magnitude of phase A is 1 pu, 1.1 pu, and 1.05 pu that continues to decrease to 0.778 pu, for the normal, SLG, and DLG faults. The negative sequence current magnitude is 0 pu initially, 0.15 pu for the SLG fault, and 0.12 pu for the DLG fault that continues to increase to 0.23 pu. The zero sequence is equal to zero as expected, since there is no path for the zero sequence current to flow, as since the VSC is ungrounded.

7.4.2.2.1 Inverse-time Overcurrent Element Response

The response of the inverse-time overcurrent element from the Mathcad relay model is illustrated in Figure 7.35. As expected, the response of the inverse-time overcurrent element in this Delta-Y-grounded case is similar to the response in the previous study case, where the transformer is Delta-Y connected. The reason is the sequence currents during the three operating conditions from both case studies are almost the same. Because these currents are

only supplied from the ungrounded VSC, as since there is no path for zero sequence current to flow due to the delta connection of the LV-side of the transformer.

Figure 7.35 (a) shows that the trip logic of the phase element (51P) and ground element (51G) did not respond to the fault for the time period the system was simulated. Again the negative sequence element (51Q) trip logic detected the fault since the negative sequence current exceeded the relay minimum pickup value and was large enough for the 51Q element to pick up during the DLG fault, as shown in Figure 7.35 (a). As a result, the final trip logic of the relay has tripped the fault as shown in Figure 7.35 (b).

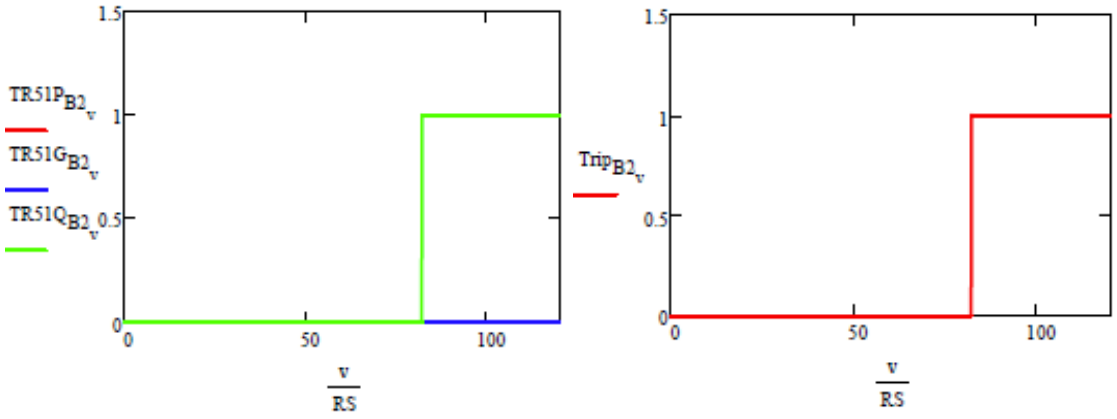

(a) (b)

Figure 7.35: (a) response of phase, ground, and negative sequence inverse-time overcurrent elements and (b) final trip logic for the Delta-Y-grounded transformer case, when the system is running without DDSRF control.

7.5. Protection Elements Response Summary

Table 7.6: Summary of protection elements response under the study.

Protection Element		Delta-Y transformer		Delta-Y-grounded transformer	
		SLG Fault (A-G)	DLG Fault (AB-G)	SLG Fault (A-G)	DLG Fault (AB-G)
With Utilizing DDSRF Control	Supervisory Overcurrent (50)	N	N	P, G	P, G
	Distance (21)	P, G	P, G	P, G	P, G
	Supervised Distance	N	N	P, G	P, G
	Inverse-time Overcurrent (51)	N	N	N	N
Without Utilizing DDSRF Control	Supervisory Overcurrent (50)	N	Q	P, G	P, G, Q
	Distance (21)	P, G	P, G	P, G	P, G
	Supervised Distance	N	Q	P, G	P, G, Q
	Inverse-time Overcurrent (51)	N	Q	N	Q

N – means the protective element did not trip the fault.

P – means the phase protective element tripped the fault.

G – means the ground protective element tripped the fault.

Q – means the negative sequence protective element tripped the fault.

Chapter 8: Summary, Conclusions, and Future Work

8.1. Summary

The results show that when the DDSRF control is used in the control of the PV VSC, the fault current is limited to less than 1.2 pu of the maximum load current with no negative sequence current for unbalanced faults. In response to the limited fault current, the protection relays have either misoperated or failed to clear some of the faults. In the collector protection study, the inverse-time overcurrent relay did not respond to the faults on the distribution line whether the HV-side of the coupling transformer was grounded and ungrounded. In the distribution protection study for ungrounded transformer, the distance elements picked up for the faults, but the final trip logic did not operate. The misoperation was because the supervisory instantaneous overcurrent relay did not trip since the fault current did not exceed its minimum pickup current. When the HV-side of the transformer is grounded however, the distance elements tripped for the SLG and DLG faults, but did not for the LL fault. Due to the limited current from the PV VSC, the mho characteristics in both case studies gave incorrect fault locations. Even though the faults were applied to the middle of the distribution line, the mho plots show the apparent fault locations are much closer to the PCC.

In addition, when running the system without the DDSRF control, the significant negative sequence current was present during the faults. Due to the existence of the negative sequence, the distance element supervised by the negative sequence instantaneous overcurrent element has picked up the DLG fault for the ungrounded case study. Similarly in the collector system side, the negative sequence inverse-time overcurrent elements have tripped for the DLG faults in both case studies since the negative sequence inverse-time overcurrent element responded to the faults.

8.2. Conclusions

In this thesis, a control scheme was developed based on the DDSRF approach. The grid-connected PV system is modeled in the ATP program, which can be then used in the ECE529 course for teaching purposes. The results and the performance of the protection relay schemes confirm previous results that the grid-connected PV system should not be treated as a conventional synchronous machine for fault analysis to determine protection scheme settings and coordination. The supervisory instantaneous overcurrent element needs to be reconsidered for the Delta-Y-ungrounded case. The mho distance element located the fault to be much closer to the PCC than the actual location, which might overreach for faults out of the zone.

When designing a protection scheme for a grid-connected PV system, the designer should know whether the inverter uses a DDSRF control or not. If an inverter that uses a DDSRF control is chosen, then the inverse-time overcurrent protection scheme should not be applied. The phase, negative sequence and ground elements will not see sufficient current to operate. If an inverter that doesn't use a DDSRF control is selected, then there will be some enough negative sequence current that can help the inverse-time overcurrent element to make decisions for unbalanced faults. Also, when the DDSRF control is not used, negative sequence current supervision can be used for the distance element to improve the protection decision, especially for the Delta-Y-ungrounded case.

8.3. Future Work

Alternate protection solutions can be studied to provide more secure performance. Other researchers have suggested using communication aided distance schemes and line current differential elements. Both need further study to see whether the supervisory elements for these schemes will pick up. Other supervisory protection elements should be considered for

the distance protection schemes. Similarly, alternative protection elements should be investigated for the collector system protection studies. This thesis did a very limited set of simulation cases. More protection case studies should be performed in the system model with different locations and different types of faults. Alternative types of renewable generators, possibly wind turbines, can be incorporated in the model and their impact on the protection scheme can be evaluated. A detailed model and a better representation of the PV source can be developed for more accurate simulation results. More case studies with PV power generation output varying by the time can be examined, with the connection of several VSCs.

Chapter 9: References

[1] M. Zeman, *Introduction to PV solar energy,* Delft University of Technology, 2003.

[2] M. Woodhouse, R. Jones-Albertus, D. Feldman, R. Fu, K. Horowitz, D. Chung, D. Jordan, S. Kurtz, *On the Path to SunShot: The Role of Advancements in Solar Photovoltaic Efficiency, Reliability, and Costs*. Golden CO, NREL, TP-6A20-65872, May 2016, [online] Available: http://www.nrel.gov/docs/fy160sti/65872.pdf.

[3] R. A. Messenger, J. Ventre, *Photovoltaic Systems Engineering, 2nd Ed*., Taylor & Francis e-Library, 2005.

[4] J. Sterling, J. McLaren, M. Taylor and K. Cory, *Treatment of Solar Generation in Electric Utility Resource Planning*. Golden CO, NREL, TP-6A20-60047, October 2013, [online] Available: https://www.osti.gov/servlets/purl/1107472.

[5] M. E. Watt, M. Oliphant, H. Outhred, and R. Collins, "Using PV to Meet Peak Summer Electricity Loads," *Proceedings of Destination Renewables, 41st Conference of the Australian and New Zealand Solar Energy Society*, Melbourne, November, 2003.

[6] C. Herig, *Using Photovoltaics to Preserve California's Electricity Capacity Reserves*. Golden CO, NREL, BR-520-31179, September 2001, [online] Available: https://www.nrel.gov/docs/fy01osti/31179.pdf.

[7] *Solar Energy and Capacity Value*. Golden CO, NREL, FS-6A20-57582, September 2013, [online] Available: https://www.nrel.gov/docs/fy13osti/57582.pdf.

[8] *IEEE Recommended Practice for Utility Interface of Photovoltaic (PV) Systems*, IEEE Standard 929-2000, 2000.

[9] *IEEE Standard for Interconnecting Distributed Resources with Electric Power Systems*, IEEE Standard 1547, 2003.

[10] *IEEE Standard Conformance Test Procedures for Equipment Interconnecting Distributed Resources with Electric Power Systems*, IEEE Standard 1547.1, 2005.

[11] *IEEE Application Guide for IEEE Std 1547(TM), IEEE Standard for Interconnecting* Distributed Resources with Electric Power Systems, IEEE Standard 1547.2, 2009.

[12] *IEEE Guide for Monitoring, Information Exchange, and Control of Distributed Resources Interconnected with Electric Power Systems*, IEEE Standard 1547.3, 2007.

[13] A. Yazdani and R. Iravani, *Voltage-sourced Converters in Power Systems*, New Jersey: John Wiley & Sons, Inc., 2010.

[14] Remus Teodorescu, Marco Liserre, and Pedro Rodriguez, *Grid Converter for Photovoltaic and Wind Power Systems*, United Kingdom: John Wiley & Sons, Inc., 2011.

[15] S. M. Holder, L. Hang, and B. K. Johnson, "Investigation of Transmission Line Protection Performance in an Electric Grid with Electronically Coupled Generation," *Proceedings of the 2013 North American Power Symposium.* Manhattan Kansas, Sept. 22-24, 2013.

[16] Joint Working Group Report, "Fault current contributions from wind plants," *2015 68th Annual Conference for Protective Relay Engineers*, College Station, TX, 2015, pp. 137-227.

[17] Ankita Roy, Brian K. Johnson, "Transmission side protection performance with Type-IV wind turbine system integration," *North American Power Symposium (NAPS) 2014*, pp. 1-6, 2014.

[18] J. Keller and B. Kroposki, *Understanding fault characteristics of inverter-based distributed energy resources.* National Renewable Energy Lab. (NREL), Golden, CO, USA, Tech. Rep. TP-550-46698, Jan. 2010.

[19] Plet, C.A.; Graovac, M.; Green, T.C.; Iravani, R., "Fault response of grid-connected inverter dominated networks," *Power and Energy Society General Meeting, 2010 IEEE*, vol., no., pp.1, 8, 25-29 July 2010.

[20] E.O. Schweitzer and H.J. Altuve, *Modern Solutions for Protection, Control, and Monitoring of Electric Power Systems*, Pullman: Schweitzer Engineering Laboratories, Inc., 2010.

[21] J.L. Blackburn, T.J. Domin, *Protective Relaying Principles and Application, 4th Ed.*, NewYork: Taylor & Francis Group, LLC, 2014.

[22] *IEEE Guide for Breaker Failure Protection of Power Circuit Breakers*, IEEE Standard C37.119-2005, 2005.

[23] P. Rodriguez, J. Pou, J. Bergas, J. I. Candela, R. P. Burgos, D. Boroyevich, "Decoupled double synchronous reference frame PLL for power converters control," *IEEE Trans. Power Electron.*, vol. 22, no. 2, pp. 584-592, Mar. 2007.

Appendix A – Distance Relay Mathcad Model

- **Supervisory Overcurrent Element Settings:**

These Instantaneous Overcurrent Elements are used to supervise the distance elements. Enter settings in secondary Amps, (leave off units) for phase (P), zero sequence (ground, G) and negative sequence (Q). Set these elements to enable the distance element, if the current exceeds a threshold, there is a fault.

Enable the relay elements you want to use (1 means enabled, 0 means disabled)

E50P1 := 1 E50P2 := 1 E50Q1 := 1

E50G1 := 1 E50G2 := 1 E50Q2 := 1

Relay Pickup Settings (default values set very small)

Level_1_50P := 1.5 Level_1_50G := 0.5 Level_1_50Q := $\frac{0.5}{3}$

- **Relay Overcurrent Element Pickup Logic:**

Initialize overcurrent elements: $Level150G\_pu_v = 0$ $Level150P\_pu_v = 0$ $Level150Q\_pu_v = 0$

Ground (zero sequence) element:

$$Level150G\_pu_v = \begin{cases} 1 \text{ if } 3\left|IA0_v\right| \geq Level\_1\_50G \\ 1 \text{ if } Level150G\_pu_{v-1} \geq 0.01 \\ 0 \text{ otherwise} \end{cases}$$

Negative sequence element:

$$Level150Q\_pu_v = \begin{cases} 1 \text{ if } \left|IA2_v\right| \geq Level\_1\_50Q \\ 1 \text{ if } Level150Q\_pu_{v-1} \geq 0.01 \\ 0 \text{ otherwise} \end{cases}$$

Phase current element (phase A or phase B or Phase C exceed pickup)

$$Level150P\_pu_v = \begin{cases} 1 \text{ if } \left|IAcpx_v\right| \geq Level\_1\_50P \\ 1 \text{ if } \left|IBcpx_v\right| \geq Level\_1\_50P \\ 1 \text{ if } \left|ICcpx_v\right| \geq Level\_1\_50P \\ 1 \text{ if } Level150P\_pu_{v-1} \geq 0.01 \\ 0 \text{ otherwise} \end{cases}$$

- **Distance Element Settings:**

Line impedance in Ohm's secondary (i.e. values seen after the CTR and PTR are factored in).

$Z1 := 0.2 + 3.7699i$ $\quad |Z1| = 3.7752$ $\quad \arg(Z1) = 86.9632 \cdot deg$

$Z0 := 3 \cdot Z1$

$\theta line := \arg(Z1)$

$Z1MAG := |Z1|$ $\quad Z1ANG := \arg(Z1)$

$Z0MAG := |Z0|$ $\quad Z0ANG := \arg(Z0)$

Distance relay k0 factor equation.

$$k0 := \frac{Z0 - Z1}{3 \cdot Z1} \qquad k0 = 0.6667$$

Distance Elements (set as percentage reach)

$Zone1P := 80\%$ $\quad Zone2P := 120\%$

$Zone1G := 80\%$ $\quad Zone2G := 120\%$

Level 2 Time Delays (default values)

$T_{DelDP} := 5cycles$ $\quad T_{DelDG} := 5cycles$

- **Phase and Ground Distance Elements:**

Convert line impedance into a vector for comparison purposes:

$$LineZ := \begin{pmatrix} 0 \\ Z1 \end{pmatrix}$$

Phase Elements:

- Calculate Mho Circles:

$\theta mho := 0deg, 0.5deg .. 360deg \qquad k := 0, 1 .. 719$

$radMho1 := Zone1G \cdot \frac{Z1MAG}{2} = 1.5101 \qquad radMho2 := Zone2G \cdot \frac{Z1MAG}{2}$

Note the divide by two for radius of circle

$offsetMho1 := Zone1G \cdot \left(\frac{Z1MAG}{2}\right) e^{j \cdot \theta line} \qquad offsetMho2 := Zone2G \cdot \left(\frac{Z1MAG}{2}\right) e^{j \cdot \theta line}$

$Zone1_k := offsetMho1 + radMho1 \cdot e^{j \cdot k \cdot 0.5deg}$

$Zone2_k := offsetMho2 + radMho2 \cdot e^{j \cdot k \cdot 0.5deg}$

$centerMho1\_G := Zone1G \cdot \frac{Z1}{2} \qquad centerMho2\_G := Zone2G \cdot \frac{Z1}{2}$

$centerMho1\_P := Zone1P \cdot \frac{Z1}{2} \qquad centerMho2\_P := Zone2P \cdot \frac{Z1}{2}$

Ground Elements:

- Now calculate impedance seen by the relay. Note that this approach will have problems for a close-in fault where the voltage falls.
- Also note that k0 is multiplied times the residual current. This model uses IR and has a 1/3 in the k0 calculation.

$ZAG_v = \frac{VAcpx_v}{IAcpx_v + k0 \cdot IRcpx_v} \qquad RAG_v = Re(ZAG_v) \qquad XAG_v = Im(ZAG_v)$

calculate impedance seen by the relay.

$ZBG_v = \frac{VBcpx_v}{IBcpx_v + k0 \cdot IRcpx_v} \qquad RBG_v = Re(ZBG_v) \qquad XBG_v = Im(ZBG_v)$

$ZCG_v = \frac{VCcpx_v}{ICcpx_v + k0 \cdot IRcpx_v} \qquad RCG_v = Re(ZCG_v) \qquad XCG_v = Im(ZCG_v)$

Phase to Ground Distance Element Pickup Logic:

Initialize Elements: $Level121DG\_pu_v = 0$ $Level221DG\_pu_v = 0$

$$Level121DG\_pu_{If} = \begin{cases} 1 \text{ if } |ZAG_{If} - centerMho1\_G| \le radMho1 \\ 1 \text{ if } |ZBG_{If} - centerMho1\_G| \le radMho1 \\ 1 \text{ if } |ZCG_{If} - centerMho1\_G| \le radMho1 \\ 1 \text{ if } Level121DG\_pu_{If-1} \ge 0.01 \\ 0 \text{ otherwise} \end{cases} \quad Level221DG\_pu_{If} = \begin{cases} 1 \text{ if } |ZAG_{If} - centerMho2\_G| \le radMho2 \\ 1 \text{ if } |ZBG_{If} - centerMho2\_G| \le radMho2 \\ 1 \text{ if } |ZCG_{If} - centerMho2\_G| \le radMho2 \\ 1 \text{ if } Level221DG\_pu_{If-1} \ge 0.01 \\ 0 \text{ otherwise} \end{cases}$$

Phase to phase elements:

$$ZABP_v = \frac{VAcpx_v - VBcpx_v}{IAcpx_v - IBcpx_v + 0.0001} \quad RABP_v = Re(ZABP_v) \quad XABP_v = Im(ZABP_v)$$

$$ZBCP_v = \frac{VBcpx_v - VCcpx_v}{IBcpx_v - ICcpx_v + 0.0001} \quad RBCP_v = Re(ZBCP_v) \quad XBCP_v = Im(ZBCP_v)$$

$$ZCAP_v = \frac{VCcpx_v - VAcpx_v}{ICcpx_v - IAcpx_v + 0.0001} \quad RCAP_v = Re(ZCAP_v) \quad XCAP_v = Im(ZCAP_v)$$

Initialize Elements: $Level121DP\_pu_v = 0$ $Level221DP\_pu_v = 0$

$$Level121DP\_pu_{If} = \begin{cases} 1 \text{ if } |ZABP_{If} - centerMho1\_P| \le radMho1 \\ 1 \text{ if } |ZBCP_{If} - centerMho1\_P| \le radMho1 \\ 1 \text{ if } |ZCAP_{If} - centerMho1\_P| \le radMho1 \\ 1 \text{ if } Level121DP\_pu_{If-1} \ge 0.01 \\ 0 \text{ otherwise} \end{cases} \quad Level221DP\_pu_{If} = \begin{cases} 1 \text{ if } |ZABP_{If} - centerMho2\_P| \le radMho2 \\ 1 \text{ if } |ZBCP_{If} - centerMho2\_P| \le radMho2 \\ 1 \text{ if } |ZCAP_{If} - centerMho2\_P| \le radMho2 \\ 1 \text{ if } Level221DP\_pu_{If-1} \ge 0.01 \\ 0 \text{ otherwise} \end{cases}$$

- **Trip Logics:**

Below is the trip logic equation, when the distance element is supervised by phase and ground instantaneous overcurrent elements.

$$TRP_d = E50P1 \wedge Level150P\_pu_d \wedge Level121DP\_pu_d \vee E50P2 \wedge Level221DP\_pu_{d-T_{DelDP}\cdot RS}$$

$$TRG_d = E50G1 \wedge Level150G\_pu_d \wedge Level121DG\_pu_d \vee E50G2 \wedge Level221DG\_pu_{d-T_{DelDG}\cdot RS}$$

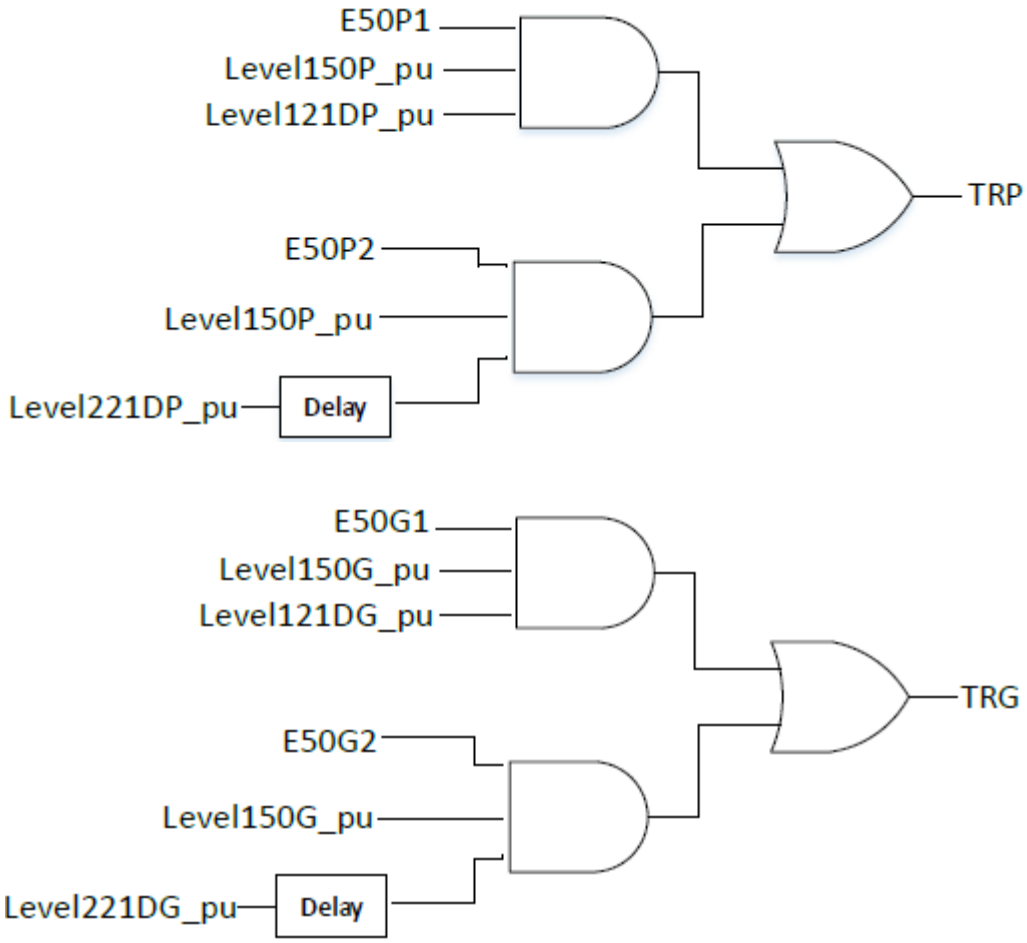

$$Trip_v = TRP_v \vee TRG_v$$

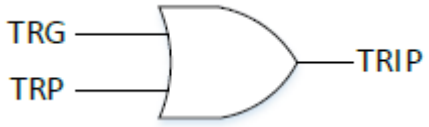

Whereas, the trip logic equation when the distance element is supervised by only the negative instantaneous overcurrent elements is shown below.

$$TRPalt_d = E50P1 \wedge Level150Q\_pu_d \wedge Level121DP\_pu_d \vee E50P2 \wedge Level150Q\_pu_d \wedge Level221DP\_pu_{d-T_{DelDP}\cdot RS}$$

$$TRGalt_d = E50Q1 \wedge Level150Q\_pu_d \wedge Level121DG\_pu_d \vee E50Q2 \wedge Level150Q\_pu_d \wedge Level221DG\_pu_{d-T_{DelDG}\cdot RS}$$

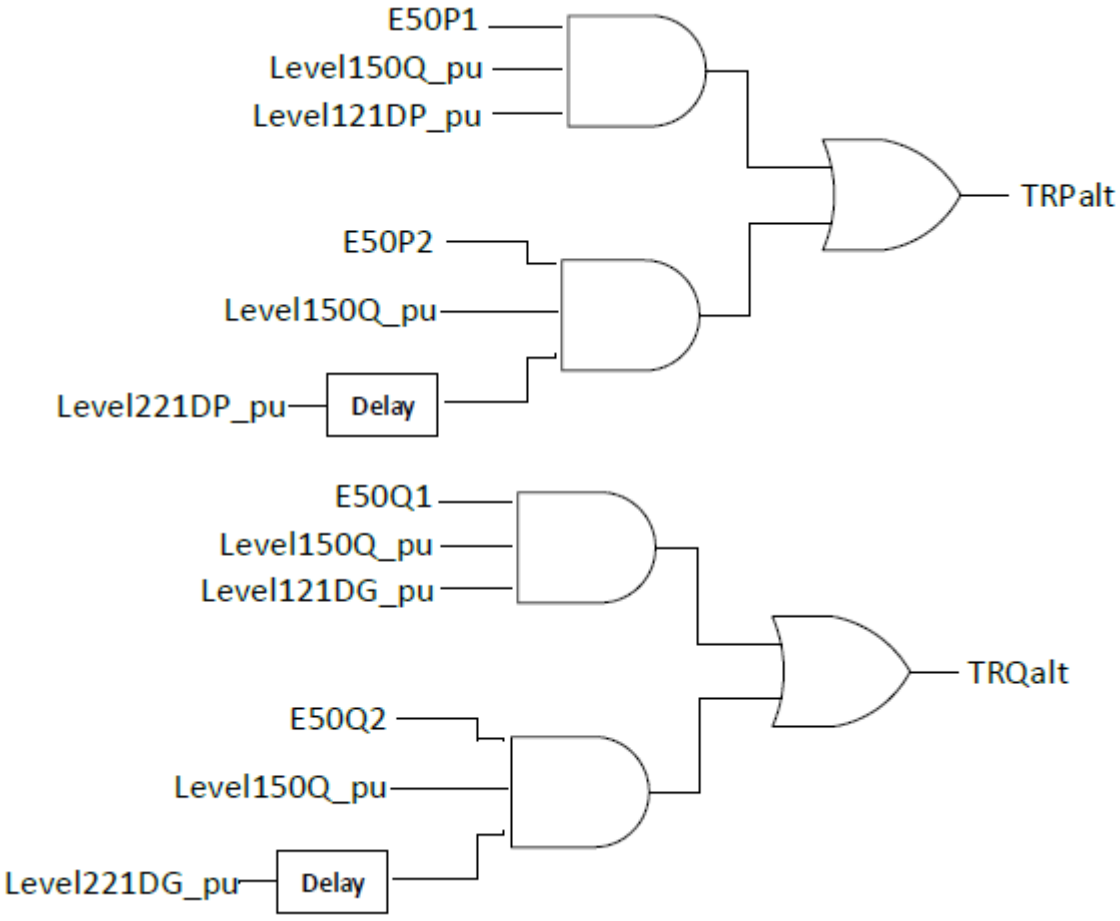

$$Tripalt_v = TRPalt_v \vee TRGalt_v$$

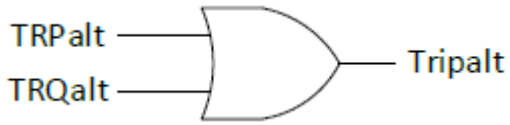

Appendix B – Inverse-time Overcurrent Relay Mathcad Model

- Enable Inverse Time Overcurrent Elements (Phase, Ground, and Negative).

$E51P_{B2} := 1 \qquad E51G_{B2} := 1 \qquad E51Q_{B2} := 1$

- Relay Element Settings:

$I_{pu\_P\_B2} := 1.5 \qquad TD_{B2\_P} := 1$

$I_{pu\_G\_B2} := 0.1 \qquad TD_{B2\_G} := 1$

$I_{pu\_Q\_B2} := 0.1 \qquad TD_{B2\_Q} := 1$

- Very Inverse Characteristic (U3)

$A_{VI} := 3.88 \qquad B_{VI} := 0.0963 \qquad p_{VI} := 2 \qquad C_{VI} := 3.88$

Model for Relay:

- Current Ratios

$$MB2_{phA_v} = \frac{|IA1cpx_v|}{I_{pu\_P\_B2}} \qquad MB2_{G_v} = \frac{3\,|IA10_v|}{I_{pu\_G\_B2}}$$

$$MB2_{phB_v} = \frac{|IB1cpx_v|}{I_{pu\_P\_B2}} \qquad MB2_{Q_v} = \frac{3\,|IA12_v|}{I_{pu\_Q\_B2}}$$

$$MB2_{phC_v} = \frac{|IC1cpx_v|}{I_{pu\_P\_B2}}$$

- Initialize angle history to 0:

$\theta B2_{PA_v} = 0sec$

$\theta B2_{PB_v} = 0sec$

$\theta B2_{PC_v} = 0sec$

$\theta B2_{G_v} = 0sec$

$\theta B2_{Q_v} = 0sec$

$$\theta B2_{PA_v} = \begin{cases} \left[\frac{\left[\left(MB2_{phA}\right)_v\right]^{pVI} - 1}{B_{VI}\left[\left(MB2_{phA_v}\right)^{pVI} - 1\right] + A_{VI}}\right] \cdot \left(\frac{1}{RS \cdot 60}\right) + \theta B2_{PA_{v-1}} & \text{if } MB2_{phA_v} \geq 1 \\ -\left[\frac{1 - \left(MB2_{phA_v}\right)^{pVI}}{C_{VI}}\right] \cdot \left(\frac{1}{RS \cdot 60}\right) + \theta B2_{PA_{v-1}} & \text{if } MB2_{phA_v} < 1 \\ 0 \text{ if } \left(MB2_{phA_v} < 1\right) \wedge \left(\theta B2_{PA_{v-1}} \leq 0\right) & \\ 0 \text{ otherwise} & \end{cases}$$

$$\theta B2_{PB_v} = \begin{cases} \left[\frac{\left[\left(MB2_{phB}\right)_v\right]^{pVI} - 1}{B_{VI}\left[\left(MB2_{phB_v}\right)^{pVI} - 1\right] + A_{VI}}\right] \cdot \left(\frac{1}{RS \cdot 60}\right) + \theta B2_{PB_{v-1}} & \text{if } MB2_{phB_v} \geq 1 \\ -\left[\frac{1 - \left(MB2_{phB_v}\right)^{pVI}}{C_{VI}}\right] \cdot \left(\frac{1}{RS \cdot 60}\right) + \theta B2_{PB_{v-1}} & \text{if } MB2_{phB_v} < 1 \\ 0 \text{ if } \left(MB2_{phB_v} < 1\right) \wedge \left(\theta B2_{PB_{v-1}} \leq 0\right) & \\ 0 \text{ otherwise} & \end{cases}$$

$$\theta B2_{PC_v} = \begin{cases} \left[\frac{\left[\left(MB2_{phC}\right)_v\right]^{pVI} - 1}{B_{VI}\left[\left(MB2_{phC_v}\right)^{pVI} - 1\right] + A_{VI}}\right] \cdot \left(\frac{1}{RS \cdot 60}\right) + \theta B2_{PC_{v-1}} & \text{if } MB2_{phC_v} \geq 1 \\ -\left[\frac{1 - \left(MB2_{phC_v}\right)^{pVI}}{C_{VI}}\right] \cdot \left(\frac{1}{RS \cdot 60}\right) + \theta B2_{PC_{v-1}} & \text{if } MB2_{phC_v} < 1 \\ 0 \text{ if } \left(MB2_{phC_v} < 1\right) \wedge \left(\theta B2_{PC_{v-1}} \leq 0\right) & \\ 0 \text{ otherwise} & \end{cases}$$

$$\theta B2G_v = \begin{cases} \left[\frac{\left[\left(MB2G\right)_v\right]^{PVI} - 1}{B_{VI}\left[\left(MB2G_v\right)^{PVI} - 1\right] + A_{VI}}\right]\cdot\left(\frac{1}{RS\cdot 60}\right) + \theta B2G_{v-1} & \text{if } MB2G_v \geq 1 \\ -\left[\frac{1 - \left(MB2G_v\right)^{PVI}}{C_{VI}}\right]\cdot\left(\frac{1}{RS\cdot 60}\right) + \theta B2G_{v-1} & \text{if } MB2G_v < 1 \\ 0 & \text{if } \left(MB2G_v < 1\right) \wedge \left(\theta B2G_{v-1} \leq 0\right) \\ 0 & \text{otherwise} \end{cases}$$

$$\theta B2Q_v = \begin{cases} \left(\frac{1}{TD_{B2\_Q}}\right)\cdot\left[\frac{\left[\left(MB2Q\right)_v\right]^{PVI} - 1}{B_{VI}\left[\left(MB2Q_v\right)^{PVI} - 1\right] + A_{VI}}\right]\cdot\left(\frac{1}{RS\cdot 60}\right) + \theta B2Q_{v-1} & \text{if } MB2Q_v \geq 1 \\ -\left[\frac{1 - \left(MB2Q_v\right)^{PVI}}{C_{VI}}\right]\cdot\left(\frac{1}{RS\cdot 60}\right) + \theta B2Q_{v-1} & \text{if } MB2Q_v < 1 \\ 0 & \text{if } \left(MB2Q_v < 1\right) \wedge \left(\theta B2Q_{v-1} \leq 0\right) \\ 0 & \text{otherwise} \end{cases}$$

Relay Element Pick Up Logic

- Ground element:

  Initialize arrays with all zeros: $pu\_51G_{B2_v} = 0$

$$pu\_51G_{B2_v} = \begin{cases} 1 \text{ if } \left|\theta B2_{G_v}\right| \geq TD_{B2\_G} \\ 1 \text{ if } pu\_51G_{B2_{v-1}} \geq 0.01 \\ 0 \text{ otherwise} \end{cases}$$

- Negative sequence element:

  Initialize arrays with all zeros: $pu\_51Q_{B2_v} = 0$

$$pu\_51Q_{B2_v} = \begin{cases} 1 \text{ if } \left|\theta B2_{Q_v}\right| \geq TD_{B2\_Q} \\ 1 \text{ if } pu\_51Q_{B2_{v-1}} \geq 0.01 \\ 0 \text{ otherwise} \end{cases}$$

- Phase current element (phase A or phase B or Phase C exceed pickup)

  Initialize arrays with all zeros: $pu\_51P_{B2_v} = 0$

$$pu\_51P_{B2_v} = \begin{cases} 1 \text{ if } \theta B2_{PA_v} \geq TD_{B2\_P} \\ 1 \text{ if } \theta B2_{PB_v} \geq TD_{B2\_P} \\ 1 \text{ if } \theta B2_{PC_v} \geq TD_{B2\_P} \\ 1 \text{ if } pu\_51P_{B2_{v-1}} \geq 0.01 \\ 0 \text{ otherwise} \end{cases}$$

- ***Trip Logic***

+

$$TR51P_{B2_v} = E51P_{B2} \wedge pu\_51P_{B2_v}$$

$$TR51G_{B2_v} = E51G_{B2} \wedge pu\_51G_{B2_v}$$

$$TR51Q_{B2_v} = E51Q_{B2} \wedge pu\_51Q_{B2_v}$$

Overall Trip Equation:

$$Trip_{B2_v} = \left(TR51P_{B2_v} \vee TR51G_{B2_v} \vee TR51Q_{B2_v}\right)$$

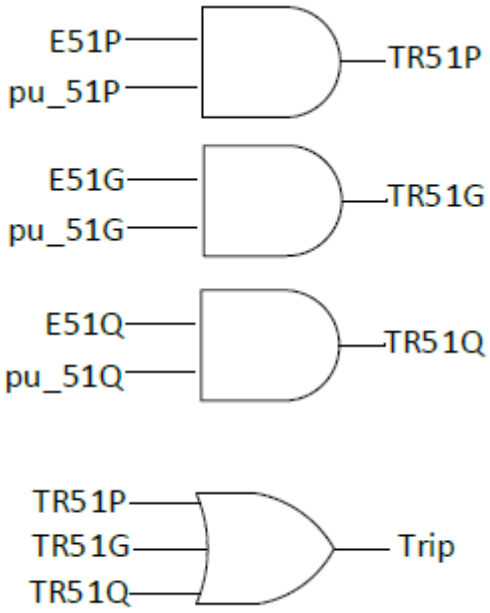

Appendix C – Inner Controller Parameters

Calculating PI controller parameters, Kp and Ki

Impedence before the transformer

$L_1 := 0.60mH \qquad X := L_1 \cdot 2 \cdot \pi \cdot 60Hz = 0.226195\,\Omega$

$\tau := 1ms$

$R := 0.04 \cdot \Omega$

$\delta := \operatorname{atan}\left(\frac{X}{R}\right) = 79.972 \cdot deg$

$R_1 := 1 \cdot 10^{-6}\Omega + R = 0.04\,\Omega$

$K_{P.1} := \frac{L_1}{\tau} = 0.6\,\Omega$

$K_{I.1} := \frac{K_{P.1} \cdot R}{L_1} = 40\,\frac{1}{F}$

Voltage Feed-forward equation:

$$H(s) = \frac{1}{1 + 8 \cdot 10^{-6} \cdot s}$$

Current Decoupling Compensator

Positive sequence:

$\omega_0 := 2 \cdot 60Hz \cdot \pi$

$\omega_0 \cdot L_1 = 0.226\,\Omega$

Negative sequence:

$-\omega_0 \cdot L_1 = -0.226\,\Omega$

Appendix D – Grid-connected PV System Model in the ATP Program

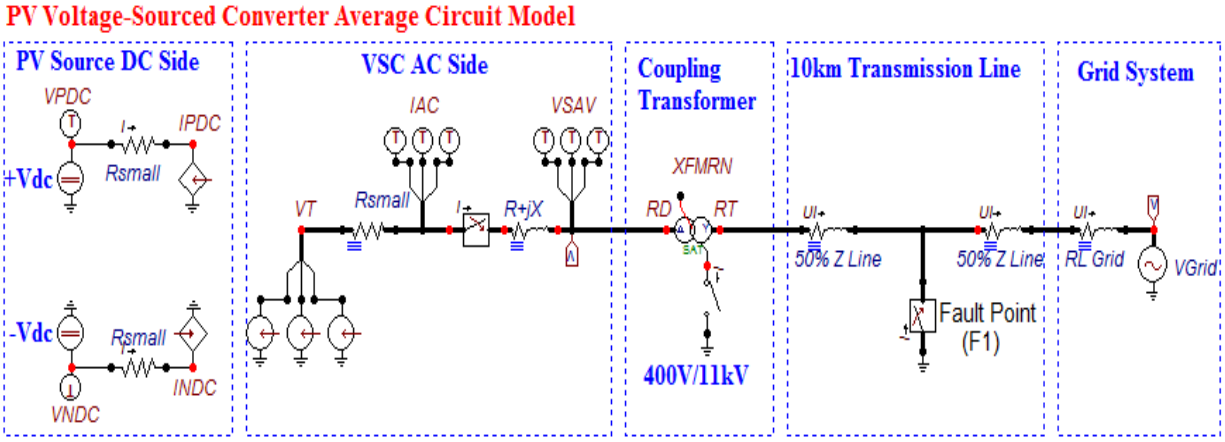

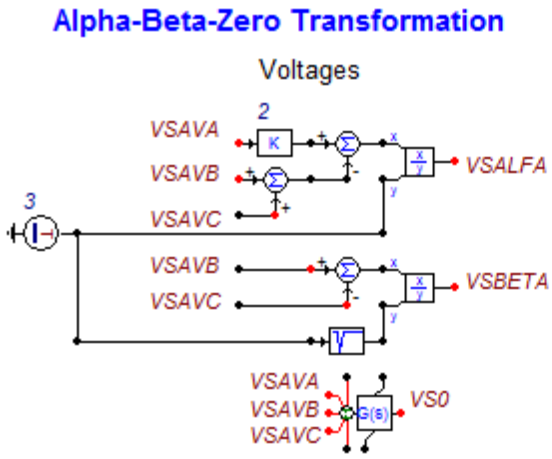

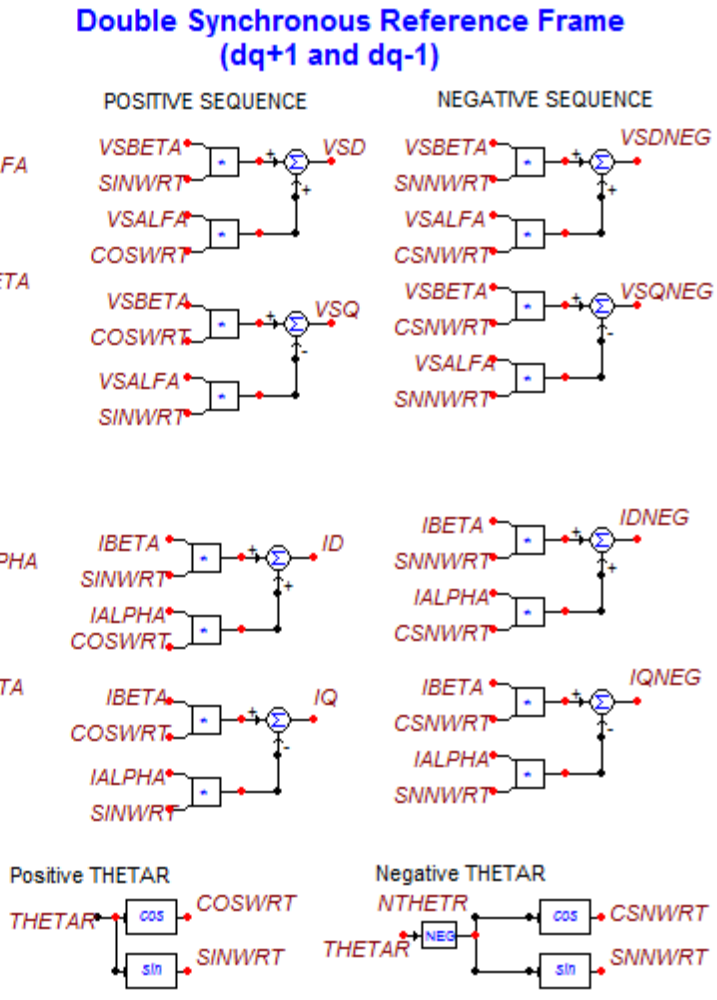

Decoulping cell for DQ+
for cancelling the effect of V- on the DQ+ frame signals

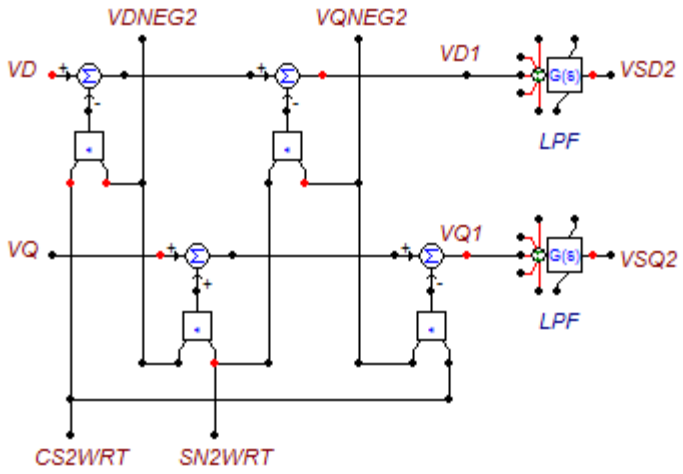

Decoulping cell for DQ-
for cancelling the effect of V+ on the DQ- frame signals

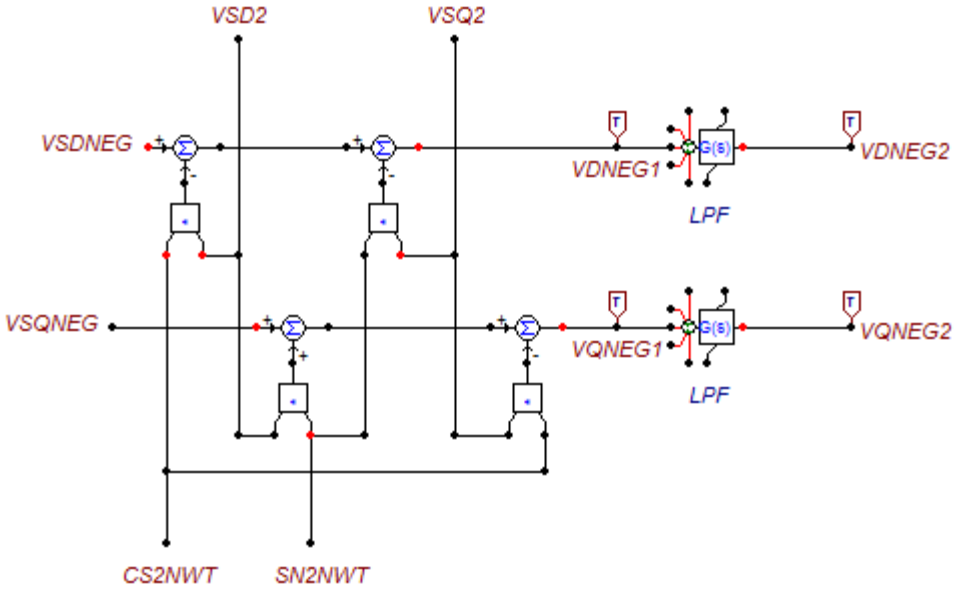

Current Decoulping cell for DQ+

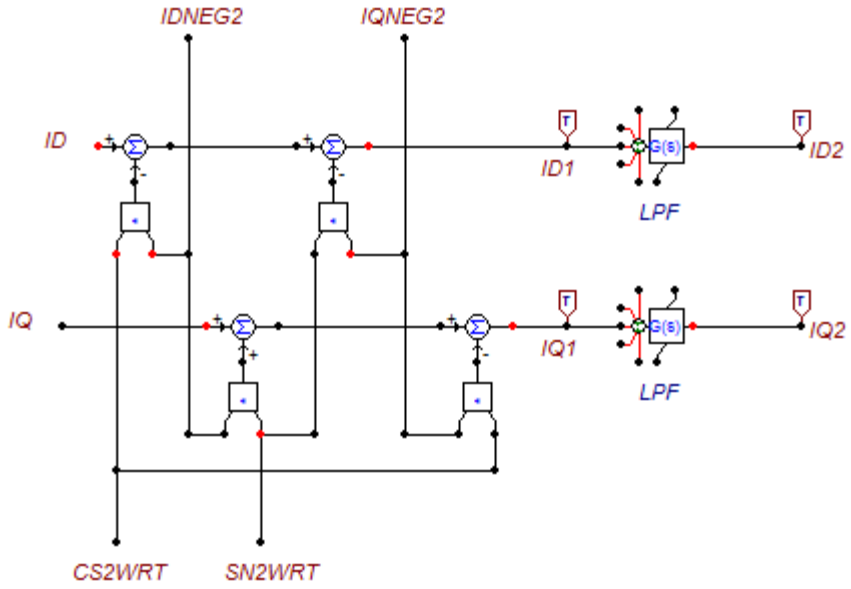

Current Decoulping cell for DQ-

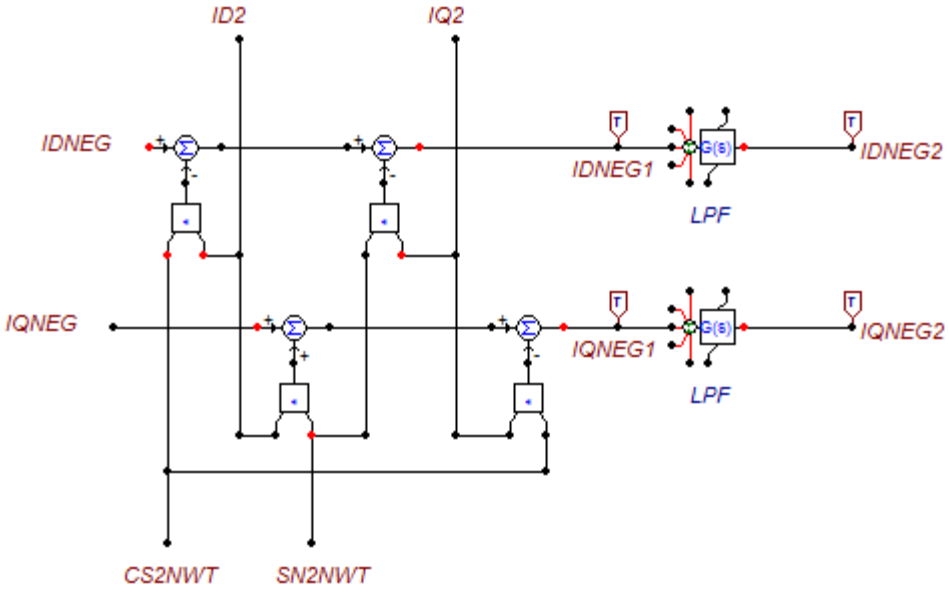

Negative Sequence Closed Loop Modulating Functions Controls

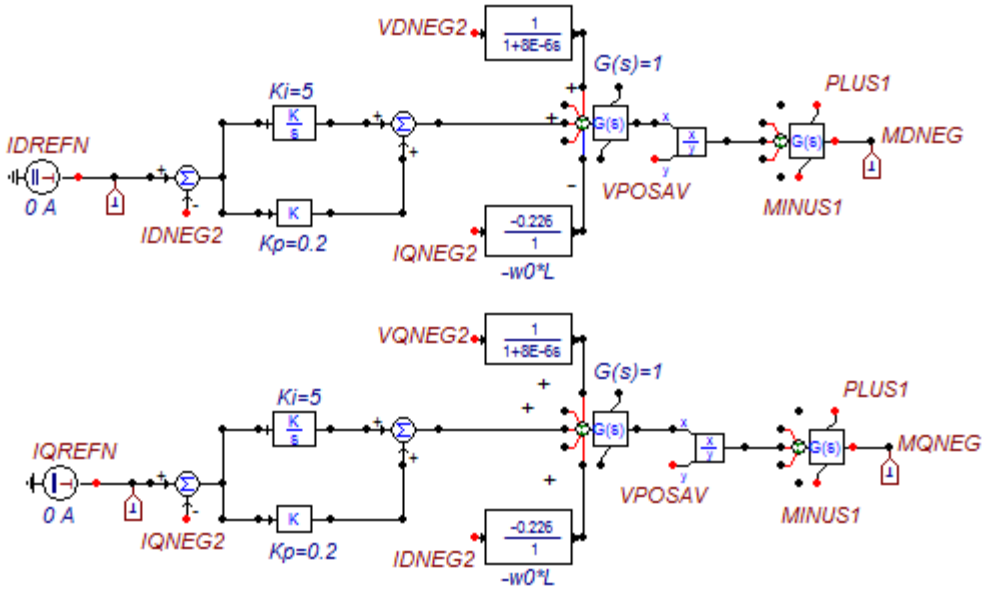

Postive Sequence Closed Loop Modulating Functions Controls

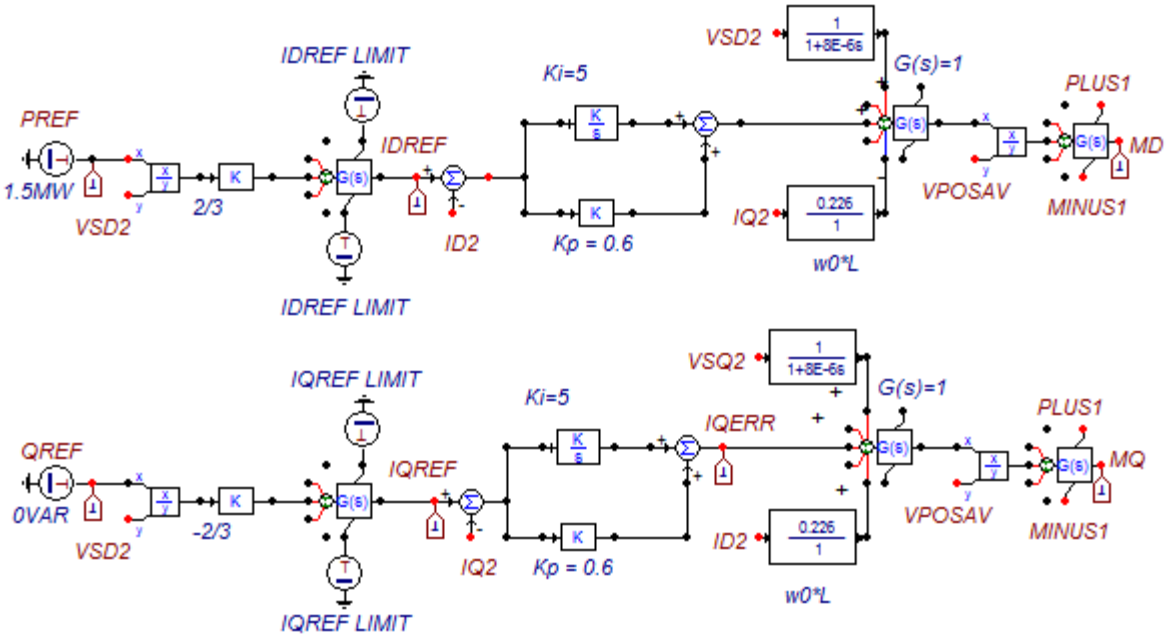

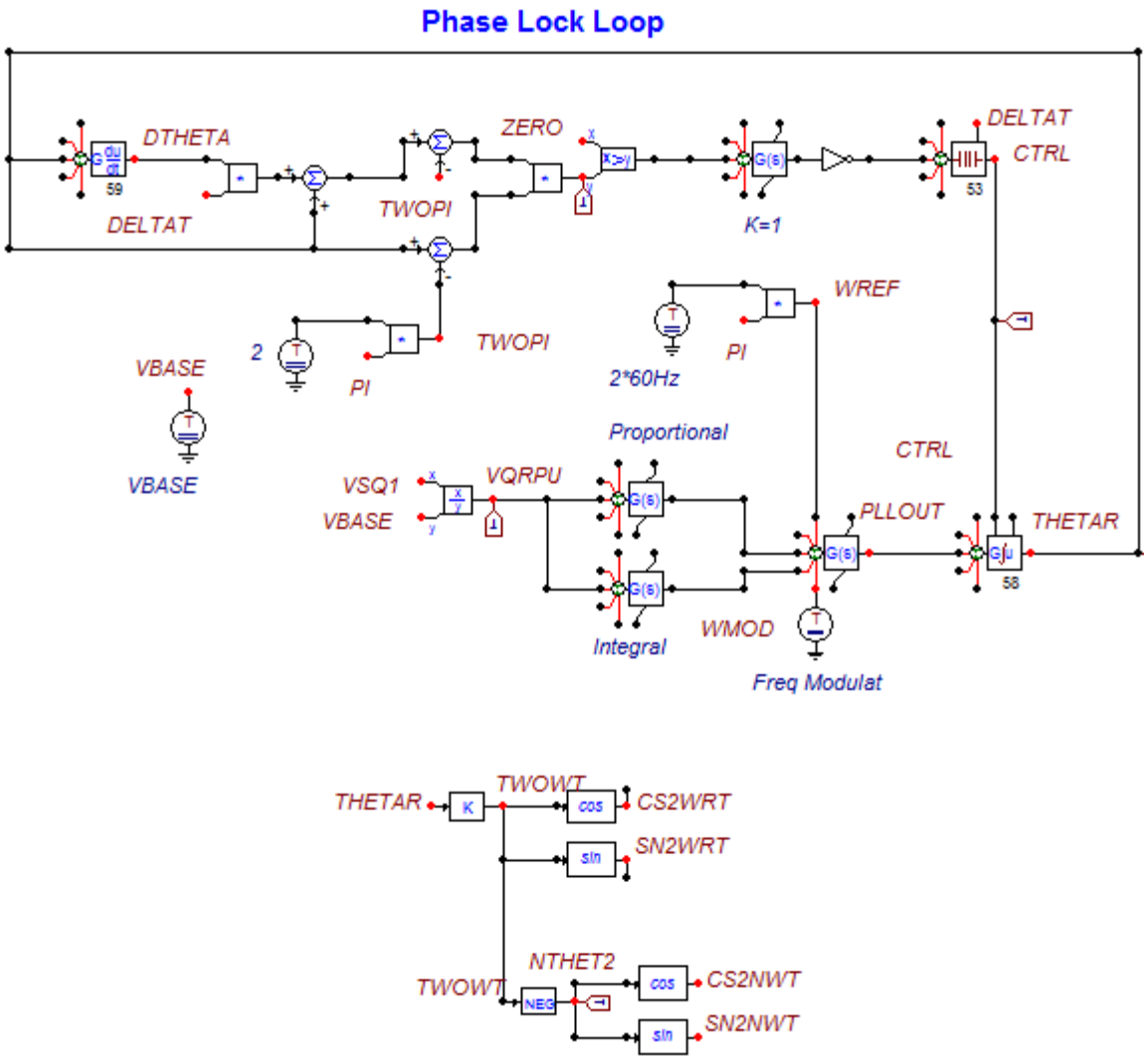
Phase Lock Loop
DTHETA
59
DELTAT
ZERO
TWOPI
K=1
DELTAT
CTRL
53
WREF
PI
2*60Hz
2
PI
TWOPI
VBASE
VBASE
Proportional
CTRL
VSQ1
VBASE
VQRPU
PLLOUT
THETAR
58
Integral
WMOD
Freq Modulat
THETAR
K
TWOWT
cos
CS2WRT
sin
SN2WRT
NTHET2
TWOWT
NEG
cos
CS2NWT
sin
SN2NWT

Convert MD and MQ alpha-beta and then to ABC domain

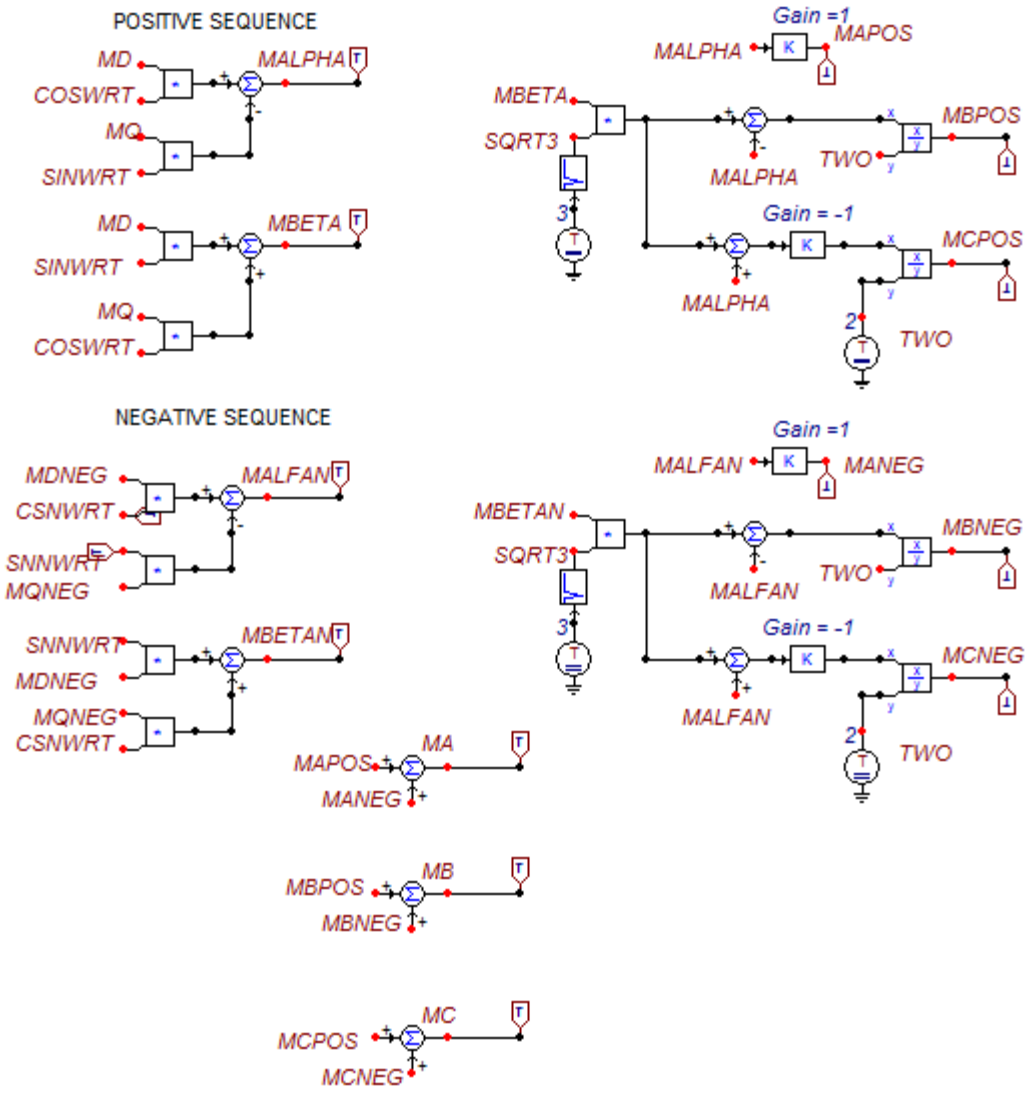

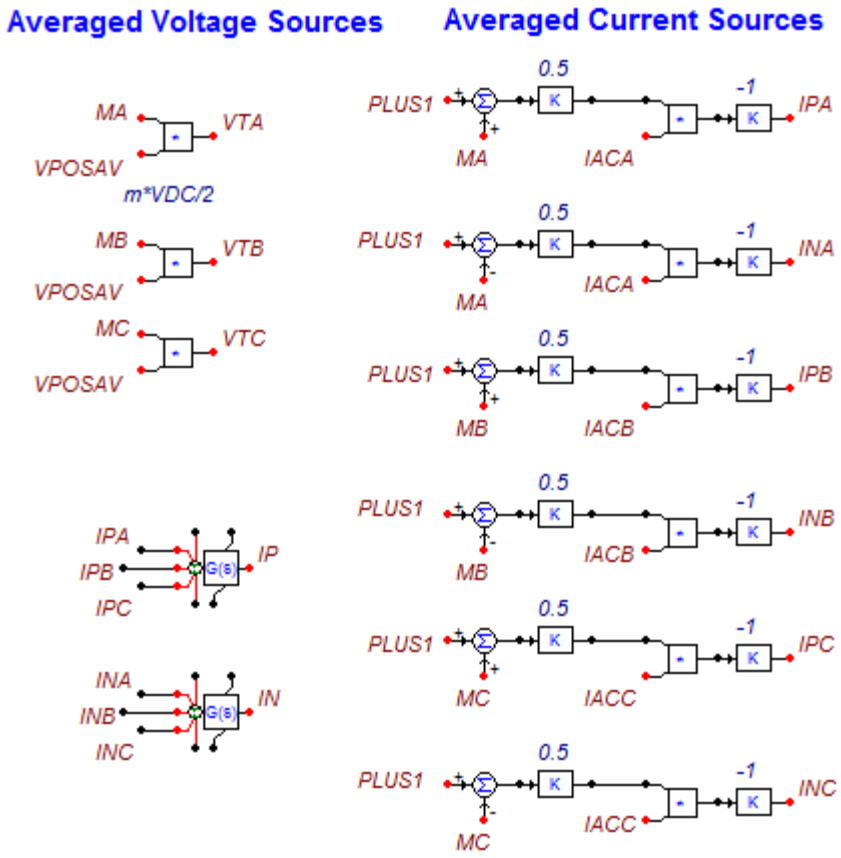
Averaged Voltage Sources
Averaged Current Sources
MA
VPOSAV
VTA
m*VDC/2
MB
VPOSAV
VTB
MC
VPOSAV
VTC
IPA
IPB
IPC
G(s)
IP
INA
INB
INC
G(s)
IN
PLUS1
0.5
MA
IACA
-1
IPA
PLUS1
0.5
MA
IACA
-1
INA
PLUS1
0.5
MB
IACB
-1
IPB
PLUS1
0.5
MB
IACB
-1
INB
PLUS1
0.5
MC
IACC
-1
IPC
PLUS1
0.5
MC
IACC
-1
INC

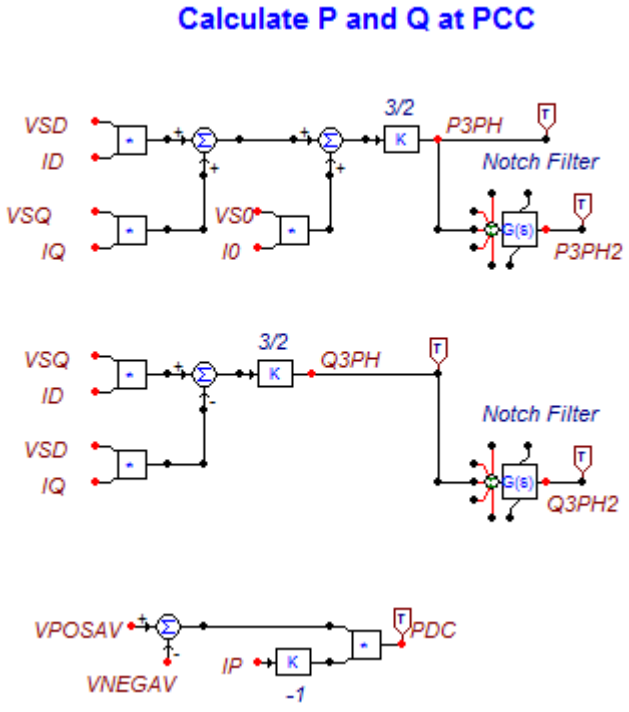
Calculate P and Q at PCC
VSD
ID
VSQ
IQ
VS0
I0
3/2
P3PH
Notch Filter
G(s)
P3PH2
VSQ
ID
VSD
IQ
3/2
Q3PH
Notch Filter
G(s)
Q3PH2
VPOSAV
VNEGAV
IP
-1
PDC